

2021-06-02

Exploring controls of the early and stepped deglaciation on the western margin of the British Irish Ice Sheet.

Benetti, S

<http://hdl.handle.net/10026.1/16979>

10.1002/jqs.3315

Journal of Quaternary Science

Wiley

All content in PEARL is protected by copyright law. Author manuscripts are made available in accordance with publisher policies. Please cite only the published version using the details provided on the item record or document. In the absence of an open licence (e.g. Creative Commons), permissions for further reuse of content should be sought from the publisher or author.

Journal of Quaternary Science

Exploring controls of the early and stepped deglaciation on the western margin of the British Irish Ice Sheet.

| | |
|-------------------------------|---|
| Journal: | <i>Journal of Quaternary Science</i> |
| Manuscript ID | JQS-20-0108.R1 |
| Wiley - Manuscript type: | Special Issue Article |
| Date Submitted by the Author: | n/a |
| Complete List of Authors: | Benetti, Sara; University of Ulster, School of Environmental Sciences Chiverrell, Richard; University of Liverpool, Department of Geography Ó Cofaigh, Colm; Durham University, Department of Geography Burke, Matthew; University of Liverpool, Department of Geography and Planning Medialdea, Alicia; The University of Sheffield; National Research Centre on Human Evolution (CENIEH), Luminescence Laboratory Small, David; Durham University, Department of Geography Ballantyne, Colin; University of St Andrews, School of Geography and Sustainable Development Bateman, Mark; University of Sheffield, Geography Callard, Louise; Durham University, Department of Geography; Newcastle University Wilson, Peter; University of Ulster, School of Environmental Sciences Fabel, Derek; University of Glasgow, Geographical and Earth Sciences clark, chris; Univ Sheffield, Dept Geography Arosio, Riccardo; Scottish Association for Marine Science; CEFAS Bradley, Sarah; The University of Sheffield, Geography Dunlop, Paul; Ulster University, School of Environmental Sciences Ely, Jeremy; University of Sheffield, Geography Gales, Jenny; National Oceanography Centre; Plymouth University, School of Biological & Marine Sciences Livingstone, Stephen; University of Sheffield, Geography Moreton, Steven; NERC Radiocarbon Facility (Environment) Purcell, Catriona; Bangor University, School of Ocean Sciences Saher, Margot; Bangor University, School of Ocean Sciences Schiele, Chris; Ulster University, School of Geography and Environmental Sciences van Landeghem, Katrien; Bangor University, School of Ocean Sciences Weilbach, Kasper; Durham University, Department of Geography |
| Keywords: | Malin Sea, Donegal, ice streams, deglaciation, retreat rate |

SCHOLARONE™
Manuscripts

1
2
3
4
5
6
7
8
9
10
11
12
13
14
15
16
17
18
19
20
21
22
23
24
25
26
27
28
29
30
31
32
33
34
35
36
37
38
39
40
41
42
43
44
45
46
47
48
49
50
51
52
53
54
55
56
57
58
59
60

Exploring controls of the early and stepped deglaciation on the western margin of the British Irish Ice Sheet

Sara Benetti^{1#}, Richard C. Chiverrell², Colm Ó Cofaigh³, Matt Burke², Alicia Medialdea^{4*}, David Small³, Colin Ballantyne⁵, Mark D. Bateman⁴, S. Louise Callard⁶, Peter Wilson¹, Derek Fabel⁷, Chris D. Clark⁴, Riccardo Arosio^{8**}, Sarah Bradley⁴, Paul Dunlop¹, Jeremy C. Ely⁴, Jenny Gales^{9***}, Stephen J. Livingstone⁴, Steven G. Moreton¹⁰, Catriona Purcell¹¹, Margot Saher¹¹, Kevin Schiele¹, Katrien Van Landeghem¹¹, Kasper Weilbach³

¹ School of Geography and Environmental Sciences, Ulster University, Coleraine, UK

² School of Environmental Sciences, University of Liverpool, Liverpool, UK

³ Department of Geography, Durham University, Durham, UK

⁴ Department of Geography, University of Sheffield, Sheffield, UK

⁵ School of Geography and Sustainable Development, University of St. Andrews, Scotland, UK

⁶ School of Geography, Politics and Sociology, University of Newcastle, Newcastle, UK

⁷ Scottish Universities Environmental Research Centre, East Kilbride, UK

⁸ Scottish Association for Marine Science, Oban PA37 1QA, UK**

⁹ National Oceanography Centre, Southampton, UK***

¹⁰ NERC Radiocarbon Laboratory, East Kilbride, UK

¹¹ School of Ocean Sciences, Bangor University, Menai Bridge, UK

Corresponding author

* *Present address:*

National Research Centre on Human Evolution (CENIEH), Burgos, Spain

** *Present address: Centre for Environment, Fisheries and Aquaculture Science, Lowestoft NR33 0HT, UK*

*** *Present address: School of Biological & Marine Sciences, Plymouth University, UK*

Running title: Deglacial rates and controls for BIIS western margin

ABSTRACT

New optically-stimulated luminescence dating and Bayesian models integrating all legacy and BRITICE-CHRONO geochronology facilitated exploration of the controls on the deglaciation of two former sectors of the British-Irish Ice Sheet, the Donegal Bay (DBIS) and Malin Sea ice-streams (MSIS). Shelf-edge glaciation occurred ~27ka, prior to the global Last Glacial Maximum, and shelf-wide retreat began 26-26.5ka at a rate of ~18.7-20.7m/a. MSIS grounding zone wedges and DBIS recessional moraines show episodic retreat punctuated by prolonged still-stands. By ~23-22ka the outer shelf (~25,000 km²) was free of grounded ice. After this time, MSIS retreat was faster (~20m/a vs. ~2-6m/a of DBIS). Separation of Irish and Scottish ice sources occurred ~20-19.5ka, leaving an autonomous Donegal ice dome. Inner Malin shelf deglaciation followed the submarine troughs reaching the Hebridean coast ~19ka. DBIS retreat formed the extensive complex of moraines in outer Donegal Bay at 20.5-19ka. DBIS retreated on land by ~17-16ka. Isolated ice caps in Scotland and Ireland persisted until ~14.5ka. Early retreat of this marine-terminating margin margins is best explained by local ice loading increasing water depths and promoting calving ice losses rather than by changes in global temperatures. Topographical controls governed the differences between the ice-stream retreat from mid-shelf to the coast.

Keywords: Malin Sea; Donegal; ice streams; deglaciation; retreat rate

1. INTRODUCTION

The assessment of the rate and style of ice sheet retreat closely relates to many globally important scientific and socio-economic questions (Stocker, 2014). Constraining the pace of ice-sheet retreat for both past and present ice sheets can improve our understanding of how large ice masses respond to local and global, internal and external forcing, such as glaciological, climatic, and oceanographic changes. Once insights gained from such knowledge are incorporated in ice sheet models, they can improve the predictions on how modern ice sheets will evolve with the current changing climate, ocean temperature and sea-level (Joughin, et al., 2014, Rignot, et al., 2010). The behaviour of ice streams is of interest as they are a major regulator of the mass balance of ice sheets (Payne, et al., 2004, Roberts, et al., 2010, Stokes, 2018, Stokes and Clark, 1999, Stokes and Clark, 2001). At ice stream termini, the reduction or loss of buttressing ice shelves can lead to thinning of upstream based ice and the acceleration of ice flow and this behaviour has been recorded in modern ice streams in Greenland and West Antarctica (Krabill, et al., 2000, Krabill, et al., 2004, Pritchard, et al., 2009, Rignot, et al., 2004a, Sonntag, et al., 2012). Additionally, ice streams react more readily than other parts of the ice margin to any perturbation in ocean circulation, atmospheric temperature and sea-ice distribution as a consequence of both thermal (melting) and mechanical (floatation and calving) stressors that occur along the margins of marine-terminating ice sheets (e.g. Hulbe, et al., 2004, Joughin, et al., 2012, Payne, et al., 2004, Scambos, et al., 2004, Shepherd, et al., 2004).

While modern ice streams are being extensively studied, the temporal resolution of such studies is limited. Numerical-glaciological, isostatic and palaeoclimatic models all require empirical constraints on past ice-sheet extent and dynamics either to direct their formulation or for the testing of model outputs (Hughes, et al., 2016). Such information over centuries and millennia can only come from palaeo-analogues, where a complete record of deglaciation may be better visible and quantifiable (Bradwell, et al., 2008, Chiverrell, et al., 2013, Hughes, et al., 2016, Svendsen, et al., 2004). The last British Irish Ice Sheet (BIIS) has been proposed as a potential analogue for sensitive areas of modern ice sheets (Clark, et al., 2012). The BIIS, at several times in the past, had an abundance of marine-terminating ice, which would have been sensitive to both climatic and oceanic forcing, and was drained by radiating ice streams, which were likely critical to BIIS dynamics and overall mass balance during retreat (e.g. Boulton and Hagdorn, 2006, Boulton, 1990, Hubbard, et al., 2009b, Pritchard, et al., 2009, Rignot, et al., 2004b, Sole, et al., 2008).

The Malin Sea includes the continental shelf to the west of Scotland, often referred to as the Malin Shelf, and the portion of the continental shelf northwest of Ireland that includes Donegal Bay (Fig. 1). The Malin Sea received flows from two large convergent ice masses derived from the Hebridean Islands, mainland Scotland, the North Channel, and the north of Ireland. Ice radiating from the mountains of Donegal in northwest Ireland formed an independent centre of ice dispersal, that not only fed ice towards the north, but also west and southwest into Donegal Bay (Fig. 1 inset). Ice in Donegal Bay was also fed from the lowland ice domes through Counties Mayo and Sligo (Greenwood and Clark, 2009a, Greenwood and Clark, 2009b). The former ice masses occupying the Malin Shelf and

1
2
3 Donegal Bay meet the fundamental geomorphological criteria for ice streams (Stokes,
4 2018, Stokes and Clark, 1999, Stokes and Clark, 2001) in the form of convergent flows and
5 ubiquitous elongated bedforms (Dove, et al., 2015, Dunlop, et al., 2010, Finlayson, et al.,
6 2014). The ice on the Malin Shelf has attracted a variety of names, including Barra Fan Ice
7 Stream (Callard, et al., 2018, Dunlop, et al., 2010, Scourse, et al., 2009), Hebrides Ice
8 Stream (Dove, et al., 2015, Small, et al., 2017a), Malin Sea Ice Stream (Wilson, et al.,
9 2019). In addition, sectors of the ice mass have also been referred to separately as other
10 names including the North Channel Ice Stream (Finlayson, et al., 2014, Finlayson, et al.,
11 2010, Hughes, et al., 2014).

12
13
14
15
16 Here, this marine-terminating ice stream is termed the Malin Sea Ice Stream (MSIS), it
17 drained between 5-10% of the BIIS and fed the southernmost glaciogenic fan on the
18 European continental margin, as well as largest sedimentary depocentre of the BIIS, the
19 Donegal-Barra Fan (DBF - Fig. 1) (Dove, et al., 2015, Howe, et al., 2012, Knutz, et al.,
20 2001). Deep water cores suggest that this portion of the ice sheet responded quickly to
21 millennial scale climate oscillations suggesting a strong link between climate cycles and
22 glaciological processes (Hibbert, et al., 2009, Knutz, et al., 2001, Scourse, et al., 2009). Its
23 sensitivity to climatic and oceanographic changes is also captured by numerical modelling
24 experiments (Hubbard, et al., 2009b, Patton, et al., 2017, Patton, et al., 2016, Patton, et al.,
25 2012a, Patton, et al., 2012b). The other marine-terminating ice stream in the southern
26 portion of the Malin Sea, was fed by ice flowing through Donegal Bay, and has surprisingly
27 never been named and is referred to here as the Donegal Bay Ice Stream (DBIS). Less is
28 known about the contribution of this ice stream to the evolution of the continental margin as
29 there is no distinct glaciogenic fan on this part of the margin similar to the DBF, but there
30 are a series of well-developed canyon systems, whose evolution was driven by meltwater
31 and sediment delivery at the shelf edge during the stages of ice advance and retreat
32 (Benetti et al., 2010; Sacchetti et al., 2012).

33
34
35
36
37
38
39 Reconstructions of the BIIS have relied heavily on onshore mapping of landforms in
40 representations of former ice limits and ice flow directions (Ballantyne, 1989, Bennett and
41 Boulton, 1993, Clark, et al., 2004, Sissons, 1980). More recently, advances in offshore
42 geomorphological mapping, through the use of bathymetric and seismic data, have allowed
43 the identification of landforms associated with ice extension and retreat on the continental
44 shelf of the Malin Sea (Arosio, et al., 2018b, Benetti, et al., 2010, Bradwell, et al., 2008,
45 Callard, et al., 2018, Dove, et al., 2015, Dunlop, et al., 2010, Howe, et al., 2012, Ó'Coifagh,
46 et al., 2012, Ó Cofaigh, et al., 2019). The marine realm has provided a better
47 characterization of the style of retreat and of the changes in ice streaming during
48 deglaciation. The dating of glacial and glacially-derived landforms and sediments, in both
49 marine and terrestrial settings, carried out as part of the NERC-funded BRITICE-CHRONO
50 project, has more recently provided key datasets, which can allow a more refined
51 chronological reconstruction of the MSIS and DBIS behaviour during the last glaciation.
52 Many of these results including full details of age controls and their stratigraphic and
53 landform contexts have been reported in a series of publications (Arosio, et al., 2018a,
54 Callard, et al., 2018, Ó Cofaigh, et al., 2019, Schiele, 2017, Small, et al., 2017a, Small, et
55 al., 2016, Tarlati, et al., 2020, Wilson, et al., 2019). In the context of BRITICE-CHRONO,
56
57
58
59
60

1
2
3 these two components of the BIIS were referred to as Transect 6 for Donegal Bay and
4 Transect 7 for the Malin Shelf (Fig. 1 inset). Here, these geochronological reconstructions
5 are brought together for the first time including both the offshore and onshore data by (1)
6 presenting the Bayesian analysis of all the geochronology, including radiocarbon, optically-
7 stimulated luminescence and cosmogenic ages, (2) using Bayesian analysis to integrate all
8 ages produced for these former ice streams; (3) providing isochrones of ice margin retreat
9 and allowing calculation of rates of retreat for both ice streams; (4) exploring the changing
10 dynamics with retreat including the separation of “Scottish” and “Irish” ice masses; and (5)
11 assessing the interplay of forcing factors in regulating the pace of ice stream retreat and
12 ultimately deglaciation.
13
14
15
16
17
18

19 2. DATA & METHODS

20 2.1 CONTEXT AND PUBLISHED AGES

21
22
23 Our aim was to constrain the timing of ice margin retreat for two adjacent marine-
24 terminating sectors of the western BIIS. This challenge was met by compiling and extending
25 an empirical dataset of quality-controlled absolute age measurements for the DBIS and the
26 MSIS. The BRITICE-CHRONO approach was to use sites with good stratigraphical or
27 geomorphological integrity and incorporate the age information within Bayesian
28 chronosequence models for the differing ice streams or glaciers (e.g. Chiverrell et al.,
29 2013). All published and new deglaciation ages are presented here for the DBIS and MSIS,
30 with all ages subject to a triage system assessed according to quality criteria (Small, et al.,
31 2017b), and here only ages deemed of good quality (green and amber) are included. A few
32 pre-LGM ages (flagged as problematic in a quality assessment of the value of legacy ages
33 for constraining deglaciation) (Small, et al., 2017b) were nonetheless used as indicators of
34 previous ice-free conditions (Fig. 1; Table 6) (Bos, et al., 2004, Colhoun, et al., 1972,
35 Jardine, et al., 1988). The new deglaciation ages include offshore radiocarbon (^{14}C) ages
36 (Table 3) (Callard, et al., 2018, Ó Cofaigh, et al., 2019) and onshore terrestrial cosmogenic
37 nuclide (TCN) ages (Table 4) (Schiele, 2017, Small, et al., 2017a, Wilson, et al., 2019) (see
38 Fig. 1 for all locations). In addition, fifteen new optically-stimulated luminescence (OSL)
39 ages have been obtained and are presented here for the first time (Table 1; Fig. 1). The
40 OSL sites were selected targeting spatial gaps in the retreat sequences and to reassess
41 sites yielding conflicting ages in the existing deglacial chronology for the region.
42
43
44
45
46
47
48

49 Details on the methods used to process all TCN and ^{14}C samples are reported in the
50 relevant publications (see Tables 3 and 4 for references). The original ^{14}C measurements
51 have been calibrated using OxCal 4.2, with for marine-derived samples the Marine-13
52 calibration curve and applying a marine reservoir correction of 0 years (Bronk Ramsey,
53 2009a, Reimer, et al., 2013). They are reported to two decimal places as cal. ka BP. ^{14}C
54 ages were calibrated afresh using consistent marine C reservoir during the Bayesian
55 modelling. Only ^{14}C ages representing latest glacial and deglaciation ages are included in
56 this paper (i.e. not younger ones). Cosmogenic ages include ^{10}Be and ^{36}Cl exposure ages
57 and, in the text, all TCN ages are rounded to the nearest 0.1 ka and shown with the ± 1
58
59
60

1
2
3 sigma external uncertainty, unless otherwise stated. To be consistent across all BRITICE-
4 Chrono publications, ^{10}Be ages presented here have been calculated using the calculator
5 formerly known as the CRONUS-Earth calculator (Developmental version; Wrapper script
6 2.3, Main calculator 2.1, constants 2.2.1, muons 1.1; Balco, et al., 2008). ^{10}Be ages are
7 calibrated using the Loch Lomond local production rate (LLPR: Fabel, et al., 2012, Small
8 and Fabel, 2015) which is linked to direct independent age control provided by limiting
9 radiocarbon ages (MacLeod, et al., 2011). All other Scottish calibration sites rely on an
10 assumed Younger Dryas deglaciation age (Borchers, et al., 2016, Marrero, et al., 2016),
11 assumed tephra age within a varve chronology (Small and Fabel, 2015), and a contested
12 radiocarbon chronology (Lowe, et al., 2019, Putnam, et al., 2019). Variation between these
13 different production rates change calculated ^{10}Be ages from 2.5% older to 6.3% younger
14 compared to LLPR. For comparison we also provide the TCN ages calculated with the
15 CRONUScalc v2.0 calculator (Marrero, et al., 2016) and using the global mean ^{10}Be
16 production rate (Borchers, et al., 2016). The resulting ages using LLPR and the global
17 production rate are statistically the same at 1 sigma (Tables 4 and 5). All ages are
18 calculated assuming a rock surface erosion rate of 1mm ka^{-1} and the LM scaling method
19 (Balco, et al., 2008). All details necessary to recalculate the TCN ages in Table 4 with
20 different calculators, reference production rates, or scaling methods can be found in the
21 original publications. Small, et al. (2017b) conveniently provides the legacy data, except for
22 the two legacy ^{36}Cl ages for which there was insufficient information in the original
23 publication. For individual locations multiple samples have been analysed typically, with the
24 site repeatability tested using the reduced Chi-squared test (see Balco, et al., 2008,
25 Heyman, et al., 2011, Small, et al., 2017a). After excluding outliers, the uncertainty
26 weighted mean and associated uncertainties for exposure ages were calculated at each
27 site.
28
29
30
31
32
33
34
35
36
37
38

39 *2.2 OPTICALLY-STIMULATED LUMINESCENCE (OSL) DATING*

40
41 Samples for OSL dating were collected from eight sites across the two transects targeting
42 glacial fluvial and deltaic outwash sands and gravels. All sites were selected based on their
43 ice-proximal context and the potential to constrain the timing for well-defined ice margins
44 (Fig. 1 and Table 2). OSL dating is underpinned by the principle that exposure to sunlight
45 zeros or bleaches an OSL signal that develops within mineral grains (typically quartz or K-
46 feldspar). The OSL signal increases with the duration of burial in sediments as the materials
47 are exposed to natural radiation increasing the charge stored within quartz or feldspar. Here
48 we use small aliquots (SA; ~20 grains) of sand-sized quartz grains separated from
49 sediments to measure the OSL signal (Duller, 2008, Murray and Wintle, 2000). For samples
50 that have been bleached heterogeneously, the measurement of multiple replicates (typically
51 here ~50) can identify those grains exposed to sunlight most recently, which are referred to
52 as a well bleached population. With heterogeneous-bleaching, statistical models are
53 required to determine an accurate age, e.g. the Minimum Age Model (MAM) (Galbraith, et
54 al., 1999) or the internal-external uncertainty (IEU) model (Thomsen, et al., 2007).
55
56
57
58
59
60

1
2
3 At all sites opaque tubes were hammered into sedimentary sections to prevent exposure to
4 sunlight during sampling. The external gamma dose rates were determined using in-situ
5 gamma spectrometry, with external beta dose rates calculated from U, Th, K and Rb
6 concentrations determined by inductively coupled plasma mass spectrometry (ICP-MS).
7 The sample preparation and analysis methods used were identical to existing studies
8 (Bateman, et al., 2018, Evans, et al., 2017). Appropriate conversion factors (Guérin, et al.,
9 2011, Guérin, et al., 2012) were applied to calculate the final total dose rate (Table 1)
10 including grain size. The sites sampled all have water tables that are presently artificially
11 low, owing to either coastal erosion or aggregate extraction. Maximum pore spaces in 180 –
12 250 µm sand are in the range between rhombohedral (26 %) and random (40 %) packing,
13 which for moderately sorted rounded to sub-rounded sands equates to saturated water
14 contents of around 30 %. In terms of palaeomoisture attenuation, contents of 23±5 % were
15 used for shallow and drier samples and 27±5 % for deeper saturated samples.
16
17
18
19
20

21 OSL analyses were performed on the 180 – 250 µm size fraction (Table 2) and using
22 aliquots each containing ~20 grains. The low proportion of quartz grains emitting an OSL
23 signal for these samples suggests the OSL signal was dominated by few grains as has
24 been the case elsewhere (e.g. Evans et al. 2017). All measured D_e distributions were
25 asymmetrically distributed and display a high over-dispersion (OD; Table 2) confirming
26 heterogeneous bleaching prior to burial. The D_e values used for age calculation (Table 2)
27 target the well bleached component of these heterogeneously bleached D_e distributions and
28 were identified by applying age models. Final D_e values for age calculation were calculated
29 using as appropriate either the Minimum Age Model (MAM) (Galbraith et al., 1999) or the
30 internal-external uncertainty (IEU) model (Thomsen, et al., 2007) with the parameters a and
31 b used in the model determined from dose recovery tests (calculating the OD of the dose
32 distribution at multiple given doses) for each site. Such an approach has been applied
33 successfully to glacial sediments elsewhere in the BISS (e.g. Bateman, et al., 2018).
34
35
36
37
38

39 2.3 BAYESIAN AGE MODELLING

40
41 Bayesian age modelling (Bronk Ramsey, 2008, Buck, et al., 1996) is an approach applied
42 routinely to integrate sets of age measurements related typically by stratigraphy, for
43 example ages from lake sediment sequences (Bronk Ramsey, 2008). The modelling refines
44 the probability distributions for individual ages and is underpinned by the series of ages
45 being presented as an order of events reasoned independently of the chronology, e.g.,
46 depth order. Increasingly the approach has been applied to spatially-distributed
47 geochronological datasets, such as the retreat of glacial margins (e.g., Bradwell, et al.,
48 2019, Chiverrell, et al., 2018, Chiverrell, et al., 2020, Chiverrell, et al., 2013). The
49 deglaciation sequence for both the DBIS (T6) and MSIS (T7) evidenced in the onshore and
50 offshore geomorphology provides a hypothetical 'relative-order' of dated events, which in
51 the terminology for the Bayesian modelling is the Prior model (Bronk Ramsey, 2008, Buck,
52 et al., 1996). The Bayesian Prior models for both ice streams were developed
53 independently of the age information and included all the geochronological samples in the
54 model structures (Bronk Ramsey, 2008, Bronk Ramsey, 2009a, Bronk Ramsey, 2009b,
55 Bronk Ramsey and Lee, 2013). These Prior models cover the ice marginal retreat from
56
57
58
59
60

1
2
3 maximum limits near the continental shelf breaks fronting DBIS and MSIS through a series
4 of well-defined ice margin configurations identified on the seafloor and stepping-back on to
5 land in Ireland and western Scotland (Callard, et al., 2018, Ó'Cofaigh, et al., 2012, Ó
6 Cofaigh, et al., 2019, Peters, et al., 2015, Peters, et al., 2016, Small, et al., 2017a, Wilson,
7 et al., 2019). The Bayesian analysis of the MSIS was not straightforward because of the
8 interaction between the MSIS draining the main ice sheet divides and more local "Irish" ice
9 that fed laterally into the ice stream. The recently mapped features in the Malin Sea
10 provided the framework for the context of ice movement (Callard, et al., 2018).
11
12
13

14 The Bayesian modelling was coded using OxCal 4.3 (Bronk Ramsey and Lee, 2013) and
15 applied uniform phase sequence models that were punctuated by boundaries located at
16 well-defined ice limits. Markov Chain Monte Carlo (MCMC) sampling was used to build
17 distributions of possible solutions, thereby generating modelling probabilities termed
18 posterior density estimates for all measured ages and boundary limits. The probabilities are
19 the product of the Prior model and the likelihood or measured age probabilities measured
20 for each sample. Each sequence was divided into retreat zones that were coded as a
21 Phase, defined as groups containing age information for sites sharing relationships with the
22 adjacent zones. In the Bayesian analysis though TCN ages at some locations were
23 consistent within a site and could be averaged using a reduced Chi-square statistic (χ^2_R)
24 (Bevington and Robinson, 2003), here the ages were included individually but grouped
25 within a Phase in the Prior model. Phases were delimited by a series of Boundary
26 commands that generated modelled age probability distributions for major ice limits. Both
27 Sequence models were run to assess outliers in time using a scaling of $10^0 - 10^4$ years and
28 Student's t-distributions to describe the outlier distribution (Bronk Ramsey, 2009b).
29 Iterations of the modelling were undertaken gradually varying the outlier probabilities for
30 individual age determinations to achieve overall model agreement indices exceeding the
31 $>60\%$ threshold advocated by Bronk Ramsey (2009a). Thereby outliers were given a
32 probability scaling of $P < 0.2$, $P < 0.5$, $P < 0.75$ and $P = 1$ (100%) on a scale of increasing
33 outlier severity. Dating bottlenecks in the Prior models were handled by increasing
34 iteratively the outlier probability for all ages in selected Phases until the model produced
35 overall agreement, which then calculates model agreement indices for all individual ages.
36 Outlier ages were identified statistically, and then scrutinised for reasons that might explain
37 the outlier behaviour either in the Prior model (e.g., the sample context) or in the
38 measurement data (e.g., nuclide inheritance). Ages were not excluded arbitrarily but
39 identified statistically and then weighted $P = 1$. Cycles of the Bayesian modelling then
40 continued decreasing and increasing other less severe outlier probabilities for subsequent
41 iterations until the overall model agreement was $> 60\%$. Samples handled as outliers ($P =$
42 1 ; 100%) are detailed in later sections.
43
44
45
46
47
48
49
50
51
52
53
54
55

56 3. RESULTS AND INTERPRETATIONS

57 This section presents the new OSL age assessments from land areas adjacent to the DBIS
58 and MSIS (Figs. 2-11; Tables 1 and 2). In addition, we summarise 71 radiocarbon ages
59
60

1
2
3 from offshore glacial and glaciomarine sediments previously presented in (Schiele, 2017),
4 (Callard, et al., 2018) and (Ó Cofaigh, et al., 2019); and 41 TCN ages already included in
5 (Schiele, 2017), (Small, et al., 2017a), and (Wilson, et al., 2019); and the legacy ages
6 published previously (Small, et al., 2017b) that have been included in the Bayesian age
7 modelling. The ages presented here may differ slightly to original published owing to
8 differences in exposure-age calculations and statistical treatments (e.g. evaluation using
9 the LLPR; (Fabel, et al., 2012, Small and Fabel, 2015).

15 3.1 OFFSHORE GEOMORPHOLOGY AND DATING

17 The geology of the Malin Shelf is characterised by series of northeast trending troughs and
18 basins, and basement blocks. Home to the former MSIS, these over-deepened troughs and
19 basins interlink from the Sea of Hebrides to the mid-shelf and were likely major flow paths
20 for ice streaming across the Malin Shelf from the Scottish Highlands and Ireland during past
21 glacial periods (Davies, et al., 1984, Dobson and Whittington, 1992). Two basins, the Malin
22 Deep and the trough of the Sea of Hebrides are separated by the Stanton Bank, a bedrock
23 high at the centre of the inner Malin Shelf (Dobson and Whittington, 1992). For the former
24 DBIS, the shelf offshore NW Ireland in the southern part of the Malin Sea has a smoother
25 profile with a gentle gradient from the mouth of Donegal Bay to the shelf edge, with
26 Donegal Bay having the characteristics of an over-deepened basin like those further to the
27 north (Fig. 1).

32 For the former MSIS, the geomorphological evidence shows the presence of a compound
33 ridge close to the shelf edge comprising a series of moraines and grounding-zone wedges
34 (GZWs) mapped from 55°30'N to 56°30'N (Callard, et al., 2018, Dunlop, et al., 2010).
35 Further to the north, a series of morainal banks with a similar N-S orientation have been
36 broadly mapped from seismic data down to 150 m water depth and are likely to be the
37 continuation of the same ice margin and to be related to the extension of the Outer
38 Hebrides Ice Cap on the Scottish continental shelf (Bradwell, et al., This volume). Moraines
39 of different orientations are observed at the boundary between the DBIS (T6) and MSIS
40 (T7) on the Malin Shelf (trending respectively NW-SE and NE-SW; Figs. 1 inset, 13, 14)
41 and it was suggested that they mark the retreat of the two ice streams in the direction of the
42 inner Malin Shelf to the north and northern Donegal to the south (Benetti, et al., 2010,
43 Dunlop, et al., 2010, ÓCofaigh, et al., 2012). In the inner part of the Malin Shelf series of
44 smaller recessional moraines and GZWs step back eastwards and become increasingly
45 abundant on the inner shelf, with De Geer moraines in the shallower waters of the sea-
46 lochs and sounds, marking the pattern and direction of retreating ice (Dove, et al., 2015,
47 Dunlop, et al., 2010, Small, et al., 2016). It has been suggested that, because of presence
48 of the over deepened troughs, retreat from the shelf back towards the Inner Hebrides was
49 likely rapid (Dove, et al., 2015), although previously estimated ice sheet retreat suggests
50 that this process was slow (Clark, et al., 2012). For the DBIS, a set of arcuate, nested
51 moraines extend across the entire continental shelf from within Donegal Bay to the shelf
52 edge up to distance of 90 to 120 km from the coastline (Benetti, et al., 2010, Dunlop, et al.,
53
54
55
56
57
58
59
60

2010, Ó'Cofaigh, et al., 2012), and they are indicative of grounded ice and a stepped glacial retreat across the shelf.

The dating of these glacial and glacially-derived landforms and sediments provides key datasets to support a more refined chronological reconstruction of the behaviour of the two ice streams during the last glaciation (Arosio, et al., 2018a, Callard, et al., 2018, Ó Cofaigh, et al., 2019, Tarlati, et al., 2020). Constraining a maximum extent of the BIIS across the Malin Sea has not been straightforward due to the presence of intense iceberg turbation at the shelf edge in correspondence with the margin of the MSIS at the shelf edge. However, the youngest radiocarbon ages obtained from shell fragments in subglacial diamicton constrains shelf edge glaciation to after 26.3 ka BP for both the MSIS and the DBIS (JC106-125VC and JC106-112VC in Table 3) (Callard, et al., 2018, Ó Cofaigh, et al., 2019). Retreat from the shelf edge has been dated using mixed foraminifera assemblages in glaciomarine muds between 26.3 and 23-24 ka BP and extensive iceberg scouring at the shelf edge across the entire margin of the Malin Sea indicate that it happened initially through intense calving. All foraminiferal and sedimentological data suggest that glaciomarine conditions prevailed during retreat. By 21 ka BP (i.e. global LGM; Clark, et al., 2009b, Hughes and Gibbard, 2015, Hughes, et al., 2013), most of the Malin Sea was free of grounded ice with glaciomarine conditions recorded offshore Tiree (JC106-149VC; Table 3) (Callard, et al., 2018) and a morainic complex of a similar age at the mouth of Donegal Bay (JC106-92VC and JC106-97VC; Table 3) (Ó Cofaigh, et al., 2019). Sedimentological evidence from the DBF suggest some marine extension of the BIIS until ~16.5 ka BP that allowed glaciomarine sediment deposition on the fan, with discrete episodes of calving recorded as peaks in ice-rafted debris (Tarlati, et al., 2020).

3.2 OSL GEOCHRONOLOGY

On the BRITICE-CHRONO project, the timing and pace of deglaciation in other sectors of the BIIS has been in part secured by optically-stimulated luminescence (OSL) dating of proglacial and ice-marginal sediments (Bateman, et al., 2018, Chiverrell, et al., 2018, Chiverrell, et al., 2020, Evans, et al., 2017, Small, et al., 2018, Smedley, et al., 2017a, Smedley, et al., 2017b). Here, we report sixteen new OSL ages, sampled between 2014 and 2016, from glacial sediments at eight terrestrial sites, three associated with DBIS and five from the north of Ireland constraining the MSIS (Tables 1-2). Exposures were logged using field sketches, vertical lithofacies logs and photo-montages following standard procedures (Evans and Benn, 2004, Thomas, et al., 2004). Other characteristics recorded included textural classifications, sorting and grain size, palaeocurrents or till fabric indicators, sedimentary structures, nature of contacts and the lithofacies.

3.2.1 OSL sites from the MSIS

OSL samples were collected from natural and quarried sediment exposures extending from in the west Altwinny Bay and Fawnmore (Co. Donegal) progressing west to east to Castleroe, Glenshesk Valley and Carey Valley in Co. Antrim, Northern Ireland (Fig. 1).

3.2.1.1 *Altwinny Bay (55.1432 N, 8.2929 W)*

A continuous coastal section is exposed at Altwinny Bay (Cullen, 2012), which is composed of sands, gravels and diamictos (Fig. 2). The sequence, from stratigraphically oldest to youngest comprises basal laminated gravels, sands, and fines, that interdigitate with largely massive gravels which are atop a weathered and granite bedrock that has been mobilised glacially. The massive gravels are interpreted as the product of ice-marginal debris flows, with the more stratified gravel, sand, and mud interbed units suggestive of deposition into a water body. Above this, there is a massive diamict containing evidence of deformation including sandy hydro-fractures injected from above. This in turn is capped by two over-consolidated matrix-supported diamicts displaying a strong clast orientation to the south and boulder pavements that suggest a subglacial origin. In the centre of the exposures these subglacial tills are capped by planar cross-stratified sands, which have flow directions to the south, probably reflecting outwash deposition with ice margin retreat. These sands appear to have been tilted and deformed suggesting proximity to and override by ice following deposition. The exposures are capped by a further series of matrix supported diamictos and finally a clast-supported massive gravel with some stratification that is associated either with later re-advance of ice and/or deposition as flow diamicts during ice retreat.

Cullen (2012) interpreted the sequence to record ice-marginal and glaciomarine debris flows from efflux jets draining ice from inland Donegal. That interpretation conflicts with the exposures observed in 2014, which show growth of the units in a southerly direction, flow directions to the southwest in the outwash sands, and lithologies of erratic clasts in the diamicts that are all consistent with an ice mass sourced from the Malin Sea rather than inland Donegal. Two OSL samples were collected T7ALTB01 (not measured) and T7ALTB02. T7ALTB01 was taken from a unit of horizontally stratified sand that forms the oldest water-lain deposits identified stratigraphically within the section (Fig. 2B). T7ALTB02 was taken from the youngest water-lain deposit in the sequence, which was composed of deformed (tilted) planar cross-stratified sands (Fig. 2F). These two samples were the most westerly onshore materials collected for the MSIS.

The asymmetric D_e distribution (Fig. 3A) derived for T7ALTB02 (Shfd15166) suggests heterogeneous bleaching prior to burial, and that a small proportion of the grains characterises the minimum dose population. The OSL age determined for T7ALTB02 30.4 ± 4.9 ka is considered slightly old relative to the dating of shelf-break glaciation at 26.3 ka BP. That said, the stratigraphical position buried by > 8 m of diamicts shows over-ride by ice and the 30.4 ± 4.9 ka could constrain the expansion of the MSIS to the coast of NW Donegal. Alternatively, this age, slightly old in the sequence, reflects potentially poor bleaching of the OSL signal, which would not be surprising given the relatively short sediment transport distances implicit in an ice contact setting.

3.2.1.2 *Fawnmore (55.1536 N, 8.0329 W)*

Located ~10.5 km east of Altwinny Bay, Fawnmore is a sand and gravel pit that has excavated an ice-marginal terrace at ~ 30 m I.O.D., and has potential to record the step

1
2
3 back of the MSIS eastward along the north coastline of Co. Donegal. Two sections were
4 examined in 2014 (Fig. 4). Section 1, although degraded, was composed of sand, gravel,
5 and fine-grained units dipping to the southeast that were capped by a massive diamicton.
6 The active workings of Section 2 displayed delta fore-set sands and gravels dipping
7 towards the southeast. Original observations at Fawnmore (McCabe, 1995) suggest ice
8 retreat to the south, however the southward delta progradation is more consistent with an
9 ice source to the north. A view supported further by the presence of erratic clasts (e.g.,
10 basalt) sourced up-ice within the MSIS. Consequently, this deposit is interpreted as a delta
11 deposited within a lake dammed by the left-lateral margin of the MSIS to the north. Three
12 OSL samples were collected: T7FAWN01 sampling rippled fine to medium sand with fine
13 laminations from section 1, and from section 2 horizontally stratified fine-medium sands
14 (T7FAWN02) and fining upward couplets of rippled to horizontally laminated fine to medium
15 sand (T7FAWN03). T7FAWN02 and T7FAWN03 were priorities for OSL because these
16 were taken from better exposed sediments that are indicative of deposition as ice proximal
17 delta fore-sets. Both samples yielded broad D_e distributions (Fig. 3D) suggestive of
18 heterogeneous bleaching prior to burial, thus a small proportion of the grains probably
19 characterises the minimum dose population. The OSL ages determined T7FAWN02
20 (Shfd15015) 25.8 ± 4.2 ka and T7FAWN03 (Shfd15168) 27.1 ± 3.7 ka are slightly old relative
21 to the geochronology for adjacent zones. These ages show wide distributions reflective of
22 the poor bleaching of the OSL signal, not unexpected given the relatively short sediment
23 transport distances associated with a small ice proximal delta topset.

31 32 *3.2.1.3 The Armoy moraine*

33 Armoy moraine is a major glacial landform in the north of Ireland and forms a series of
34 interlinked ridges hummocks and kettle-holes that extend discontinuously for 50 km
35 between Articlave and Ballycastle (Figs. 1 inset, 13) (Knight, 2004, Knight, 2008a, Knight,
36 2008b). It is generally agreed that the moraine, given the orientation of its arcuate
37 morphology, marks advance of ice from southwestern Scotland into Northern Ireland, but
38 the timing is not well constrained. The samples collected at Castleroe, Glenshesk Valley
39 and Carey Valley are all distributed along the length of, or immediately down ice from, the
40 moraine. The objective was to constrain the timing of this ice incursion into the north of
41 Ireland.

42 Castleroe (55.0987 N, 6.6363 W): Within the outwash sands and gravels immediately down
43 ice from the Armoy moraine, 4 km southeast of Coleraine and west of the River Bann, a
44 small dormant sand and gravel pit is set within an undulating bench of glacial sediments
45 (Knight, 2004). The sections, when visited in September 2014, showed a fragmentary
46 sequence of what are probably high-energy outwash sands and gravels beneath a massive
47 diamicton containing occasional gravel layers. The sequence is then capped by a unit of
48 clay-silt glaciolacustrine rhythmites containing occasional drop-stones (Fig. 5). Three
49 samples were taken from the middle to lower part of the sequence within the outwash
50 sands and gravels, with T7CAST01 highest in the sequence sampling horizontally stratified
51 coarse sand). Towards the base of a >10 m thick sequence samples of planar cross
52 stratified sands with fine laminations (T7CAST02) and rippled and planar cross set fine to
53
54
55
56
57
58
59
60

1
2
3 coarse sands with fine laminations (T7CAST03) were taken (Fig. 5). All three samples
4 targeted appropriate lithofacies for OSL dating within the lower and middle part of the
5 sequence, but unfortunately sand-rich facies did not feature within the uppermost
6 glaciolacustrine unit.
7
8

9 Both samples yielded broad De distributions with T7CAST02 asymmetric (Fig. 3C)
10 suggestive of heterogeneous bleaching prior to burial, thus a small proportion of the grains
11 characterises the minimum dose population. The OSL age determined for T7CAST01
12 (Shfd15015) is too old at 48.1 ± 4.8 ka and predates a younger sample that was taken from
13 lower in the sequence. T7CAST01 sampled a thin sand unit within high energy gravel
14 outwash lain down potentially in deep channels of back-bar gravel fore-sets, which may
15 have limited the potential for re-setting of the OSL signal. The De distribution for T7CAST02
16 is slightly better behaved with a younger population of aliquots and yielded an age of
17 38.3 ± 3.8 ka. Chronologically 38.3 ± 3.8 ka predates the MSIS advance to the shelf break
18 (Callard, et al., 2018), but the stratigraphical location of these samples beneath 6 m thick
19 diamicts and evidence for deformation of the outwash sediments samples is intriguing.
20 Taken at face value the T7CAST02 (Shfd15168) age of 38.3 ± 3.8 ka may relate to an earlier
21 advance of the ice sheet during the build up towards the LGM. These older
22 glaciofluvial/deltaic sediments at Castleroe were then incorporated within the Armoy
23 Moraine, with ice advance adding the diamict and the uppermost proglacial glaciolacustrine
24 muds as a lake formed between the MSIS and inland 'Irish' ice. The alternative hypothesis
25 is that the Castleroe outwash units are younger and relate to the most recent deglaciation,
26 but where the OSL signals have not been reset for these samples.
27
28
29
30
31
32

33 Glenshesk Valley (55.1447 N, 6.2211 W): East of the Armoy Moraine and 7 km south from
34 Ballycastle, Glenshesk is one of a series of valleys where water ponded when dammed by
35 ice to the west at Armoy and in the north towards the coast at Ballycastle. Within the
36 Glenshesk valley a set of broad and relatively flat drift surfaces occur, which are
37 stratigraphically above glacial features (drumlinized till) associated with Irish ice (Knight,
38 2008a). These drift surfaces are believed to be associated with water flow and damming
39 between Irish and Scottish ice and could only be deposited when Scottish sourced ice
40 formed margins at the Armoy moraine (Knight, 2004). A small gravel pit within one of these
41 surfaces reveals it to be composed of distal glaciofluvial sands and gravels, with the
42 uppermost near-surface sequence showing sands capped by planar cross-stratified
43 gravels. Two samples (T7GLEN01 and T7GLEN02) were collected from units of rippled
44 medium sands (Fig. 6), both yielding asymmetric De distributions (Fig. 3E) suggestive of
45 heterogeneous bleaching and a small minimum dose population. The De distribution for
46 T7GLEN02 (Shfd15170) is better behaved and yields a younger age of 23.6 ± 3.4 ka, with
47 T7GLEN01 (Shfd15017) 30.4 ± 4.2 ka probably too old. Both samples were lain down in
48 similar environments and so the between sample differences in signal resetting probably
49 simply reflect the heterogeneity of bleaching in these environments.
50
51
52
53
54
55

56 Carey Valley 55.1918 N, 6.1555 W: Further east still, the Carey Valley is ~6 km east of
57 Ballycastle and ~2 km inland of the present coastline to the north. Situated down-ice from
58 the most eastern end of the Armoy moraine, the valley contains a set of terraced flat-topped
59
60

1
2
3 surfaces that form a deltaic sequence, which has been subsequently incised. This
4 sequence, which is described by McCabe and Eyles (1988), is composed of two lower
5 diamictons separated by gravelly debris flows. The upper sequence comprises a classic
6 Gilbert-type delta sequence of horizontal fine-grained silty bottom-sets, gently dipping
7 gravel and sand fore-set beds, and planar massive top-set gravels (Fig. 7). These
8 sediments were interpreted to reflect deposition into an open marine setting to the north
9 (McCabe and Eyles, 1988). Given the high elevation of the deposit surface at 113 m above
10 O.D. this seems unlikely and instead we suggest it was deposited within a lake dammed by
11 Scottish ice at the Armoy Moraine near the coast. Two OSL samples were taken from the
12 deltaic sequence, targeting horizontally stratified fine to medium sands in the bottom-set
13 units (T7CARV01) and an upper sample (T7CARV02) from planar cross-stratified sand in
14 the delta fore-sets. Both samples yielded broad and slightly asymmetric De distributions
15 (Fig. 3B) suggestive of heterogeneous bleaching, but contain small minimum dose
16 populations producing similar ages of 22.6 ± 2.4 ka (T7CARV01: Shfd15169) and 22.1 ± 2.4
17 ka (T7CARV02: Shfd15018).
18
19

20 Taken as a group these sites constraining the Armoy Moraine highlight the challenges of
21 dating heterogeneously bleached materials, but the cluster of three OSL ages ranging
22 23.6 ± 3.4 to 22.1 ± 2.4 ka from Glenshesk and Carey Valley are in broad agreement. The
23 OSL ages from Castleroe are interesting, but suboptimal in terms of their stratigraphical
24 position and the youngest of the age measurements may instead constrain the build-up of
25 regional ice to $\sim 38.3 \pm 3.8$ ka. Those sediments were perhaps deposited, and then later
26 ridden over by MSIS ice and incorporated into the Armoy Moraine. Alternatively, given
27 $\sim 38.3 \pm 3.8$ ka predates evidence for ice free conditions in western Scotland (Jardine, et al.,
28 1988), potentially the OSL signal were not reset completely for those samples during the
29 last depositional cycle.
30
31

32 3.2.2 OSL dating sites in the Donegal Mountains and flanking the DBIS

33 3.2.2.1 Lough Nacung (55.0405 N, 8.2132 W)

34 Located in the Donegal Mountains, the Gweedore Valley contains the Clady River which
35 drains these uplands westwards to the coast near Bunbeg (Fig. 1). Immediately
36 downstream of Lough Nacung and south of the Clady River, a large sand and gravel pit has
37 been excavated into dome-shaped low valley-side hillocks at elevations of 93 m (Cullen,
38 2012). The setting is within the mountain interior of Donegal and glacial landforms
39 therein are more likely to relate to the Donegal Ice Dome, though the exit to the valley
40 reaches the coast between the DBIS (T6) and MSIS (T7). The exposures, visited in
41 September 2014, comprised a Gilbert-type deltaic sequence of massive basal gravels,
42 capped by steeply dipping sand- and gravel fore-sets, and capped by planar gravel top-sets
43 (Fig. 8). The sequence has been interpreted by Cullen (2012) as subaqueous fan
44 sediments capped by an ice-distal deltaic sequence. The apparent dip direction of the
45 deltaic fore-sets suggests delta progradation toward the northwest. Deltaic sedimentation
46 was likely within a lake dammed to the north and west by coalesced MSIS and DBIS ice
47 masses and fed by ice sourced to the east in Poisoned Glen, Donegal Mountains. Two
48 samples were collected from units of rippled medium sands (T6LNAC01) and rippled
49
50
51
52
53
54
55
56
57
58
59
60

1
2
3 medium to coarse sands (T6LNAC02) located toward the top of the fore-sets. These
4 samples potentially constrain sedimentation within a lake that could only have existed whilst
5 ice was present to the northwest. Both samples yielded broad De distributions (Fig. 9C)
6 suggestive of heterogeneous bleaching and contain a small minimum dose population.
7 They produced ages of 109.4 ± 8.4 ka (T6LNAC01: Shfd15173) and 132.0 ± 10.5 ka
8 (T6LNAC02: Shfd15014) that though similar do not overlap within uncertainties.
9

10
11 The ages for the Lough Nacung delta are substantially too old relative to the LGM shelf-
12 break maxima for the MSIS and DBIS (Callard, et al., 2018, Peters, et al., 2015, Peters, et
13 al., 2016). The lack of evidence for overriding by ice in the sequence in the form of
14 deformation and disruption of the Gilbert-type delta poses questions about the Donegal ice
15 dome. It seems implausible having ice margins at the shelf break and ice-free enclaves in
16 the Donegal Mountains, and so a more likely explanation is poor resetting of the OSL signal
17 in these uppermost fore-set sands of this ice proximal delta. TCN ages for three glacially
18 transported granite boulders at Poisoned Glen ~8 km up ice from the delta produced a
19 mean age of 16.9 ± 0.7 ka and indicate that the Derryveagh Mountains (north Donegal) were
20 largely deglaciated by ~18–17 ka (Wilson, et al., 2019). The relatively short sediment
21 transport distances implicit in this ice proximal delta lend further support to the poor
22 resetting of the OSL signal.
23
24
25
26
27

28 3.2.2.2 *Glenulra (54.3023 N, 9.4330 W)*

29
30 Located near the coast on the southern flanks of Donegal Bay, the exposures at Glenulra
31 are a small aggregate pit and natural river-cut exposures in part incised probably by glacial
32 meltwater. The exposures show a sequence cut into an ice contact delta with a surface at
33 80 m I.O.D. (Ballantyne and Ó Cofaigh, 2017, Hallissy, 1911, Hinch, 1913, McCabe, et al.,
34 2007a). The sediments at Glenulra Quarry and Farm are an important site for the evolution
35 of the Irish Ice Sheet, though the glaciological interpretation of the sequence and the
36 chronology is equivocal (Ballantyne and Ó Cofaigh, 2017, McCabe, et al., 2007a). McCabe,
37 et al. (2007a) described a sequence of basal high density gravelly flows, ~ 16 m of bedded
38 muddy fine-grained units and sands, overlain by 5 m of dipping gravelly delta fore-sets
39 prograding northwards onshore to offshore and capped by planar massive gravel delta top-
40 set (Fig. 10). Marine fauna occur throughout, and have been ^{14}C dated by analysing
41 mixture of reworked *Arctica islandica* shells from the basal gravels and gravel delta top-set,
42 and *in situ* monospecific *Elphidium clavatum* from muds interpreted as glaciomarine in
43 origin (McCabe, et al., 2007a).
44
45
46
47
48

49 Reconstructions of regional ice flows affecting the Glenulra area show ice generated in the
50 mountains in the southern part of Co. Mayo extended north to Donegal Bay (Greenwood
51 and Clark, 2009a, Greenwood and Clark, 2009b, Synge, 1963, Synge, 1965). Offshore in
52 Donegal Bay, mapping of submarine landforms affirm the extension of ice northwards from
53 land offshore including a late stage set of moraines extending from Killala Bay 20 km east
54 of Glenulra (Fig. 14) (Ó'Cofaigh, et al., 2012), but moraines with geometries reflecting ice
55 extending westwards from the Irish Midlands to the continental shelf break dominate and
56 suggest that the DBIS came close to or impinged on the north coast of Mayo (Ó'Cofaigh, et
57 al., 2012). McCabe, et al. (2007a) interpreted the Glenulra ^{14}C ages as reflecting high
58
59
60

1
2
3 relative sea levels from 26 to 45 ka, perhaps discontinuously, but implying substantial
4 isostatic depression. That would require the proximity and some persistence of a thick ice
5 sheet for a significant period before the LGM. Fifteen ^{14}C ages have been obtained for the
6 sequence, with the ages ranging from 21.1 ± 0.2 to 39.5 ± 0.5 ^{14}C ka BP. The eleven ages
7 for reworked *Arctica islandica* shells can only provide maximal constraint on the sequence
8 and the ages may predate reworking by millennia. Ballantyne and Ó Cofaigh (2017)
9 summarise an alternative view that ice cover in Ireland was limited before 32 ka supported
10 by ^{14}C dating of organic and faunal remains from various sites. Were the *Arctica islandica*
11 shells found at Glenulra reworked from the sea floor in Donegal Bay, those ^{14}C ages imply
12 ice-free conditions in those waters prior to any build-up of land-based ice and advance to
13 shelf-break glaciation 27.8–27.6 ka (Ballantyne and Ó Cofaigh, 2017). The four ^{14}C ages for
14 monospecific *Elphidium clavatum* from Glenulra form a tighter cluster spanning 23.7 ± 0.1
15 to 21.1 ± 0.2 ^{14}C ka BP and include the youngest ^{14}C age in the sequence. The ages for
16 these foraminifera, if in situ, suggest also significant isostatic depression and proximity to a
17 thick ice sheet 27.8–25.3 cal ka BP (McCabe, et al., 2007a). Given the timing for shelf-
18 break glaciation presented here, the Glenulra ^{14}C ages suggest either i) the site was not run
19 over by ice during the LGM advance requiring an implausibly thin DBIS, ii) there was
20 preservation of the Glenulra deposits under the ice sheet, and iii) that all the ^{14}C ages are
21 from reworked marine fauna and only provide maximal ages for the deposits (Ballantyne
22 and Ó Cofaigh, 2017). The third scenario potentially still requires high relative sea levels
23 (80 m OD) after 25.3 cal ka BP during deglaciation assuming the deposits are glaciomarine
24 (Ballantyne and Ó Cofaigh, 2017), although a niche glaciolacustrine setting is an alternative
25 hypothesis forming between the DBIS and local ice thereby receiving reworked glaciomarine
26 fauna. Regional striae patterns on the north Mayo coast (Smith, et al., 2008) point to the
27 deflection of ice feeding the DBIS via Bunatrahair and Killala Bays towards the west and
28 northwest.

29
30
31 To address some of these palaeoenvironmental and geochronological uncertainties, this
32 key site was revisited to apply OSL dating to the uppermost deltaic sediments. In November
33 2014, the upper Glenulra Quarry (54.3023 N, 9.4330 W) sequence displayed the uppermost
34 3 m comprising a thin diamicton beneath gently dipping sand and gravel fore-sets that were
35 in turn capped by a planar geometry gravelly delta top-set (Fig. 10). The exposures were
36 restricted with talus and the patchy nature of aggregate extraction, but the dip to the
37 uppermost fore-sets appeared to vary from a W to SW which differs to McCabe, et al.
38 (2007a) who recorded a northerly dip to the fore-sets. A summary conclusion might be that
39 the sediment efflux direction was variable, which supported in Geological Survey Ireland
40 mapping showing a north-flowing down valley meltwater input, but also coast parallel west
41 flowing meltwater channels feeding towards the Glenulra delta (Meehan, 2013). A DBIS
42 origin to the sediment efflux provides a mechanism for the reworking of marine fauna. Two
43 samples (T6GULR01, T6GULR02) were collected for OSL dating from rippled medium to
44 fine sands with fine laminations. These sampled units are located from the top of the
45 sequence within the gravelly topsets. Both samples constrain potentially sedimentation
46 within either a small ice marginal lake or proglacial glaciomarine delta flanking Donegal
47 Bay, with two OSL ages that overlap within uncertainties at 25.2 ± 1.9 ka (T6GULR01:
48
49
50
51
52
53
54
55
56
57
58
59
60

1
2
3 Shfd15172) and 24.1 ± 1.9 ka (T6GULR02: Shfd15012). Both samples yielded asymmetric
4 De distributions (Fig. 9B) suggestive of heterogeneous bleaching, contain a small minimum
5 dose population and are probably maximal ages for the delta. The youngest of these,
6 24.1 ± 1.9 ka, slightly post-dates though overlaps within uncertainties the youngest of the
7 Glenulra ^{14}C ages at 25.4 ± 0.3 cal ka BP. Regardless, all the chronology from Glenulra is
8 old relative to the DBIS retreat sequence, and we favour an interpretation that the fauna is
9 ostensibly reworked, and that the delta developed as a niche lake ponded between DBIS
10 and inland Irish ice with an active delta topset $\sim 24.1 \pm 1.9$ ka (T6GULR02: Shfd15012).

14 3.2.2.3 Brockhill (54.2782 N, 9.3964 W)

16 McCabe, et al. (1986) described an extensive area of glaciofluvial outwash deposits west of
17 the drumlins in the low ground feeding towards Bunatrahir Bay. Located ~ 8 km southeast
18 from Glenulra and ~ 3 km inland of the present coast, the aggregate pit at Brockhill is
19 excavated into a flat drift surface that appears to form an ice-contact delta with an ice
20 margin located to the south. McCabe, et al. (1986) encountered in >20 m of vertical
21 thickness of deposit with a basal 6-7 m comprising horizontally bedded and rippled sands
22 delta toe-sets, ~ 13 m of massive to normally-graded matrix-supported gravel giving way to
23 planar cross-bed sands, a delta fore-set unit, dipping broadly north, and the sequence is
24 capped by ~ 1 -2m of planar cobble and pebbly top-set gravels. In November 2014, at the
25 time of sampling, only the upper half of the sequence was exposed showing sandy delta
26 fore-sets capped by gravel delta topsets. Two samples were collected from the middle
27 (T6BROC01) and top (T6BROC02) of the sandy fore-sets (Fig. 11). Both samples were
28 collected from units of rippled fine to medium sands, with the aim of constraining the
29 unzipping of ice retreating inland into Co. Mayo. Both samples yielded asymmetric De
30 distributions (Fig. 9A) suggestive of heterogeneous bleaching, contain a small minimum
31 dose population and produced ages of 44.4 ± 4.1 ka (T6BROC01: Shfd15171) and paired
32 small aliquot and single grain (SG) measurements for the second sample of 39.1 ± 3.8 ka
33 (T6BROC02: Shfd15013) and 45.8 ± 8.2 ka (T6BROC02: Shfd15013-SG). There is no real
34 evidence for subsequent overriding by ice, and so the most likely explanation is poor
35 resetting of the OSL signal given the relatively short sediment transport distances implicit in
36 this ice proximal delta.
37
38
39
40
41
42
43
44
45
46

47 3.3 SYNTHESIS OF PUBLISHED ONSHORE AGES

48 The Bayesian age modelling uses the new geochronological data obtained during the
49 BRITICE-CHRONO project (Table 4) and already published (Schiele, 2017, Small, et al.,
50 2017a, Wilson, et al., 2019), alongside clusters of previously published geochronological
51 information at several onshore locations in Scotland and Ireland (Tables 5 and 6). These
52 are predominantly TCN ages (Table 5) but include some radiocarbon ages from various
53 organic material recovered in mostly glaciomarine sediments in coastal proximal settings
54 (Table 6).
55
56
57

58 Legacy TCN research from before BRITICE-CHRONO includes the Bloody Foreland
59 moraine and other sites in the Donegal and Ox mountains (Ballantyne, et al., 2007,
60

1
2
3 Ballantyne and Ó Cofaigh, 2017, Clark, et al., 2009a). In Hebridean ice feeders towards the
4 MSIS, other ages come from Arran, South Uist (Ballantyne and Small, 2018, Finlayson, et
5 al., 2014, Small, et al., 2016, Stone and Ballantyne, 2006). BRITICE-CHRONO conducted a
6 program of sampling at 12 suitable locations distributed across the two transects aiming to
7 fill in gaps in the existing datasets or resolve issues with the previous dating (Fig. 1 for
8 locations). Small, et al. (2017a) presented 17 ^{10}Be exposure ages from glacial boulders and
9 bedrock at sites across western Scotland within the area drained by the MSIS. These TCN
10 ages include measurements on Tiree, Mull, Jura, Mingulay and Barra. Wilson, et al. (2019)
11 presented 20 new ^{10}Be and ^{36}Cl surface exposure ages from six sites in Donegal, including
12 Malin Head, Rosguill, and Poisoned Glen in northern Donegal and Glencolumbkille, Kilcar
13 and Blue Stacks Mountains in southern Donegal, and Schiele (2017) worked on 4 ^{10}Be
14 samples from Ben Bulbin in Co. Sligo. Some TCN samples at the boundary between the
15 two transects have used for ensuing Bayesian modelling in both transects (Table 7).
16
17
18
19
20

21 Overall, all these ages provide evidence of the timing of the BIIS first landfall across the
22 Malin Sea and ensuing retreat further inland ultimately towards isolated mountain glaciers.
23 Sites around the coastline of Donegal (including Malin Head, Bloody Foreland, Aran Island,
24 Belderg Pier and Fiddauntawnanoneen; Tables 5-6) indicate that the ice margin around
25 20.5 ka, was at the Donegal and north Mayo coasts. In Scotland, ice landfall occurred first
26 at Tiree at around the same time (20.6 ± 1.2 ka) and slightly later in Mingulay (18.9 ± 1.0 ka)
27 on the Outer Hebrides. The TCN age at Malin Head were used alongside ^{14}C chronology
28 from Corvish to suggest an early separation of Scottish-sourced ice and Donegal-sourced
29 ice by ~ 20.7 ka (Wilson, et al., 2019). This implied that by this time a marine embayment
30 extended eastward along the north coast of Donegal, separating ice flowing north and
31 northeast from the Donegal Ice Centre from the retreating MSIS. The northern mountains of
32 Donegal (Poisoned Glen and Errigal Col) were largely deglaciated by ~ 18 -17 ka (Wilson, et
33 al., 2019). By 17.5-16.5 ka the ice margin straddled the fjords, islands and peninsulas of
34 the western seaboard of Scotland, and the Outer Hebrides Ice Cap had shrunk to expose
35 most of the southern Outer Hebridean islands (Small, et al., 2017a). In north Co. Mayo, the
36 five younger ^{10}Be exposure ages from glacially transported boulders within the moraine
37 system on the northern slopes of the Ox Mountains (Table 5) indicate that ice persisted in
38 much or all Donegal Bay and covered south-west Donegal as late as 17 ka. By ~ 15.0 ka
39 the Donegal Ice Centre had shrunk to a small ice cap or ice field of very limited extent on
40 the Blue Stack Mountains (Wilson, et al., 2019).
41
42
43
44
45
46
47
48
49

50 3.4 BAYESIAN MODELS

51
52 Bayesian age modelling of all the dating control for both transects has calculated the timing
53 for the advance and retreat of the DBIS and the MSIS (Figs. 12-14, 16; Table 7). Additional
54 coastal and inland sites with organic remains dated to before the LGM and after
55 deglaciation in both Scotland and Ireland were used to identify ice free conditions before
56 and after the last glacial advance and are discussed in the next section in the context of the
57 Bayesian models (Table 6). Ultimately both Bayesian analyses produced conformable age
58 models with an overall agreement indices of 188% for the DBIS and 119% for the MSIS,
59
60

1
2
3 both exceeding the >60 % threshold advocated by Bronk Ramsey (2009a). Iterative cycles
4 of the Bayesian modelling varying the outlier probabilities led to the identification of the
5 outlier ages shown on Fig. 12. Italics from now on denote the posterior density estimates or
6 modelled ages derived from the Bayesian modelling to distinguish them from the
7 unmodelled individual ages obtained for samples directly-dated.
8
9

10 3.4.1 Malin Sea Ice Stream

11
12 Basal constraint on the retreat model for the MSIS is provided by radiocarbon ages
13 obtained for faunal remains and organic deposits in western Scotland denoting ice free
14 conditions before the advances to LGM limits (Bos, et al., 2004, Brown, et al., 2007,
15 Jardine, et al., 1988). At Sourlie on the Ayrshire coast (Fig. 13) in the inner feeder zone of
16 the MSIS (Finlayson, et al., 2014, Finlayson, et al., 2010), organic pockets of sediment in
17 cold-stage fluvial sediments between two glacial diamicts yielded antler of *Rangifer*
18 *tarandus* with the collagen extract dated to $29,900 \pm 420$ BP (SRR-3023) and plant debris
19 dated to $29,290 \pm 350$ BP (SRR-3146) (Bos, et al., 2004, Jardine, et al., 1988). Support for
20 ice free conditions in the hinterland of the MSIS is provided further east in central Scotland
21 by equivalent organic-rich sediments at Balglass Burn, north of Glasgow (Brown, et al.,
22 2007) spanning 39.8 – 32.8 ka BP. The Bayesian modelling (Fig. 12A) has produced
23 modelled age probability distributions for ice dynamics in the MSIS sector. Organic sites in
24 western Scotland show ice free conditions around 34.4 ± 1.8 ka and provide maximum
25 constraint on the build-up and extension of ice into the Malin Sea. In zone 1, on the outer
26 shelf, the youngest ^{14}C ages on shells reworked into over consolidated diamicts (Callard, et
27 al., 2018) constrain shelf break glaciation to 27.9 ± 2.2 ka (BL0), before marine fauna in the
28 softer overlying glacial marine diamict indicated rapid retreat to the zone 2 moraines by $26.3 \pm$
29 0.3 ka (BL1; Fig. 13).
30
31

32
33 Decline of ice in the more open Malin Sea proceeded with an ice margin >120 km wide
34 retreating east reaching BL2 at 23.5 ± 0.3 , BL3 at 22 ± 0.3 and BL4 at 21.2 ± 0.5 ka (Fig.
35 13). Deglaciation of zone 2 vacated the Malin Deep (> -150 m) and the outer portion of the
36 Hebrides Trough (> -150 m) to establish a series of grounding zone wedges and the BL2
37 ice margin east and landward of Stanton Banks. Glacial marine sediments in front of BL2
38 yielded basal ^{14}C ages ranging 23.2 ± 0.3 to 22.1 ± 0.3 ka BP and denote ice-free
39 conditions on the inner Malin shelf by 23.5 ± 0.3 ka (BL2). The constraint on BL3 is
40 provided by TCN and OSL ages from northwest Donegal, with boulders on the Bloody
41 Foreland and Malin Head peninsulas forming a coherent grouping. Two of the Bloody
42 Foreland granite boulder ages were treated as outliers leaving seven consistent TCN ages.
43 The OSL age from Altwinny Bay, notwithstanding the substantial uncertainty, is an outlier in
44 this grouping, and the age of 30.4 ± 4.9 ka (T7ALTB02) is intriguing given that the sand unit
45 sampled was beneath thick diamict units, which reflects later over-riding by ice. It is feasible
46 that the thin outwash predates ice advance and may be better positioned in zone 1 of the
47 Bayesian sequence model. The deltaic deposits at Fawnmore, though on the face of it a
48 little old, are given the wide uncertainties conformable with the Bayesian model. Together,
49 these ages constrain zone 3 ice margin retreat to BL3 by 22 ± 0.3 ka. BL4 is constrained by
50 TCN ages from Tiree (inner Hebrides) and OSL ages from outwash draining into lakes
51
52
53
54
55
56
57
58
59
60

1
2
3 ponded by Scottish ice impinging on the lowlands of the north of Ireland broadly at the
4 Armoy Moraine (Knight, 2004, Knight, 2008a). Evidence of ice-free conditions from zone
5 4/5 marine core (149VC) is provided by a shell fragment in a soft diamicton dated to $20.2 \pm$
6 0.2 cal. ka BP (Callard, et al., 2018). These ages constrain BL4 at 21.2 ± 0.5 ka (Fig. 13).

7
8
9 BL5 at 20 ± 0.3 ka and BL6 at 19.5 ± 0.3 ka (Fig. 13) describe the MSIS dividing into
10 increasingly separate lobes with the ice margin in the Sea of Hebrides entering the fjord
11 landscape of western Scotland and further south, Scottish ice extended across the North
12 Channel impinging on the lowlands north of Ireland. The cluster of TCN ages from Rosguill
13 document the retreat of ice margins from the outer headlands of the north of Ireland into the
14 mountains of Donegal (Wilson, et al., 2019), and across the Malin Sea, TCN measurements
15 from Mingulay (southern Outer Hebrides) (Small, et al., 2017a) are very similar in age. In
16 the Bayesian model, the Rosguill and Mingulay clusters are conformable as a single
17 grouping, though the overall model performance is better with Rosguill before Mingulay.
18 The pragmatic interpretation is that the BL5 to BL6 limits were established between $20 \pm$
19 0.3 ka and BL6 at 19.5 ± 0.3 ka (Fig. 13). Boundary limits documenting the step back of
20 increasingly separated ice lobes into the fjords of western Scotland and into the mountains
21 of Donegal integrates evidence distributed across the Malin Sea. BL7 at 19 ± 0.3 ka is
22 constrained between TCN ages in the southern Outer Hebrides (Mingulay), and ^{14}C dated
23 evidence of ice-free conditions at Corvish (Donegal) (McCabe and Clark, 2003). There is
24 strong geographical spread to the age constraint on BL8 at 18.1 ± 0.7 ka and BL9 at $14.9 \pm$
25 1.5 ka (Fig. 13), and this is supported by an array of dated TCN sites on Mull, Jura, North
26 Barra and Arran. The three ages treated as outliers within zone 9 were two TCN ages from
27 Jura that Ballantyne, et al. (2014) had previously interpreted as too young owing to the
28 probable burial of the boulders under a former cover of sediment and/or peat. Three more
29 TCN ages obtained more recently from Jura included a further slightly young age (S3-Jura)
30 (Small, et al., 2017a) and was also handled as an outlier. Together four of Jura TCN ages
31 form a coherent set within the Bayesian model. Ultimate deglaciation of the western
32 Scottish Highlands occurred by 14.3 ± 1.8 ka (BL10) (Fig. 13).

3.4.2 Donegal Bay Ice Stream

33
34
35
36
37
38
39
40
41
42
43
44
45
46
47
48
49
50
51
52
53
54
55
56
57
58
59
60
There are fewer locations in the hinterland of the DBIS that constrain ice free conditions
predating MIS 2 advances, though Colhoun, et al. (1972) described organic freshwater silts
and fine sands at Derryvree (Co Fermanagh; Fig. 14) that nestled between two thick
diamict sheets from a road-cut exposure of a drumlin (54.3031 N, 7.4411 W). The
Derryvree cold stage organic deposits yielded an age of 30.5 ± 1.1 ^{14}C ka BP (Birm-166)
and indicate ice free conditions (Colhoun, et al., 1972). Bayesian modelling indicates a
maximum constraint on the build-up and extension of ice into Donegal Bay at 35.1 ± 3.2 ka
(pre-LGM ice free conditions; Figs. 12B; 14), in a similar age range to the western coastline
of Scotland, further to the north (Bos, et al., 2004, Jardine, et al., 1988).

In zone 1 (Fig. 14), on the outer shelf, the youngest ^{14}C ages on shells reworked into over
consolidated diamicts constrain shelf break glaciation to 26.6 ± 1.3 ka (BL0) and the
establishment of the shelf break moraine (BL1) at 26.3 ± 0.1 ka (BL1). In zone 2, moving
landwards, a series of ^{14}C ages from glacial marine muds constrain ice free conditions in the

1
2
3 outer Donegal Bay across a series of arcuate sea floor moraines. These ^{14}C ages with the
4 more landwards zone 3 chronology constrains BL2 to $22.9 \pm 0.7 \text{ ka}$. Zone 3 contains a
5 series of nine ^{10}Be ages from Bloody Foreland (Clark, et al., 2009a, Wilson, et al., 2019)
6 and two from Aran Island (Cullen, 2012, Wilson, et al., 2019) both in northwest Donegal.
7 The location of these sites is marginal to both the DBIS and MSIS, and probably developed
8 a suture between the two ice-masses with ice margin retreat. Two of the Bloody Foreland
9 ages plot too young and were handled as outliers, with all the others forming a coherent
10 grouping. These sites constrain deglaciation of the outer headlands and islands of
11 northwest Donegal and correlate with BL3 ice margins in Donegal Bay to $20.5 \pm 0.3 \text{ ka}$ (Fig.
12 14). Zone 4 comprises dating of ice-free conditions moving further east into Donegal Bay
13 and a series of marine fauna ^{14}C dated on the north coast of County Mayo. Our attempt to
14 date the uppermost deltaic deposits by OSL dating logically form part of this cluster but
15 form a clear 'too old' outlier in the Bayesian model. The zone 4 chronology and bracketing
16 ages in zone 5, constrain the BL4 limit to $19 \pm 0.4 \text{ ka}$. Interestingly, the modelling combines
17 together ^{14}C ages from the Donegal Bay moraine complex and the Killala Bay moraines,
18 thus suggesting that they are not statistically differentiated and therefore part of a single
19 phase of the ice margin. Within this phase, it is possible that the Killala Bay moraines
20 represent a rapid and short-lived advance of an ice tongue from the north Mayo coast due
21 to de-buttressing of northward-flowing ice caused by retreat of the DBIS.
22
23
24
25
26
27
28

29 Zones 5-7 record the stepping back of ice margins from Donegal Bay into the flanking
30 mountain regions in counties Donegal, Mayo, and Sligo. Zone 5 integrates dating
31 information from typically the coastal fringe around the mountains of Donegal and includes
32 six locations yielding eighteen TCN ages. These form a coherent grouping in the Bayesian
33 model, with three of four ^{36}Cl ages from Kilcar too old and probably compromised by
34 nuclide inheritance though the fourth age is consistent within that grouping. Elsewhere, one
35 of three ^{10}Be ages from Poisoned Glen, north Donegal, appears too young and one of five
36 ^{10}Be ages from Glencolumbkille, southwest Donegal (MAL-05: Ballantyne, et al., 2007,
37 Wilson, et al., 2019). Together, these thirteen ages form a conformable group and constrain
38 retreat of ice margins on-land into the mountains of Donegal by $16.8 \pm 0.5 \text{ ka}$ (BL5). In zone
39 6, eight ^{10}Be ages came from the northern Ox Mountains, south of Donegal Bay, and were
40 published originally by Clark, et al. (2009a). Later authors have rationalised the division of
41 the ages into two clusters regarding the five younger ages (mean $16.6 \pm 0.6 \text{ ka}$) as better
42 constraint on deglaciation, with the older cluster affected by nuclide inheritance (Ballantyne
43 and Ó Cofaigh, 2017, Wilson, et al., 2019). These five ages form a conformable grouping
44 and constrain retreat of ice margins further inland to the Ox Mountains and BL6 by $15.3 \pm$
45 0.6 ka . Deglaciation of zone 7 of the DBIS is constrained by TCN ages from Eglish Valley in
46 the Blue Stack Mountains and Binn Ghulbain (Ben Bulbin) in County Sligo. These TCN
47 ages form a broadly conformable set, with two of the Eglish Valley ages and two of Binn
48 Ghulbain ages handled as outliers. In total, four TCN from the two localities indicate that by
49 $13.9 \pm 0.4 \text{ ka}$ (BL7) the mountains of the inner DBIS had deglaciated (Fig. 14).
50
51
52
53
54
55
56
57
58
59
60

4. DISCUSSION

The seafloor geomorphology (Benetti, et al., 2010, Bradwell, et al., 2008, Callard, et al., 2018, Dove, et al., 2015, Dunlop, et al., 2010, Howe, et al., 2012, Ó Cofaigh, et al., 2012, Ó Cofaigh, et al., 2019) and terrestrial landforms in western Scotland, the north of Ireland and around Donegal Bay suggest the presence of former ice streaming across both the Malin Shelf and Donegal Bay (Clark, et al., 2012, Finlayson, et al., 2014, Finlayson, et al., 2010, Greenwood and Clark, 2009a, Greenwood and Clark, 2009b, McCabe, 2008). However, these two adjoining sectors of the former BIIS display clearly different characteristics and rates of retreat during the last glaciation and deglacial period (Figs. 13-16).

The MSIS had a wide ice margin (120 km; Fig. 13) that remained so as the ice retreated across the shelf. The shelf topography is characterised by pronounced areas of deeper water, with normal and adverse slopes corresponding to the major seabed troughs, including the Malin Deep and extensions of the Hebrides Trough (Fig. 16), both separated by the Stanton Banks bedrock high (Lewisian Gneiss) (Dobson and Whittington, 1992). The geomorphological features associated with ice margin retreat across this outer to mid shelf topography are complex systems of GZWs, while moraines and much smaller GZWs are found mostly in the inner shelf and close to the coastline and are much smaller in size (Callard, et al., 2018, Dove, et al., 2015, Dunlop, et al., 2010, Howe, et al., 2012). Conversely, the DBIS was less wide (ca 80 km) decreasing in width as the ice margin retreated landward and had a very gently normal-sloped bed (only the innermost part of the bay displays an adverse slope) and a distinct pattern of closely-spaced recessional moraines across the shelf (Benetti, et al., 2010, Ó Cofaigh, et al., 2019). Some lateral moraines (Fig. 14) exist in a position that suggest the presence of a distinct small ice lobe extending northwards into the bay at some stage during deglaciation (Benetti, et al., 2010, Ó Cofaigh, et al., 2019).

From ice free conditions in the hinterlands of the MSIS and DBIS ~33 ka (Colhoun, et al., 1972, Jardine, et al., 1988), glacial landforms and the presence of radiocarbon dated subglacial diamicts at the shelf edge show that between 28 and 26.5 ka the BIIS had grown to its maximum extent with ice grounded to the shelf edge (Fig. 16). Evidence across the continental shelf of the western BIIS suggests that this ice margin extended also north and south of the Malin Sea, following predominantly the shelf edge at 140 to 150 m (current) water depth from Northern Scotland to northern Porcupine Bank, with coalescing ice from Scotland and Ireland (Benetti, et al., 2010, Bradwell, et al., This volume, Ó Cofaigh, et al., This volume, Schiele, 2017). This recognition that the BIIS extended to the edge of the Malin Shelf led Wilson, et al. (2019) to suggest that the Donegal ice dome was of sufficient thickness to have buried all mountain summits. This hypothesis is supported by thermo-mechanical models of ice-sheet build-up and decay driven by proxy climate data (Hubbard, et al., 2009a) which predict thick cold-based ice over many summits. There is further support for these ice thicknesses elsewhere in Ireland (Ballantyne, et al., 2011, Ballantyne and Ó Cofaigh, 2017, Ballantyne and Small, 2018, Ballantyne and Stone, 2015), and demonstrations that the last ice sheet overtopped all mountain summits in northwest Scotland (Ballantyne and Small, 2018, Fabel, et al., 2012). This build-up of ice, from

1
2
3 Greenland Stadial (GS) 4 into the beginning of GS-3, occurs relatively early within the
4 context of the global LGM and predated the maximum in global ice volume (Fig. 15).
5 Variations in SST across the North Atlantic Ocean and variations in air temperature prior to
6 the global LGM may indicate that changes in ocean and atmospheric circulation patterns
7 that could have resulted in an increase in atmospheric moisture transport from the Equator
8 to the Poles that is concomitant with a cooling at the northern latitudes favouring the
9 accumulation of snow and ice (Clark, et al., 2009b, Hughes and Gibbard, 2015, Hughes, et
10 al., 2013, Khodri, et al., 2001, Lambeck, et al., 2014). In the Malin Sea, shelf edge
11 glaciation appears to be relatively short-lived. By 26.5 ka the ice sheet had already started
12 to retreat from the shelf edge and extensive iceberg scouring at the shelf edge across the
13 entire margin of the Malin Sea indicates that it happened initially through intense calving.
14 This is also prior to the global LGM and occurred during cold conditions of GS-3. It is
15 possible, as suggested by Ó Cofaigh, et al. (2019) and Callard, et al. (2018), that this early
16 retreat was related to the growth of the BIIS and driven by local ice loading increasing water
17 depths and promoting calving ice loss rather than by any changes in oceanic and
18 atmospheric temperatures. This early retreat coincides with the timing of Heinrich event 2
19 and the increased flux of BIIS sourced IRD to the Donegal-Barra Fan at both MD04-2822
20 (Hibbert, et al., 2009) and MD05-2006 (Knutz, et al., 2001, Knutz, et al., 2002) (Fig. 15D).

27 After the maximum extension in Donegal Bay ~26.6 ka, the retreat and pullback of the DBIS
28 margins across the outer shelf was occurring at a rate of ca. 20 m a⁻¹. Subsequently, we
29 observe a clear pattern of episodic retreat and then stabilisations of the ice margin each
30 marked by a morainic ridge on the shelf; more than 25 such moraines can be counted
31 across the Donegal Bay shelf and even more are visible in sub-surface geophysical data
32 (Benetti, et al., 2010, Ó Cofaigh, et al., 2019). For the Malin Shelf in contrast an extensive
33 GZW complex (zone 2: Fig. 13) is observed on the outer shelf for the entire width of the ice
34 stream margin (Callard, et al., 2018). This outer portion of the MSIS displays one of the
35 lower rates in retreat for the MSIS (18.7 m a⁻¹; Fig. 15B), and this is smaller than the retreat
36 rate for the corresponding zone of the DBIS (Fig. 15A). The timing of formation of the
37 GZWs in this zone is consistent with the reconstructed 600 to 1500 years for the deposition
38 of GZWs during ice stream retreat in Antarctica prior to the Holocene (paleo-Pine Island ice
39 stream) (Jakobsson, et al., 2012). After the initial retreat from the shelf edge, there is a
40 switch in the relative magnitude of retreat rates and in the MSIS they are five to ten times
41 faster than the DBIS (Fig. 15A vs. 15B). This could be related to the shape of the underlying
42 bed. The Malin Shelf displays a clear reverse-sloping bed into the Malin Deep and
43 Hebridean Trough (zones 3 and 5: Fig. 13), where we observe retreat rates of ~25-29 m a⁻¹,
44 that could have contributed to an accelerated ice loss compared to the much more gently
45 inclined DBIS bed (Fig. 15A). When grounding lines retreat onto reverse-sloped beds
46 theoretical and numerical models predict that instability of the ice margin can be triggered
47 by increases in ice thickness at the grounding line, which in turns favours an increase in ice
48 flow across it. This mechanism, termed marine ice-sheet instability (MISI), has been
49 advocated in explanations of the dynamics of many West Antarctic outlets (DeConto and
50 Pollard, 2016, Favier, et al., 2014, Schoof, 2007). Whether the water depths are sufficient
51 for MISI to have occurred in the Malin Sea remains to be tested. Overall, the rates of retreat
52
53
54
55
56
57
58
59
60

1
2
3 across the margin at this time appear to be between 1.5 and 10 times slower than those of
4 other ice streams of the former BIIS, Laurentide Ice Sheet, Fennoscandian Ice Sheet, and
5 for Greenland Ice Sheet (Hughes, et al., 2012, Scourse, et al., This volume, Stokes, et al.,
6 2014, Winsborrow, et al., 2010).
7
8

9 Foraminiferal and sedimentological data developed for the sector suggest that glaciomarine
10 conditions prevailed during ice margin retreat across the Malin Shelf (Callard, et al., 2018).
11 Across the entire ice front there is a distinct reduction in retreat rates once the margins
12 reached constrictions in width at the headlands and islands of Donegal and Scotland; this is
13 particularly the case in the mid-Malin Shelf (10 m a^{-1} in zone 4; Fig. 13) and outer Donegal
14 Bay ($2\text{-}5.4 \text{ m a}^{-1}$ in zones 3/4; Fig. 14). Within this area, the Donegal Bay Moraine (zone 4;
15 Fig 14) represents a major stillstand at 20.5 - 19 ka. The assessment here of ages
16 developed for the Donegal Bay and Killala Bay moraines cannot be differentiated
17 statistically (Fig. 12B) to distinguish the Killala Bay moraines as a temporally distinct
18 readvance as previously suggested (Ó'Cofaigh, et al., 2012, Ó Cofaigh, et al., 2019).
19 Instead, it is likely that all the moraines mapped within zone 4 (Fig. 14) were the product of
20 oscillating ice positions from different source areas around Donegal Bay and formed around
21 the same time. It appears likely that the Donegal and Mayo headlands and underlying
22 bedrock highs visible in the sub-bottom data (Benetti, et al., 2010, Schiele, 2017) acted as
23 shallow and constricted pinning points during the retreat thus slowing ice loss (Favier, et al.,
24 2012) and favouring the formation of this moraine complex, at this time fed by entirely Irish-
25 based ice, now a separate Donegal Ice Dome. In attempting to resolve the temporal
26 linkages between MSIS and DBIS we highlight a less well resolved region between Malin
27 Beg and Bloody Foreland, which occupies both the developing suture between the two ice
28 streams during their respective maximum and later retreat. This sector is rendered even
29 more complex by the growing influence of the ice dome over the Donegal mountains on the
30 geomorphology. The exact timing of the separation of Scottish and Irish Ice in the Malin
31 Sea is resolved for the first time here by the MSIS Bayesian model, which brackets it
32 between 20 and 19.5 ka (Figs. 13; 16). Thus, separation of Scottish and Irish Ice in the
33 Malin Sea occurs quite early during deglaciation, a feature not present in previous
34 reconstructions; (see DATED: Hughes, et al., 2016). This timing of 20-19.5 ka coincides
35 with equivalent data from the north Irish Sea basin showing the pullback of ice on land in
36 northeast Ireland (Ballantyne and Ó Cofaigh, 2017, Chiverrell, et al., 2018, McCabe, 2008,
37 McCabe, et al., 2007b). Here we show the reduced contributions of ice from the North
38 Channel into the Irish Sea, which accords with evidence for an ice-free western Irish Sea
39 and the margins of the Irish Sea Ice-stream positioned to the north of the Isle of Man
40 receiving flows solely from SW Scotland (Galloway Hills Ice Dome) and the English Lake
41 District by 20-19 ka (Chiverrell, et al., 2018, Scourse, et al., This volume). Ice persisted
42 longer over Donegal Bay than on the Malin Shelf. Compared to the DBIS sector, the ice
43 margin of the MSIS was still straddling the entire width of the Malin Shelf, through a series
44 of deep troughs and smaller headlands (Fig. 13). By 20 ka, Tiree was already seaward of
45 the ice margin, but the remainder of the Inner and Outer Hebrides were still glaciated.
46 Rapid retreat in the Minch Trough between 20 – 18.5 ka and the drawdown of ice lead to
47 Hebridean ice masses becoming glaciologically independent shortly before ~18.5 ka
48
49
50
51
52
53
54
55
56
57
58
59
60

1
2
3 (Bradwell, et al., This volume) and leading to the development of a separate Outer Hebrides
4 Ice Dome (Small, et al., 2017a). A differential pattern of retreat developed to the northeast
5 and southeast once the separation of MSIS and DBIS initiated, and the Outer Hebrides Ice
6 Dome became independent. Seismic and bathymetric data behind Stanton Bank show a
7 stepped retreat to the southeast between Tiree and Mull (Callard, et al., 2018) but that is
8 not resolved in terms of timing by the BRITICE-CHRONO sampling.
9

10
11 Around 20 to 18.5 ka, the retreat of the MSIS was proceeding at a slightly slower pace of
12 $\sim 20 \text{ m a}^{-1}$ compared to earlier retreat, and which may reflect stabilisation of ice margins at
13 constricted fjord mouths of western Scotland. The net MSIS retreat rates are between 10-
14 28 m a^{-1} throughout and do not vary much at all, so the changes in net pace are subtle.
15 That said, there is better geomorphological evidence for pinning and stabilisation points, for
16 example the larger GZWs and moraines, so the actual pace of retreat may have included
17 faster and slower episodes not resolved by the net axial ice margin retreat rate data that
18 emerges from the Bayesian age modelling. This is a pattern of retreat observed commonly
19 in marine-based paleo-ice streams (Bradwell, et al., This volume, Jakobsson, et al., 2012,
20 Larter, et al., 2009, Newton and Huuse, 2017, Ottesen, et al., 2005, Shaw, et al., 2006,
21 Winsborrow, et al., 2010). Between 21 and 15.4 ka, the reduction in the flux of subglacially-
22 derived material, measured using radiogenic Pb isotope data, to the continental shelf is
23 interpreted as the result of the break-up of the ice-stream in western Scotland (Arosio, et
24 al., 2018a) and glaciomarine conditions are still indicated in the shelf sediments around the
25 Scottish coastline (Callard, et al., 2018). Sedimentological evidence from the Donegal-Barra
26 Fan suggests some marine extension of the BIIS until as late as $\sim 16.5 \text{ ka}$ that allowed
27 glaciomarine sediment deposition on the fan, with discrete episodes of calving recorded as
28 peaks in ice-rafted debris between 18 and $\sim 16.5 \text{ ka}$ (Tarlatti, et al., 2020).
29
30
31
32
33
34
35

36 Between 19 and $\sim 16.8 \text{ ka}$, an increase in retreat rate, from an average of around 3.7 to 25
37 m a^{-1} , is however observed in the inner part of Donegal Bay (Zone 5; Fig. 14), inshore of
38 the extensive Donegal Bay and Killala Bay moraine complex that occupies the outer bay. At
39 this location, the reverse sloped bed (Fig. 15B) is likely to have accelerated through MIS1
40 processes (DeConto and Pollard, 2016, Favier, et al., 2014, Schoof, 2007). The overall
41 driver, beyond instability, of retreat at this stage is unclear as it is happening within
42 Greenland Stadial 2 (GS-2) and therefore atmospheric warming is unlikely to be a
43 significant control (Fig. 15). Lack of significant change in foraminifera assemblages across
44 the Malin Sea also suggest that the final stages of deglaciation were not likely driven by
45 changes in sea temperature but more probably by local sea level changes and / or thinning
46 of the ice sheet. This is supported by modelled water depths for the inner and outer MSIS
47 derived from a glacio-isostatic adjustment model (Bradley, et al., 2011) rerun to account for
48 the ice thicknesses from the latest BRITICE-CHRONO ice sheet reconstruction and
49 accounting for global ice sheet variations (Fig. 15A-B). This suggests maximum water
50 depths occurred at 20-16 ka in the later part of GS-2. Retreat to a fully terrestrially-based
51 Donegal Ice Dome occurred within 1-1.5 ka after 16.8 ka and corresponds with the timing of
52 Heinrich event 1. Deglaciation at low ground around Donegal Bay was widespread by 15.3
53 ka when ice free conditions are also recorded in the Ox Mountains (zones 6 & 7, Fig. 14).
54
55
56
57
58
59
60

5. CONCLUSIONS

New OSL ages combined with Bayesian modelling of legacy and BRITICE-CHRONO ages along with consideration of their stratigraphic and landform contexts has allowed us to reconstruct ice advance to the continental shelf edge and withdrawal from here and back across the marine to terrestrial transition (Fig. 16). We summarise the main aspects and the coastal and inland radiocarbon ages show that Donegal and Scotland were ice free at low elevations around 34-35 ka. However, by 27.9-26.6 ka the BIIS had reached its maximum extent reaching the shelf break of the Malin Sea extending distances of ~190 km from the Donegal and ~280 km from the Scottish coastlines. Geomorphological and sedimentological evidence in the form of subglacial diamict, moraines and grounding zone wedges show a continuous ice margin developed at the shelf edge, fed by ice flow from two confluent ice streams, the Malin Sea and the Donegal Bay ice streams. Bayesian modelling of the geochronology shows that retreat from maximum started synchronously along the entire shelf edge of the Malin Sea by 26.3 ka. Compared with the onset of ice retreat globally this is surprisingly early. The Malin Sea Ice Stream retreated at a rate of ~19 m a⁻¹ and the Donegal Bay Ice Stream at ~20 m a⁻¹ both across the outer shelf between 26.3 and 22.5-23 ka. The outer shelf GZWs in the northern part of the Malin Sea and recessional moraines in the southern part, offshore NW Ireland, indicate that episodic retreat was separated by still-stand or oscillation of the ice margins. The Bayesian modelling struggles to resolve the duration of still-stands, but the scale of the landforms suggests some persistence of the ice margins at these locations.

By 23-22 ka the outer shelf (an area of about ~25,000 km²) was already free of grounded ice and ice margin retreat continued at a slower net rate across mid-shelf between 23.5 and 20.5 ka, with the ice margin sitting across the central Malin Sea, near the NW Irish coastline, and across the outer part and mouth of Donegal Bay. The separation between Irish-based and Scottish-based ice seems to have occurred just after this time around 20-19.4 ka, leaving behind an autonomous ice dome over the uplands of Donegal. Thereafter, mass loss of ice on the inner Malin shelf was focussed along major submarine troughs and took place over the ensuing two thousand years at a net rate of 16-27 m a⁻¹ with an ice margin positioned close to the present coastline within the Sea of Hebrides at 19ka. In Donegal Bay retreat during this time was punctuated by still-stands building moraines and retreat occurred at a much slower pace of 2 - 5.4 m a⁻¹. The Donegal Bay and Killala Bay moraines at the mouth of the bay record a major ice margin stillstand between 20.5 and 19 ka, with the moraines of different orientations suggesting oscillating ice positions driven by different source areas around Donegal Bay. Once the ice margin started retreating further from this position, the rate of retreat drastically accelerated to 25 m a⁻¹, likely due to the reverse-slope bed in the inner part of the bay. By 17 - 16 ka ice had retreated onto land and may have persisted as isolated ice caps in both Scotland and Ireland at least until ca 14.9-13.9 ka.

1
2
3 Our chronologically-constrained reconstruction suggests that the early retreat of the marine-
4 terminating western margin of the BIIS was initially driven by local ice loading that
5 increased water depths promoting ice losses by calving, rather than forcing by rises in
6 ocean and atmospheric temperatures. Retreat from the mid-shelf to the coastline
7 proceeded at differing paces between ice-streams and was affected by the presence of
8 topographic controls, including pinning points at underlying bedrock outcrops and
9 constrictions between coastal headlands of Scotland and Ireland, and by the presence of
10 reverse-slope beds underneath portions of the ice streams. Thinning of the ice sheet could
11 have also driven the onset of stages comprising relatively more rapid retreat close to the
12 coastlines of Ireland and Scotland. The timing and rates of retreat for the two ice streams
13 seem largely unrelated to global atmospheric and oceanographic changes, except for the
14 final stage transition into ice-free conditions before 14-13 ka.
15
16
17
18
19
20
21

22 Acknowledgements

23
24 This research was funded by the UK Natural Environment Research Council consortium
25 grant NE/J007196/1 BRITICE-CHRONO. The work was supported by the NERC
26 Radiocarbon Facility and NERC Cosmogenic Isotope Facility Analysis. Thanks to the staff
27 at the SUERC AMS Laboratory, East Kilbride for carbon isotope measurements. We thank
28 the officers and crew of the RRS James Cook for their assistance with data acquisition, as
29 well as the British Geological Survey and UK National Oceanography Centre for vibro- and
30 piston core collection respectively, during cruise JC106. Also thanks to the entire BRITICE-
31 CHRONO consortium for fruitful discussions over the duration of the project and the two
32 anonymous reviewers for their constructive comments.
33
34
35
36
37
38

39 References

- 40
41
42 Arosio R, Crocket KC, Nowell GM, Callard SL, Howe JA, Benetti S, Fabel D, Moreton S,
43 Clark CD. 2018a. Weathering fluxes and sediment provenance on the SW Scottish shelf
44 during the last deglaciation. *Marine Geology* **402**: 81-98. DOI:
45 10.1016/j.margeo.2017.08.017
46 Arosio R, Dove D, Ó Cofaigh C, Howe JA. 2018b. Submarine deglacial sediment and
47 geomorphological record of southwestern Scotland after the Last Glacial Maximum. *Marine*
48 *Geology* **403**: 62-79. DOI: 10.1016/j.margeo.2018.04.012
49 Balco G, Stone JO, Lifton NA, Dunai TJ. 2008. A complete and easily accessible means of
50 calculating surface exposure ages or erosion rates from ¹⁰Be and ²⁶Al measurements.
51 *Quaternary Geochronology* **3**: 174-195. DOI: 10.1016/j.quageo.2007.12.001
52 Ballantyne CK. 1989. The Loch Lomond Readvance on the Isle of Skye, Scotland: Glacier
53 reconstruction and palaeoclimatic implications. *Journal of Quaternary Science* **4**: 95-108.
54 DOI: 10.1002/jqs.3390040201
55 Ballantyne CK, McCarroll D, Stone JO. 2007. The Donegal ice dome, northwest Ireland:
56 Dimensions and chronology. *Journal of Quaternary Science* **22**: 773-783
57
58
59
60

- 1
2
3 Ballantyne CK, McCarroll D, Stone JO. 2011. Periglacial trimlines and the extent of the
4 Kerry-Cork Ice Cap, SW Ireland. *Quaternary Science Reviews* **30**: 3834-3845. DOI:
5 10.1016/j.quascirev.2011.10.006
6 Ballantyne CK, Ó Cofaigh C. 2017. The last Irish Ice Sheet: extent and chronology. In
7 *Advances in Irish Quaternary Studies*. Springer; 101-149.
8 Ballantyne CK, Small D. 2018. The Last Scottish Ice Sheet. *Earth and Environmental*
9 *Science Transactions of the Royal Society of Edinburgh* **110**: 93-131. DOI:
10 10.1017/s1755691018000038
11 Ballantyne CK, Stone JO. 2015. Trimlines, blockfields and the vertical extent of the last ice
12 sheet in Southern Ireland. *Boreas* **44**: 277-287. DOI: 10.1111/bor.12109
13 Ballantyne CK, Wilson P, Gheorghiu D, Rodés À. 2014. Enhanced rock-slope failure
14 following ice-sheet deglaciation: timing and causes. *Earth Surface Processes and*
15 *Landforms* **39**: 900-913. DOI: 10.1002/esp.3495
16 Bateman MD, Evans DJA, Roberts DH, Medialdea A, Ely J, Clark CD. 2018. The timing and
17 consequences of the blockage of the Humber Gap by the last British–Irish Ice Sheet.
18 *Boreas* **47**: 41-61. DOI: 10.1111/bor.12256
19 Benetti S, Dunlop P, ÓCofaigh C. 2010. Glacial and glacially-related features on the
20 continental margin of northwest Ireland mapped from marine geophysical data. *Journal of*
21 *Maps* **2010**: 14-29
22 Bennett MR, Boulton GS. 1993. Deglaciation of the younger dryas or Loch Lomond Stadial
23 ice-field in the northern Highlands, Scotland. *Journal of Quaternary Science* **8**: 133-145.
24 DOI: 10.1002/jqs.3390080206
25 Berger A, Loutre MF. 1991. Insolation values for the climate of the last 10 million years.
26 *Quaternary Science Reviews* **10**: 297-317. DOI: 10.1016/0277-3791(91)90033-Q
27 Bevington PR, Robinson DK. 2003. Data reduction and error analysis for the physical
28 sciences. McGraw-Hill: Boston, Mass. ; London
29 Bintanja R, van de Wal RSW, Oerlemans J. 2005. Modelled atmospheric temperatures and
30 global sea levels over the past million years. *Nature* **437**: 125-128
31 Bond G, Heinrich H, Broecker W, Labeyrie L, McManus J, Andrews J, Huon S, Jantschik R,
32 Clasen S, Simet C, Tedesco K, Klas M, Bonani G, Ivy S. 1992. Evidence for massive
33 discharges of icebergs into the North Atlantic ocean during the last glacial period. *Nature*
34 **360**: 245-249
35 Borchers B, Marrero S, Balco G, Caffee M, Goehring B, Lifton N, Nishiizumi K, Phillips F,
36 Schaefer J, Stone J. 2016. Geological calibration of spallation production rates in the
37 CRONUS-Earth project. *Quaternary Geochronology* **31**: 188-198. DOI:
38 10.1016/j.quageo.2015.01.009
39 Bos JAA, Dickson JH, Coope GR, Jardine WG. 2004. Flora, fauna and climate of Scotland
40 during the Weichselian Middle Pleniglacial – palynological, macrofossil and coleopteran
41 investigations. *Palaeogeography, Palaeoclimatology, Palaeoecology* **204**: 65-100. DOI:
42 10.1016/s0031-0182(03)00724-7
43 Boulton G, Hagdorn M. 2006. Glaciology of the British Isles Ice Sheet during the last glacial
44 cycle: form, flow, streams and lobes. *Quaternary Science Reviews* **25**: 3359-3390. DOI:
45 10.1016/j.quascirev.2006.10.013
46 Boulton GS. 1990. Sedimentary and sea level changes during glacial cycles and their
47 control on glacial marine facies architecture. *Glacial marine environments: processes and*
48 *sediments*: 15-52
49 Bradley SL, Milne GA, Shennan I, Edwards R. 2011. An improved glacial isostatic
50 adjustment model for the British Isles. *Journal of Quaternary Science* **26**: 541-552. DOI:
51 10.1002/jqs.1481
52
53
54
55
56
57
58
59
60

- 1
2
3 Bradwell T, Fabel D, Clark C, Chiverrell RC, Small D, Smedley RK, Saher M, Moreton S,
4 Dove D, Callard SL, Duller GAT, Medialdea A, Bateman MB, Burke MJ, McDonald N,
5 Gilgannon S, Morgan S, Roberts DH, Ó Cofaigh C. This volume. Pattern, style and timing of
6 British-Irish Ice Sheet advance and retreat over the last 45,000 years: evidence from NW
7 Scotland and the adjacent continental shelf. *Journal of Quaternary Science*:
8 Bradwell T, Small D, Fabel D, Clark CD, Chiverrell RC, Saher MH, Dove D, Callard SL,
9 Burke MJ, Moreton SG, Medialdea A, Bateman MD, Roberts DH, Golledge NR, Finlayson
10 A, Morgan S, Cofaigh C. 2019. Pattern, style and timing of British–Irish Ice Sheet retreat:
11 Shetland and northern North Sea sector. *Journal of Quaternary Science*. DOI:
12 10.1002/jqs.3163
13
14 Bradwell T, Stoker MS, Golledge NR, Wilson CK, Merritt JW, Long D, Everest JD, Hestvik
15 OB, Stevenson AG, Hubbard AL, Finlayson AG, Mathers HE. 2008. The northern sector of
16 the last British Ice Sheet: Maximum extent and demise. *Earth-Science Reviews* **88**: 207-
17 226. DOI: 10.1016/j.earscirev.2008.01.008
18
19 Bronk Ramsey C. 2008. Deposition models for chronological records. *Quaternary Science*
20 *Reviews* **27**: 42-60. DOI: 10.1016/j.quascirev.2007.01.019
21
22 Bronk Ramsey C. 2009a. Bayesian analysis of radiocarbon dates. *Radiocarbon* **51**: 337-
23 360
24
25 Bronk Ramsey C. 2009b. Dealing with outliers and offsets in radiocarbon dating.
26 *Radiocarbon* **51**: 1023-1045
27
28 Bronk Ramsey C, Lee S. 2013. Recent and Planned Developments of the Program Oxcal.
29 *Radiocarbon* **55**: 720-730
30
31 Brown EJ, Rose J, Coope RG, Lowe JJ. 2007. An MIS 3 age organic deposit from Balglass
32 Burn, central Scotland: palaeoenvironmental significance and implications for the timing of
33 the onset of the LGM ice sheet in the vicinity of the British Isles. *Journal of Quaternary*
34 *Science* **22**: 295-308. DOI: 10.1002/jqs.1028
35
36 Buck CE, Cavanagh WG, Litton CD. 1996. Bayesian Approach to Interpreting
37 Archaeological Data:
38 Callard SL, Cofaigh C, Benetti S, Chiverrell RC, Van Landeghem KJJ, Saher MH, Gales
39 JA, Small D, Clark CD, Livingstone SJ, Fabel D, Moreton SG. 2018. Extent and retreat
40 history of the Barra Fan Ice Stream offshore western Scotland and northern Ireland during
41 the last glaciation. *Quaternary Science Reviews* **201**: 280-302. DOI:
42 10.1016/j.quascirev.2018.10.002
43
44 Chiverrell RC, Smedley RK, Small D, Ballantyne CK, Burke MJ, Callard SL, Clark CD,
45 Duller GAT, Evans DJA, Fabel D, van Landeghem K, Livingstone S, Ó Cofaigh C, Thomas
46 GSP, Roberts DH, Saher M, Scourse JD, Wilson P. 2018. Ice margin oscillations during
47 deglaciation of the northern Irish Sea Basin. *Journal of Quaternary Science*. DOI:
48 10.1002/jqs.3057
49
50 Chiverrell RC, Thomas GSP, Burke M, Medialdea A, Smedley R, Bateman M, Clark C,
51 Duller GAT, Fabel D, Jenkins G, Ou X, Roberts HM, Scourse J. 2020. The evolution of the
52 terrestrial-terminating Irish Sea glacier during the last glaciation. *Journal of Quaternary*
53 *Science*. DOI: 10.1002/jqs.3229
54
55 Chiverrell RC, Thrasher IM, Thomas GSP, Lang A, Scourse JD, van Landeghem KJJ,
56 McCarroll D, Clark CD, ÓCofaigh C, Evans DJA, Ballantyne CK. 2013. Bayesian modelling
57 the retreat of the Irish Sea Ice Stream. *Journal of Quaternary Science* **28**: 200-209. DOI:
58 10.1002/jqs.2616
59
60 Clark CD, Evans DJA, Khatwa A, Bradwell T, Jordan CJ, Marsh SH, Mitchell WA, Bateman
MD. 2004. Map and GIS database of glacial landforms and features related to the last
British Ice Sheet. *Boreas* **33**: 359-375. DOI: 10.1111/j.1502-3885.2004.tb01246.x

- 1
2
3 Clark CD, Hughes ALC, Greenwood SL, Jordan C, Sejrup HP. 2012. Pattern and timing of
4 retreat of the last British-Irish Ice Sheet. *Quaternary Science Reviews* **44**: 112-146. DOI:
5 10.1016/j.quascirev.2010.07.019
6
7 Clark CD, Ely JC, Greenwood S.L, Hughes ALC, Meehan R, Barr I.D, Bateman
8 MD, Bradwell T, Doole J, Evans DJA, Jordan CJ, Monteys X, Pellicer XM, Sheehy
9 M. 2018. BRITICE Glacial Map, version 2: a map and GIS database of glacial landforms of
10 the last British–Irish Ice Sheet. *Boreas* **47**: 11-27. DOI 10.1111/bor.12273.
11
12 Clark J, McCabe AM, Schnabel C, Clark PU, McCarron S, Freeman SPHT, Maden C, Xu S.
13 2009a. Cosmogenic ¹⁰Be chronology of the last deglaciation of western Ireland, and
14 implications for sensitivity of the Irish ice sheet to climate change. *Bulletin of the Geological
15 Society of America* **121**: 3-16
16
17 Clark PU, Dyke AS, Shakun JD, Carlson AE, Clark J, Wohlfarth B, Mitrovica JX, Hostetler
18 SW, McCabe AM. 2009b. The Last Glacial Maximum. *Science* **325**: 710-4. DOI:
19 10.1126/science.1172873
20
21 Colhoun EA, Dickson JH, McCabe AM, Shotton FW. 1972. A Middle Midlandian freshwater
22 series at Derryvree, Maguiresbridge, County Fermanagh, Northern Ireland. *Proceedings of
23 the Royal Society of London. Series B. Biological Sciences* **180**: 273-292. DOI:
24 10.1098/rspb.1972.0018
25
26 Cullen C. 2012. Deciphering the geomorphic and sedimentary record of the last Irish Ice
27 Sheet in NW Donegal, Ireland: implications for glacial dynamics and decay configurations.
28 In *Geography and Archaeology*. National University of Ireland, Galway: NUI Galway; 434.
29
30 Davies HC, Dobson MR, Whittington RJ. 1984. A revised seismic stratigraphy for
31 Quaternary deposits on the inner continental shelf west of Scotland between 55°30'N and
32 57°30'N. *Boreas* **13**: 49-66. DOI: 10.1111/j.1502-3885.1984.tb00059.x
33
34 DeConto RM, Pollard D. 2016. Contribution of Antarctica to past and future sea-level rise.
35 *Nature* **531**: 591-597. DOI: 10.1038/nature17145
36
37 Dietze M, Kreuzer S, Burow C, Fuchs MC, Fischer M, Schmidt C. 2016. The abanico plot:
38 Visualising chronometric data with individual standard errors. *Quaternary Geochronology*
39 **31**: 12-18. DOI: 10.1016/j.quageo.2015.09.003
40
41 Dobson MR, Whittington RJ. 1992. Aspects of the geology of the Malin Sea area. Basins on
42 the Atlantic seaboard: 291-311
43
44 Dove D, Arosio R, Finlayson A, Bradwell T, Howe JA. 2015. Submarine glacial landforms
45 record Late Pleistocene ice-sheet dynamics, Inner Hebrides, Scotland. *Quaternary Science
46 Reviews* **123**: 76-90. DOI: 10.1016/j.quascirev.2015.06.012
47
48 Duller GAT. 2008. Single-grain optical dating of Quaternary sediments: why aliquot size
49 matters in luminescence dating. *Boreas* **37**: 589-612
50
51 Dunlop P, Shannon R, McCabe M, Quinn R, Doyle E. 2010. Marine geophysical evidence
52 for ice sheet extension and recession on the Malin Shelf: New evidence for the western
53 limits of the British Irish Ice Sheet. *Marine Geology* **276**: 86-99. DOI:
54 10.1016/j.margeo.2010.07.010
55
56 Evans DJA, Bateman MD, Roberts DH, Medialdea A, Hayes L, Duller GAT, Fabel D, Clark
57 CD. 2017. Glacial Lake Pickering: stratigraphy and chronology of a proglacial lake dammed
58 by the North Sea Lobe of the British-Irish Ice Sheet. *Journal of Quaternary Science* **32**: 295-
59 310. DOI: 10.1002/jqs.2833
60
61 Evans DJA, Benn DI. 2004. *A Practical Guide to the Study of Glacial Sediments. A Practical
62 Guide to the Study of Glacial Sediments*:
63
64 Fabel D, Ballantyne CK, Xu S. 2012. Trimlines, blockfields, mountain-top erratics and the
65 vertical dimensions of the last British-Irish Ice Sheet in NW Scotland. *Quaternary Science
66 Reviews* **55**: 91-102. DOI: 10.1016/j.quascirev.2012.09.002

- 1
2
3 Favier L, Durand G, Cornford SL, Gudmundsson GH, Gagliardini O, Gillet-Chaulet F,
4 Zwinger T, Payne AJ, Le Brocq AM. 2014. Retreat of Pine Island Glacier controlled by
5 marine ice-sheet instability. *Nature Climate Change* **4**: 117-121. DOI: 10.1038/nclimate2094
6 Favier L, Gagliardini O, Durand G, Zwinger T. 2012. A three-dimensional full Stokes model
7 of the grounding line dynamics: effect of a pinning point beneath the ice shelf. *The*
8 *Cryosphere* **6**: 101-112. DOI: 10.5194/tc-6-101-2012
9
10 Finlayson A, Fabel D, Bradwell T, Sugden D. 2014. Growth and decay of a marine
11 terminating sector of the last British–Irish Ice Sheet: a geomorphological reconstruction.
12 *Quaternary Science Reviews* **83**: 28-45. DOI: 10.1016/j.quascirev.2013.10.009
13
14 Finlayson A, Merritt J, Browne M, Merritt J, McMillan A, Whitbread K. 2010. Ice sheet
15 advance, dynamics, and decay configurations: evidence from west central Scotland.
16 *Quaternary Science Reviews* **29**: 969-988. DOI: 10.1016/j.quascirev.2009.12.016
17
18 Galbraith RF, Roberts RG, Laslett GM, Yoshida H, Olley JM. 1999. Optical dating of single
19 and multiple grains of quartz from Jinmium rock shelter, northern Australia: Part I,
20 experimental design and statistical models. *Archaeometry* **41**: 339-364. DOI:
21 10.1111/j.1475-4754.1999.tb00987.x
22
23 Greenwood SL, Clark CD. 2009a. Reconstructing the last Irish Ice Sheet 1: changing flow
24 geometries and ice flow dynamics deciphered from the glacial landform record. *Quaternary*
25 *Science Reviews* **28**: 3085-3100. DOI: 10.1016/j.quascirev.2009.09.008
26
27 Greenwood SL, Clark CD. 2009b. Reconstructing the last Irish Ice Sheet 2: a
28 geomorphologically-driven model of ice sheet growth, retreat and dynamics. *Quaternary*
29 *Science Reviews* **28**: 3101-3123. DOI: 10.1016/j.quascirev.2009.09.014
30
31 Guérin G, Mercier N, Adamiec G. 2011. Dose-rate conversion factors: update. *Ancient TL*
32 **29**: 5-8
33
34 Guérin G, Mercier N, Nathan R, Adamiec G, Lefrais Y. 2012. On the use of the infinite
35 matrix assumption and associated concepts: A critical review. *Radiation Measurements* **47**:
36 778-785. DOI: 10.1016/j.radmeas.2012.04.004
37
38 Hallissy T. 1911. Part 7. Geology. *Proceedings of the Royal Irish Academy. Section C:*
39 *Archaeology, Celtic Studies, History, Linguistics, Literature* **31**: 7.1-7.22
40
41 Heyman J, Stroeve AP, Harbor JM, Caffee MW. 2011. Too young or too old: Evaluating
42 cosmogenic exposure dating based on an analysis of compiled boulder exposure ages.
43 *Earth and Planetary Science Letters* **302**: 71-80. DOI: 10.1016/j.epsl.2010.11.040
44
45 Hibbert FD, Austin WEN, Leng MJ, Gatliff RW. 2009. British Ice Sheet dynamics inferred
46 from North Atlantic ice-rafted debris records spanning the last 175 000 years. *Journal of*
47 *Quaternary Science* **25**: 461-482. DOI: 10.1002/jqs.1331
48
49 Hinch JDW. 1913. The Shelly Drift of Glenultra and Belderrig, Co. Mayo. *The Irish*
50 *Naturalist*. **22**: 1-6
51
52 Howe JA, Dove D, Bradwell T, Gafeira J. 2012. Submarine geomorphology and glacial
53 history of the Sea of the Hebrides, UK. *Marine Geology* **315-318**: 64-76. DOI:
54 10.1016/j.margeo.2012.06.005
55
56 Hubbard A, Bradwell T, Golledge N, Hall A, Patton H, Sugden D, Cooper R, Stoker M.
57 2009a. Dynamic cycles, ice streams and their impact on the extent, chronology and
58 deglaciation of the British-Irish ice sheet. *Quaternary Science Reviews* **28**: 758-776
59
60 Hubbard A, Bradwell T, Golledge N, Hall A, Patton H, Sugden D, Cooper R, Stoker M.
2009b. Dynamic cycles, ice streams and their impact on the extent, chronology and
deglaciation of the British–Irish ice sheet. *Quaternary Science Reviews* **28**: 758-776. DOI:
10.1016/j.quascirev.2008.12.026
Hughes ALC, Clark CD, Jordan CJ. 2014. Flow-pattern evolution of the last British Ice
Sheet. *Quaternary Science Reviews* **89**: 148-168. DOI: 10.1016/j.quascirev.2014.02.002

- 1
2
3 Hughes ALC, Gyllencreutz R, Lohne OS, Mangerud J, Svendsen JI. 2016. The last
4 Eurasian ice sheets - a chronological database and time-slice reconstruction, DATED-1.
5 *Boreas* **45**: 1-45. DOI: 10.1111/bor.12142
6
7 Hughes ALC, Rainsley E, Murray T, Fogwill CJ, Schnabel C, Xu S. 2012. Rapid response
8 of Helheim Glacier, southeast Greenland, to early Holocene climate warming. *Geology* **40**:
9 427-430. DOI: 10.1130/G32730.1
10
11 Hughes PD, Gibbard PL. 2015. A stratigraphical basis for the Last Glacial Maximum (LGM).
12 *Quaternary International* **383**: 174-185. DOI: 10.1016/j.quaint.2014.06.006
13
14 Hughes PD, Gibbard PL, Ehlers J. 2013. Timing of glaciation during the last glacial cycle:
15 evaluating the concept of a global 'Last Glacial Maximum' (LGM). *Earth-Science Reviews*
16 **125**: 171-198. DOI: 10.1016/j.earscirev.2013.07.003
17
18 Hulbe CL, MacAyeal DR, Denton GH, Kleman J, Lowell TV. 2004. Catastrophic ice shelf
19 breakup as the source of Heinrich event icebergs. *Paleoceanography* **19**: PA1004 1-15.
20 DOI: 10.1029/2003pa000890
21
22 Jakobsson M, Anderson JB, Nitsche FO, Gyllencreutz R, Kirshner AE, Kirchner N, O'Regan
23 M, Mohammad R, Eriksson B. 2012. Ice sheet retreat dynamics inferred from glacial
24 morphology of the central Pine Island Bay Trough, West Antarctica. *Quaternary Science*
25 *Reviews* **38**: 1-10. DOI: 10.1016/j.quascirev.2011.12.017
26
27 Jardine WG, Dickson JH, Haughton PDW, Harkness DD, Bowen DQ, Sykes GA. 1988. A
28 late Middle Devensian interstadial site at Sourlie, near Irvine, Strathclyde. *Scottish Journal*
29 *of Geology* **24**: 288. DOI: 10.1144/sjg24030288
30
31 Joughin I, Alley RB, Holland DM. 2012. Ice-Sheet Response to Oceanic Forcing. *Science*
32 **338**: 1172-1176. DOI: 10.1126/science.1226481
33
34 Joughin I, Smith BE, Medley B. 2014. Marine Ice Sheet Collapse Potentially Under Way for
35 the Thwaites Glacier Basin, West Antarctica. *Science* **344**: 735-738. DOI:
36 10.1126/science.1249055
37
38 Khodri M, Leclainche Y, Ramstein G, Braconnot P, Marti O, Cortijo E. 2001. Simulating the
39 amplification of orbital forcing by ocean feedbacks in the last glaciation. *Nature* **410**: 570-
40 574. DOI: 10.1038/35069044
41
42 Knight J. 2004. Sedimentary evidence for the formation mechanism of the Armoy moraine
43 and late Devensian glacial events in the north of Ireland. *Geological Journal* **39**: 403-417.
44 DOI: 10.1002/gj.964
45
46 Knight J. 2008a. Armoy Moraine. In *North of Ireland: Field Guide*, Whitehouse NJ, Roe HM,
47 McCarron S, Knight J (eds). Quaternary Research Association: London; 187-193.
48
49 Knight J. 2008b. Carey and Glenshesk valleys. In *North of Ireland: Field Guide*, Whitehouse
50 NJ, Roe HM, McCarron S, Knight J (eds). Quaternary Research Association: London; 194-
51 203.
52
53 Knutz PC, Austin WEN, John W Jones E. 2001. Millennial-scale depositional cycles related
54 to British ice sheet variability and North Atlantic paleocirculation since 45 kyr B.P., Barra
55 Fan, U.K. margin. *Paleoceanography* **16**: 53-64. DOI: 10.1029/1999PA000483
56
57 Knutz PC, Hall IR, Zahn R, Rasmussen TL, Kuijpers A, Moros M, Shackleton NJ. 2002.
58 Multidecadal ocean variability and NW European ice sheet surges during the last
59 deglaciation. *Geochemistry, Geophysics, Geosystems* **3**: 1077
60
61 Krabill W, Abdalati W, Frederick E, Manizade S, Martin C, Sonntag J, Swift R, Thomas R,
62 Wright W, Yungel J. 2000. Greenland Ice Sheet: High-elevation balance and peripheral
63 thinning. *Science* **289**: 428-430. DOI: 10.1126/science.289.5478.428
64
65 Krabill W, Hanna E, Huybrechts P, Abdalati W, Cappelen J, Csatho B, Frederick E,
66 Manizade S, Martin C, Sonntag J, Swift R, Thomas R, Yungel J. 2004. Greenland Ice
67 Sheet: Increased coastal thinning. *Geophysical Research Letters* **31**: 1-4. DOI:
68 10.1029/2004GL021533

- 1
2
3 Lambeck K, Rouby H, Purcell A, Sun Y, Sambridge M. 2014. Sea level and global ice
4 volumes from the Last Glacial Maximum to the Holocene. *Proc Natl Acad Sci U S A* **111**:
5 15296-303. DOI: 10.1073/pnas.1411762111
6
7 Larter RD, Graham AGC, Gohl K, Kuhn G, Hillenbrand C-D, Smith JA, Deen TJ, Livermore
8 RA, Schenke H-W. 2009. Subglacial bedforms reveal complex basal regime in a zone of
9 paleo-ice stream convergence, Amundsen Sea embayment, West Antarctica. *Geology* **37**:
10 411-414. DOI: 10.1130/G25505A.1
11
12 Lowe J, Matthews I, Mayfield R, Lincoln P, Palmer A, Staff R, Timms R. 2019. On the
13 timing of retreat of the Loch Lomond ('Younger Dryas') Readvance icefield in the SW
14 Scottish Highlands and its wider significance. *Quaternary Science Reviews* **219**: 171-186.
15 DOI: 10.1016/j.quascirev.2019.06.034
16
17 MacLeod A, Palmer A, Lowe J, Rose J, Bryant C, Merritt J. 2011. Timing of glacier
18 response to Younger Dryas climatic cooling in Scotland. *Global and Planetary Change* **79**:
19 264-274. DOI: 10.1016/j.gloplacha.2010.07.006
20
21 Marrero SM, Phillips FM, Borchers B, Lifton N, Aumer R, Balco G. 2016. Cosmogenic
22 nuclide systematics and the CRONUScalc program. *Quaternary Geochronology* **31**: 160-
23 187. DOI: 10.1016/j.quageo.2015.09.005
24
25 McCabe A, Haynes JR, MacMillan NF. 1986. Late Pleistocene tidewater glaciers and
26 glaciomarine sequences from north County Mayo, Republic of Ireland. *Journal of*
27 *Quaternary Science* **1**: 73-84
28
29 McCabe AM. 1995. Fawnmore - ice marginal terrace. In *North West Donegal. Field*
30 *Guide.*, Wilson P (ed). Irish Association for Quaternary Studies: Dublin; 67-70.
31
32 McCabe AM. 2008. Glacial geology and geomorphology: the landscapes of Ireland.
33 Dunedin Academic Press, Edinburgh
34
35 McCabe AM, Clark PU. 2003. Deglacial chronology from county Donegal, Ireland:
36 Implications for deglaciation of the British-Irish ice sheet. *Journal of the Geological Society*
37 **160**: 847-855
38
39 McCabe AM, Clark PU, Clark J. 2007a. Radiocarbon constraints on the history of the
40 western Irish ice sheet prior to the Last Glacial Maximum. *Geology* **35**: 147-150
41
42 McCabe AM, Clark PU, Clark J, Dunlop P. 2007b. Radiocarbon constraints on readvances
43 of the British-Irish Ice Sheet in the northern Irish Sea Basin during the last deglaciation.
44 *Quaternary Science Reviews* **26**: 1204-1211. DOI: 10.1016/j.quascirev.2007.01.010
45
46 McCabe AM, Eyles N. 1988. Sedimentology of an ice-contact glaciomarine delta, Carey
47 Valley, Northern Ireland. *Sedimentary Geology* **59**: 1-14
48
49 Meehan R. 2013. North Mayo. In *Geological Survey Ireland Geological Mapping*.
50 Geological Survey Ireland: Dublin.
51
52 Murray AS, Wintle AG. 2000. Luminescence dating of quartz using an improved single-
53 aliquot regenerative-dose protocol. *Radiation Measurements* **32**: 57-73. DOI:
54 10.1016/S1350-4487(99)00253-X
55
56 Newton AMW, Huuse M. 2017. Glacial geomorphology of the central Barents Sea:
57 Implications for the dynamic deglaciation of the Barents Sea Ice Sheet. *Marine Geology*
58 **387**: 114-131. DOI: <https://doi.org/10.1016/j.margeo.2017.04.001>
59
60 Ó'Cofaigh C, Dunlop P, Benetti S. 2012. Marine geophysical evidence for Late Pleistocene
ice sheet extent and recession off northwest Ireland. *Quaternary Science Reviews* **44**: 147-
159. DOI: 10.1016/j.quascirev.2010.02.005
Ó'Cofaigh C, Callard L, Roberts DH, Chiverrell RC, Ballantyne CK, Evans D, Saher M, Van
Landeghem K, Benetti S, Burke MJ, Clark C, Duller G, Fabel D, Livingstone S, Medialdea
A, Moreton S, Sacchetti F, Smedley RK. This volume. Timing and pace of ice-sheet
withdrawal across the marineterrestrial transition west of Ireland during the last glaciation.
Journal of Quaternary Science:

- 1
2
3 Ó Cofaigh C, Weilbach K, Lloyd JM, Benetti S, Callard SL, Purcell C, Chiverrell RC, Dunlop
4 P, Saher M, Livingstone SJ, Van Landeghem KJJ, Moreton SG, Clark CD, Fabel D. 2019.
5 Early deglaciation of the British-Irish Ice Sheet on the Atlantic shelf northwest of Ireland
6 driven by glacioisostatic depression and high relative sea level. *Quaternary Science*
7 *Reviews* **208**: 76-96. DOI: 10.1016/j.quascirev.2018.12.022
- 8 Ottesen D, Dowdeswell JA, Rise L. 2005. Submarine landforms and the reconstruction of
9 fast-flowing ice streams within a large Quaternary ice sheet: The 2500-km-long Norwegian-
10 Svalbard margin (57°–80°N). *GSA Bulletin* **117**: 1033-1050. DOI: 10.1130/B25577.1
- 11 Patton H, Hubbard A, Andreassen K, Auriac A, Whitehouse PL, Stroeven AP, Shackleton
12 C, Winsborrow M, Heyman J, Hall AM. 2017. Deglaciation of the Eurasian ice sheet
13 complex. *Quaternary Science Reviews* **169**: 148-172. DOI:
14 10.1016/j.quascirev.2017.05.019
- 15 Patton H, Hubbard A, Andreassen K, Winsborrow M, Stroeven AP. 2016. The build-up,
16 configuration, and dynamical sensitivity of the Eurasian ice-sheet complex to Late
17 Weichselian climatic and oceanic forcing. *Quaternary Science Reviews* **153**: 97-121. DOI:
18 10.1016/j.quascirev.2016.10.009
- 19 Patton H, Hubbard A, Glasser NF, Bradwell T, Golledge NR. 2012a. The last Welsh Ice
20 Cap: Part 1 - Modelling its evolution, sensitivity and associated climate. *Boreas*: n/a-n/a.
21 DOI: 10.1111/j.1502-3885.2012.00300.x
- 22 Patton H, Hubbard A, Glasser NF, Bradwell T, Golledge NR. 2012b. The last Welsh Ice
23 Cap: Part 2 - Dynamics of a topographically controlled icecap. *Boreas*: n/a-n/a. DOI:
24 10.1111/j.1502-3885.2012.00301.x
- 25 Payne AJ, Vieli A, Shepherd AP, Wingham DJ, Rignot E. 2004. Recent dramatic thinning of
26 largest West Antarctic ice stream triggered by oceans. *Geophysical Research Letters* **31**: 1-
27 4. DOI: 10.1029/2004GL021284
- 28 Peck VL, Hall IR, Zahn R, Elderfield H, Grousset F, Hemming SR, Scourse JD. 2006. High
29 resolution evidence for linkages between NW European ice sheet instability and Atlantic
30 Meridional Overturning Circulation. *Earth and Planetary Science Letters* **243**: 476-488. DOI:
31 10.1016/j.epsl.2005.12.023
- 32 Peck VL, Hall IR, Zahn R, Grousset F, Hemming SR, Scourse JD. 2007. The relationship of
33 Heinrich events and their European precursors over the past 60 ka BP: a multi-proxy ice-
34 rafted debris provenance study in the North East Atlantic. *Quaternary Science Reviews* **26**:
35 862-875. DOI: 10.1016/j.quascirev.2006.12.002
- 36 Peters JL, Benetti S, Dunlop P, Ó Cofaigh C. 2015. Maximum extent and dynamic
37 behaviour of the last British–Irish Ice Sheet west of Ireland. *Quaternary Science Reviews*
38 **128**: 48-68. DOI: 10.1016/j.quascirev.2015.09.015
- 39 Peters JL, Benetti S, Dunlop P, Ó Cofaigh C, Moreton SG, Wheeler AJ, Clark CD. 2016.
40 Sedimentology and chronology of the advance and retreat of the last British-Irish Ice Sheet
41 on the continental shelf west of Ireland. *Quaternary Science Reviews* **140**: 101-124. DOI:
42 10.1016/j.quascirev.2016.03.012
- 43 Pritchard HD, Arthern RJ, Vaughan DG, Edwards LA. 2009. Extensive dynamic thinning on
44 the margins of the Greenland and Antarctic ice sheets. *Nature* **461**: 971-5. DOI:
45 10.1038/nature08471
- 46 Putnam AE, Bromley GRM, Rademaker K, Schaefer JM. 2019. In situ ¹⁰Be production-rate
47 calibration from a ¹⁴C-dated late-glacial moraine belt in Rannoch Moor, central Scottish
48 Highlands. *Quaternary Geochronology* **50**: 109-125. DOI: 10.1016/j.quageo.2018.11.006
- 49 Rasmussen SO, Bigler M, Blockley SP, Blunier T, Buchardt SL, Clausen HB, Cvijanovic I,
50 Dahl-Jensen D, Johnsen SJ, Fischer H, Gkinis V, Guillevic M, Hoek WZ, Lowe JJ, Pedro
51 JB, Popp T, Seierstad IK, Steffensen JP, Svensson AM, Vallelonga P, Vinther BM, Walker
52 MJC, Wheatley JJ, Winstrup M. 2014. A stratigraphic framework for abrupt climatic changes

- 1
2
3 during the Last Glacial period based on three synchronized Greenland ice-core records:
4 Refining and extending the INTIMATE event stratigraphy. *Quaternary Science Reviews*
5 **106**: 14-28. DOI: 10.1016/j.quascirev.2014.09.007
6 Rasmussen TL, Thomsen E, Moros M. 2016. North Atlantic warming during Dansgaard-
7 Oeschger events synchronous with Antarctic warming and out-of-phase with Greenland
8 climate. *Sci Rep* **6**: 20535. DOI: 10.1038/srep20535
9 Reimer PJ, Bard E, Bayliss A, Beck JW, Blackwell PG, Bronk Ramsey C, Buck CE, Cheng
10 H, Edwards RL, Friedrich M, Grootes PM, Guilderson TP, Haflidason H, Hajdas I, Hatté C,
11 Heaton TJ, Hoffmann DL, Hogg AG, Hughen KA, Kaiser KF, Kromer B, Manning SW, Niu
12 M, Reimer RW, Richards DA, Scott EM, Southon JR, Staff RA, Turney CSM, van der Plicht
13 J. 2013. IntCal13 and Marine13 radiocarbon age calibration curves 0-50,000 years cal BP.
14 *Radiocarbon* **55**: 1869-1887. DOI: 10.2458/azu_js_rc.55.16947
15 Rignot E, Braaten D, Gogineni SP, Krabill WB, McConnell JR. 2004a. Rapid ice discharge
16 from southeast Greenland glaciers. *Geophysical Research Letters* **31**: L10401 1-4. DOI:
17 10.1029/2004GL019474
18 Rignot E, Casassa G, Gogineni P, Krabill W, Rivera A, Thomas R. 2004b. Accelerated ice
19 discharge from the Antarctic Peninsula following the collapse of Larsen B ice shelf.
20 *Geophysical Research Letters* **31**: L18401 1-4. DOI: 10.1029/2004GL020697
21 Rignot E, Koppes M, Velicogna I. 2010. Rapid submarine melting of the calving faces of
22 West Greenland glaciers. *Nature Geoscience* **3**: 187-191. DOI: 10.1038/ngeo765
23 Roberts DH, Long AJ, Davies BJ, Simpson MJR, Schnabel C. 2010. Ice stream influence
24 on West Greenland Ice Sheet dynamics during the Last Glacial Maximum. *Journal of*
25 *Quaternary Science* **25**: 850-864. DOI: <https://doi.org/10.1002/jqs.1354>
26 Scambos TA, Bohlander JA, Shuman CA, Skvarca P. 2004. Glacier acceleration and
27 thinning after ice shelf collapse in the Larsen B embayment, Antarctica. *Geophysical*
28 *Research Letters* **31**: L18402 1-4. DOI: 10.1029/2004GL020670
29 Schiele CK. 2017. Timing, forcing and onshore-offshore correlations on the western margin
30 of the British-Irish Ice Sheet. In *School of Geography and Environmental Sciences*. Ulster
31 University: Coleraine.
32 Schoof C. 2007. Ice sheet grounding line dynamics: Steady states, stability, and hysteresis.
33 *Journal of Geophysical Research: Earth Surface* **112**. DOI: 10.1029/2006JF000664
34 Scourse JD, Chiverrell RC, Smedley RK, Small D, Burke MJ, Saher M, Landeghem KJJV,
35 Duller GAT, Cofaigh C , Bateman M, Benetti S, Bradley S, Callard SL, Evans DJA, Fabel
36 D, Jenkins GTH, McCarron S, Medialdea A, Moreton S, Praeg D, Roberts DH, Clark CD.
37 This volume. Maximum extent and readvance dynamics of the Irish Sea Ice Stream and
38 Irish Sea Glacier since the Last Glacial Maximum. *Journal of Quaternary Science*:
39 Scourse JD, Haapaniemi AI, Colmenero-Hidalgo E, Peck VL, Hall IR, Austin WEN, Knutz
40 PC, Zahn R. 2009. Growth, dynamics and deglaciation of the last British-Irish ice sheet: the
41 deep-sea ice-rafted detritus record. *Quaternary Science Reviews* **28**: 3066-3084. DOI:
42 10.1016/j.quascirev.2009.08.009
43 Shaw J, Piper DJW, Fader GBJ, King EL, Todd BJ, Bell T, Batterson MJ, Liverman DGE.
44 2006. A conceptual model of the deglaciation of Atlantic Canada. *Quaternary Science*
45 *Reviews* **25**: 2059-2081. DOI: 10.1016/j.quascirev.2006.03.002
46 Shepherd A, Wingham D, Rignot E. 2004. Warm ocean is eroding West Antarctic ice Sheet.
47 *Geophys. Res. Lett.* **31**:
48 Sissons JB. 1980. The Loch Lomond Advance in the Lake District, northern England.
49 *Transactions of the Royal Society of Edinburgh: Earth Sciences* **71**: 13-27. DOI:
50 10.1017/S0263593300013468
51 Small D, Benetti S, Dove D, Ballantyne CK, Fabel D, Clark CD, Gheorghiu DM, Newall J,
52 Xu S. 2017a. Cosmogenic exposure age constraints on deglaciation and flow behaviour of
53
54
55
56
57
58
59
60

- 1
2
3 a marine-based ice stream in western Scotland, 21–16 ka. *Quaternary Science Reviews*
4 **167**: 30-46. DOI: 10.1016/j.quascirev.2017.04.021
- 5 Small D, Clark CD, Chiverrell RC, Smedley RK, Bateman MD, Duller GAT, Ely JC, Fabel D,
6 Medialdea A, Moreton SG. 2017b. Devising quality assurance procedures for assessment
7 of legacy geochronological data relating to deglaciation of the last British-Irish Ice Sheet.
8 *Earth-Science Reviews* **164**: 232-250. DOI: 10.1016/j.earscirev.2016.11.007
- 9 Small D, Fabel D. 2015. A Lateglacial ^{10}Be production rate from glacial lake shorelines in
10 Scotland. *Journal of Quaternary Science* **30**: 509-513. DOI: 10.1002/jqs.2804
- 11 Small D, Rinterknecht V, Austin WEN, Bates R, Benn DI, Scourse JD, Bourlès DL, Hibbert
12 FD. 2016. Implications of ^{36}Cl exposure ages from Skye, northwest Scotland for the timing
13 of ice stream deglaciation and deglacial ice dynamics. *Quaternary Science Reviews* **150**:
14 130-145. DOI: 10.1016/j.quascirev.2016.08.028
- 15 Small D, Smedley RK, Chiverrell RC, Scourse JD, Cofaigh C, Duller GAT, McCarron S,
16 Burke MJ, Evans DJ, Fabel D, Gheorghiu DM, Thomas GSP, Xu S, Clark CD. 2018. Trough
17 geometry was a greater influence than climate-ocean forcing in regulating retreat of the
18 marine-based Irish-Sea Ice Stream. *Bulletin of the Geological Society of America* **130**:
19 1981-1999. DOI: 10.1130/B31852.1
- 20 Smedley RK, Chiverrell RC, Ballantyne CK, Burke MJ, Clark CD, Duller GAT, Fabel D,
21 McCarroll D, Scourse JD, Small D, Thomas GSP. 2017a. Internal dynamics condition
22 centennial-scale oscillations in marinebased ice-stream retreat. *Geology* **45**: 787-790. DOI:
23 10.1130/G38991.1
- 24 Smedley RK, Scourse JD, Small D, Hiemstra JF, Duller GAT, Bateman MD, Burke MJ,
25 Chiverrell RC, Clark CD, Davies SM, Fabel D, Gheorghiu DM, McCarroll D, Medialdea A,
26 Xu S. 2017b. New age constraints for the limit of the British–Irish Ice Sheet on the Isles of
27 Scilly. *Journal of Quaternary Science* **32**: 48-62. DOI: 10.1002/jqs.2922
- 28 Smith MJ, Knight J, Field KS, Harrison S. 2008. Glacial striae observations for Ireland
29 compiled from historic records. *Journal of Maps* **4**: 378-398. DOI: 10.4113/jom.2008.1035
- 30 Sole A, Payne T, Bamber J, Nienow P, Krabill W. 2008. Testing hypotheses of the cause of
31 peripheral thinning of the Greenland Ice Sheet: Is land-terminating ice thinning at
32 anomalously high rates? *Cryosphere* **2**: 205-218. DOI: 10.5194/tc-2-205-2008
- 33 Sonntag J, Manizade S, Krabill W, Linkswiler M, Yungel J. 2012. Progressive thinning of
34 Greenland's west-central flank and northwest coastal margin from operation icebridge laser
35 altimetry. 1553-1556. DOI: 10.1109/IGARSS.2012.6350815
- 36 Stocker T. 2014. *Climate change 2013 : the physical science basis : Working Group I*
37 *contribution to the Fifth assessment report of the Intergovernmental Panel on Climate*
38 *Change*
- 39 Stokes CR. 2018. Geomorphology under ice streams: Moving from form to process. *Earth*
40 *Surface Processes and Landforms* **43**: 85-123. DOI: 10.1002/esp.4259
- 41 Stokes CR, Clark CD. 1999. Geomorphological criteria for identifying Pleistocene ice
42 streams. *Annals of Glaciology* **28**: 67-74
- 43 Stokes CR, Clark CD. 2001. Palaeo-ice streams. *Quaternary Science Reviews* **20**: 1437-
44 1457
- 45 Stokes CR, Corner GD, Winsborrow MCM, Husum K, Andreassen K. 2014. Asynchronous
46 response of marine-terminating outlet glaciers during deglaciation of the Fennoscandian ice
47 sheet. *Geology* **42**: 455-458. DOI: 10.1130/G35299.1
- 48 Stone JO, Ballantyne CK. 2006. Dimensions and deglacial chronology of the Outer
49 Hebrides Ice Cap, northwest Scotland: implications of cosmic ray exposure dating. *Journal*
50 *of Quaternary Science* **21**: 75-84. DOI: 10.1002/jqs.933
- 51 Svendsen JI, Alexanderson H, Astakhov VI, Demidov I, Dowdeswell JA, Funder S,
52 Gataullin V, Henriksen M, Hjort C, Houmark-Nielsen M, Hubberten HW, Ingolfsson O,
53
54
55
56
57
58
59
60

- 1
2
3 Jakobsson M, Kjær KH, Larsen E, Lokrantz H, Lunkka JP, Lyså A, Mangerud J,
4 Matiouchkov A, Murray A, Möller P, Niessen F, Nikolskaya O, Polyak L, Saarnisto M,
5 Siegert C, Siegert MJ, Spielhagen RF, Stein R. 2004. Late Quaternary ice sheet history of
6 northern Eurasia. *Quaternary Science Reviews* **23**: 1229-1271
7
8 Synge FM. 1963. The Glaciation of the Nephin Beg Range, County Mayo. *Irish Geography*
9 **4**: 397-403. DOI: 10.1080/00750776309555569
10
11 Synge FM. 1965. The glaciation of west mayo. *Irish Geography* **5**: 372-386. DOI:
12 10.1080/00750776509555630
13
14 Tarlati S, Benetti S, Callard SL, Cofaigh CÓ, Dunlop P, Georgiopoulou A, Edwards R, Van
15 Landeghem K, Saher M, Chiverrell R, Fabel D, Moreton S, Morgan S, Clark CD. 2020. Final
16 deglaciation of the Malin Sea through meltwater release and calving events. *Scottish*
17 *Journal of Geology*. DOI: 10.1144/sjg2019-010
18
19 Thomas GSP, Chiverrell R, Huddart D. 2004. Ice-marginal depositional responses to
20 readvance episodes in the Late Devensian deglaciation of the Isle of Man. *Quaternary*
21 *Science Reviews* **23**: 85-106. DOI: 10.1016/j.quascirev.2003.10.012
22
23 Thomsen KJ, Murray AS, Bøtter-Jensen L, Kinahan J. 2007. Determination of burial dose in
24 incompletely bleached fluvial samples using single grains of quartz. *Radiation*
25 *Measurements* **42**: 370-379. DOI: 10.1016/j.radmeas.2007.01.041
26
27 Van Kreveld S, Sarnthein M, Erlenkeuser H, Grootes P, Jung S, Nadeau MJ, Pflaumann U,
28 Voelker A. 2000. Potential links between surging ice sheets, circulation changes, and the
29 Dansgaard-Oeschger cycles in the Irmiger Sea, 60-80 kyr. *Paleoceanography* **15**: 425-442.
30 DOI: 10.1029/1999PA000464
31
32 Waelbroeck C, Lougheed BC, Vazquez Riveiros N, Missiaen L, Pedro J, Dokken T, Hajdas
33 I, Wacker L, Abbott P, Dumoulin JP, Thil F, Eynaud F, Rossignol L, Fersi W, Albuquerque
34 AL, Arz H, Austin WEN, Came R, Carlson AE, Collins JA, Dennielou B, Desprat S, Dickson
35 A, Elliot M, Farmer C, Giraudeau J, Gottschalk J, Henderiks J, Hughen K, Jung S, Knutz P,
36 Lebreiro S, Lund DC, Lynch-Stieglitz J, Malaize B, Marchitto T, Martinez-Mendez G,
37 Mollenhauer G, Naughton F, Nave S, Nurnberg D, Oppo D, Peck V, Peeters FJC, Penaud
38 A, Portilho-Ramos RDC, Repschlager J, Roberts J, Ruhlemann C, Salgueiro E, Sanchez
39 Goni MF, Schonfeld J, Scussolini P, Skinner LC, Skonieczny C, Thornalley D, Toucanne S,
40 Rooij DV, Vidal L, Voelker AHL, Wary M, Weldeab S, Ziegler M. 2019. Consistently dated
41 Atlantic sediment cores over the last 40 thousand years. *Sci Data* **6**: 165. DOI:
42 10.1038/s41597-019-0173-8
43
44 Wilson P, Ballantyne CK, Benetti S, Small D, Fabel D, Clark CD. 2019. Deglaciation
45 chronology of the Donegal Ice Centre, north-west Ireland. *Journal of Quaternary Science*
46 **34**: 16-28. DOI: 10.1002/jqs.3077
47
48 Winsborrow MCM, Andreassen K, Corner GD, Laberg JS. 2010. Deglaciation of a marine-
49 based ice sheet: Late Weichselian palaeo-ice dynamics and retreat in the southern Barents
50 Sea reconstructed from onshore and offshore glacial geomorphology. *Quaternary Science*
51 *Reviews* **29**: 424-442. DOI: 10.1016/j.quascirev.2009.10.001
52
53
54
55
56
57
58
59
60

TABLES

Table 1 Radioactivity and dose rate data for luminescence samples.

| Site | Sample | Depth (m) | Water (%) | U (ppm)* | Th (ppm)* | K (%) * | Rb (ppm)* | Beta dose-rate (Gy/ka) | Gamma dose-rate (Gy/ka) | Cosmic dose-rate (Gy/ka) | Total dose-rate (Gy/ka) |
|------------------|----------|-----------|-----------|-----------|-----------|-----------|-----------|------------------------|-------------------------|--------------------------|-------------------------|
| Brockhill Quarry | T6BROC01 | 7 | 27 | 1.22±0.12 | 3.0±0.3 | 1.5±0.08 | 42.9±4.29 | 0.782±0.060 | 0.452±0.030 | 0.088±0.004 | 1.339±0.074 |
| | T6BROC02 | 5 | 27 | 1.03±0.10 | 2.4±0.24 | 1.3±0.07 | 39.4±3.94 | 0.902±0.078 | 0.477±0.032 | 0.111±0.006 | 1.507±0.084 |
| Glenulra Quarry | T6GULR01 | 2.3 | 27 | 1.65±0.17 | 4.4±0.44 | 2.1±0.11 | 72.5±7.25 | 1.270±0.109 | 0.760±0.050 | 0.156±0.008 | 2.207±0.120 |
| | T6GULR02 | 2 | 27 | 1.70±0.17 | 4.7±0.47 | 2.0±0.10 | 64.6±6.46 | 1.228±0.105 | 0.636±0.042 | 0.162±0.008 | 2.047±0.113 |
| Lough Nacung | T6LNAC01 | 5 | 27 | 0.66±0.07 | 1.6±0.2 | 0.8±0.04 | 25.3±2.53 | 0.485±0.042 | 0.317±0.021 | 0.111±0.006 | 0.928±0.047 |
| | T6LNAC02 | 3 | 27 | 0.82±0.08 | 3.0±0.3 | 2.0±0.10 | 53.1±5.31 | 1.120±0.101 | 0.563±0.038 | 0.143±0.007 | 1.841±0.108 |
| Altwinny Bay | T7ALTB02 | 10 | 27 | 1.04±0.10 | 3.9±0.39 | 1.9±0.10 | 51.3±5.13 | 1.109±0.97 | 0.584±0.039 | 0.064±0.003 | 1.775±0.105 |
| Carey Valley | T7CARV01 | 12 | 27 | 1.22±0.12 | 5.0±0.5 | 1.4±0.07 | 49.7±4.97 | 0.882±0.074 | 0.519±0.034 | 0.054±0.003 | 1.474±0.081 |
| | T7CARV02 | 8 | 27 | 1.39±0.14 | 6.3±0.63 | 1.7±0.09 | 62.7±6.27 | 1.067±0.091 | 0.530±0.032 | 0.080±0.004 | 1.697±0.095 |
| Castleroe | T7CAST01 | 10 | 23 | 0.37±0.04 | 1.3±0.13 | 0.60±0.03 | 16.8±1.68 | 0.375±0.033 | 0.211±0.014 | 0.064±0.003 | 0.663±0.036 |
| | T7CAST02 | 15 | 23 | 0.37±0.04 | 1.2±0.12 | 0.60±0.03 | 15.9±1.59 | 0.373±0.033 | 0.207±0.014 | 0.041±0.002 | 0.635±0.036 |
| Fawnmore | T7FAWN02 | 5 | 27 | 1.17±0.12 | 4.7±0.47 | 1.30±0.07 | 44.9±4.49 | 0.823±0.070 | 0.573±0.038 | 0.111±0.006 | 1.525±0.079 |
| | T7FAWN03 | 3 | 27 | 1.27±0.13 | 6.6±0.66 | 1.60±0.08 | 53.8±5.38 | 1.010±0.084 | 0.625±0.042 | 0.142±0.007 | 1.798±0.094 |
| Glenshesk Valley | T7GLEN01 | 2 | 27 | 1.06±0.11 | 4.3±0.43 | 0.80±0.04 | 28.2±2.82 | 0.555±0.044 | 0.440±0.030 | 0.164±0.008 | 1.178±0.054 |
| | T7GLEN02 | 3 | 27 | 1.13±0.11 | 4.9±0.49 | 0.90±0.05 | 35.4±3.54 | 0.621±0.050 | 0.386±0.039 | 0.144±0.007 | 1.170±0.057 |

*The analytical chemistry laboratory did not provide uncertainties on individual U, Th, K or Rb concentrations. Based on replicate analyses, uncertainties of 10% were assumed for U, Th and Rb, and 5% for K, and these uncertainties were propagated through the dose rate calculations.

Table 2 Luminescence equivalent dose and age data.

| Site | Sample | Labcode | Analysis | Grain size (μm) | DR OD (%) | Total analysed* | n | OD (%) | Age model† | a value or Sigma-b‡ | D _e (Gy) | Age (ka) |
|---------------------|----------|-----------|----------|---------------------------------|--------------|--------------------|----|--------|---------------|------------------------|---------------------|----------|
| Brockhill Quarry | T6BROC01 | Shfd15171 | SA | 180-250 | 12 | 102 | 60 | 60 | IEU | 0.307 | 59.43±4.37 | 44.4±4.1 |
| | T6BROC02 | Shfd15013 | SA | 212-250 | | 96 | 48 | 65 | IEU | 0.307 | 58.97±4.66 | 39.1±3.8 |
| | T6BROC02 | Shfd15013 | SG | 212-250 | | 1600 | 29 | 36 | IEU | 0.307 | 68.96±11.8 | 45.8±8.2 |
| Glenuira Quarry | T6GULR01 | Shfd15172 | SA | 180-250 | | 76 | 53 | 45 | IEU | 0.307 | 55.68±2.71 | 25.2±1.9 |
| | T6GULR02 | Shfd15012 | SA | 180-250 | 6 | 144 | 51 | 65 | IEU | 0.307 | 49.3±2.71 | 24.1±1.9 |
| Lough Nacung | T6LNAC01 | Shfd15173 | SA | 180-250 | | 92 | 36 | 40 | IEU | 0.307 | 243±13 | 109±8.4 |
| | T6LNAC01 | Shfd15173 | SG | 180-250 | | 3200 | 33 | 34 | IEU | 0.189 | 77.8±5.01 | 83.8±6.9 |
| | T6LNAC02 | Shfd15014 | SA | 180-250 | 6 | 48 | 25 | 71 | IEU | 0.307 | 63.6±6.32 | 132±11 |
| Altwinny Bay | T7ALT02 | Shfd15166 | SA | 180-250 | | 97 | 35 | 56 | MAM | 0.20 | 54.0±8.16 | 30.4±4.9 |
| Carey Valley | T7CARV01 | Shfd15169 | SA | 212-250 | | 80 | 43 | 65 | MAM | 0.10 | 42.04±2.41 | 22.6±2.4 |
| | T7CARV02 | Shfd15018 | SA | 212-250 | 6 | 160 | 40 | 37 | MAM | 0.10 | 41.36±2.61 | 22.1±2.4 |
| Castleroe | T7CAST01 | Shfd15167 | SA | 212-250 | | 72 | 57 | 42 | MAM | 0.10 | 31.91±2.67 | 48.1±4.8 |
| | T7CAST02 | Shfd15016 | SA | 212-250 | 6 | 70 | 45 | 58 | MAM | 0.10 | 24.29±2.02 | 38.3±3.8 |
| Fawnmore | T7FAWN02 | Shfd15015 | SA | 212-250 | | 78 | 34 | 65 | MAM | 0.20 | 41.34±5.28 | 25.8±4.2 |
| | T7FAWN03 | Shfd15168 | SA | 212-250 | 20 | 103 | 45 | 70 | MAM | 0.20 | 46.43±7.08 | 27.1±3.7 |
| Glenshesk Valley | T7GLEN01 | Shfd15017 | SA | 212-250 | 17 | 120 | 52 | 70 | MAM | 0.20 | 36.66±3.32 | 30.4±4.2 |
| | T7GLEN02 | Shfd15170 | SA | 212-250 | | 78 | 55 | 80 | MAM | 0.20 | 32.24±2.42 | 23.6±3.4 |

*Total analysed is the number of small aliquots or single grains measured for a sample, while the column headed 'n' is the number of small aliquots of single grains accepted for De modelling.

†Shows the age model used, either the Minimum Age Model (MAM) or the internal–external uncertainty (IEU) model.

‡Where the IEU model was used, the first parameter 'a' is given in this column. The second parameter 'b' is 1.5 for all samples. For samples analysed using the MAM, the value given here is that for sigma b.

Table 3 Previously published BRITICE-CHRONO ¹⁴C ages included in this paper.

| Transect | Cruise-Core | Code | Sample ID | Latitude | Longitude | Depth (m) | Sample type | Sample depth (cm) | Stratigraphical context | Conventional Radiocarbon Age (years BP) | +/- 1σ (radiocarbon yrs BP) | Reference |
|----------|-------------|---------------|---|-----------|-----------|-----------|--------------------------------|-------------------|--|---|-----------------------------|------------------------------|
| T6 | CE08-018VC | UCIAMS-133552 | CE_08-018_CC | 54.98 | -9.92 | 122 | Mixed Forams | core catcher | Marine sands and gravels (deglacial), contained fine sands (w/forams) | 20170 | 90 | Ó Cofaigh <i>et al.</i> 2019 |
| T6 | JC106-92VC | Beta432793 | T6-92VC-259cm | 54.405517 | -9.1768 | 75 | Foraminifera-mixed benthic | 259-260 | Diamict | 16250 | 60 | Schiele, 2017 |
| T6 | JC106-97VC | Beta432794 | T6-97VC-468cm | 54.454783 | -9.17203 | 75 | Foraminifera-mixed benthic | 468-469 | Compact deformed mud | 16350 | 60 | Schiele, 2017 |
| T6 | JC106-099VC | UCIAMS-164429 | T6-099VC-474 | 54.60363 | -9.33564 | 99 | Foraminifera | 474 | From laminated clay and silts. Mid unit, no diamict at base. | 17180 | 80 | Ó Cofaigh <i>et al.</i> 2019 |
| T6 | JC106-101VC | UCIAMS-164431 | T6-101VC-548-551 | 54.61307 | -9.42068 | 100 | Foraminifera | 548-551 | From laminated clay and silts. Mid unit, no diamict at base. | 20110 | 120 | Ó Cofaigh <i>et al.</i> 2019 |
| T6 | JC106-102VC | UCIAMS-164437 | T6-102VC-247 | 54.62345 | -9.5189 | 90.5 | Foraminifera | 247 | From laminated clay and silts. Mid unit, no diamict at base. | 21000 | 110 | Ó Cofaigh <i>et al.</i> 2019 |
| T6 | JC106-103VC | SUERC-63558 | T6-103VC-145 | 54.64063 | -9.59722 | 100 | Foraminifera | 145 | From laminated clay and silts. Mid unit, no diamict at base. | 22521 | 70 | Ó Cofaigh <i>et al.</i> 2019 |
| T6 | JC106-112VC | SUERC-63584 | T6-112VC-51 | 54.84513 | -10.18137 | 125 | Shell fragment | 51 | Diamict interpreted as subglacial till | 22582 | 67 | Ó Cofaigh <i>et al.</i> 2019 |
| T6 | JC106-112VC | SUERC-63585 | T6-112VC-59.5 | 54.84513 | -10.18137 | 125 | Shell fragment | 59.5 | Diamict interpreted as subglacial till | 22572 | 71 | Ó Cofaigh <i>et al.</i> 2019 |
| T7 | JC106-125VC | SUERC-72873 | T7JC106-125VC11555.73367167-9.251471389 | 56.47296 | -8.70696 | 150 | Foraminifera, mixed assemblage | 223-225 | Glaciomarine/ice proximal: alternating laminated silt and clay with IRD rich mud, not overconsolidated | 20200 | 80 | Callard <i>et al.</i> , 2018 |
| T7 | JC106-125VC | SUERC-72874 | T7JC106-125VC11755.73367167-9.251471389 | 56.47296 | -8.70696 | 150 | Foraminifera, mixed assemblage | 369-372 | Glaciomarine/ice proximal: alternating laminated silt and clay with IRD rich mud, not overconsolidated | 22030 | 100 | Callard <i>et al.</i> , 2018 |
| T7 | JC106-146VC | UCIAMS-176382 | T7-146VC-223 | 56.48404 | -8.44641 | 158 | Foraminifera, mixed assemblage | 389-392 | Soft diamict, possibly glaciomarine/ice proximal - IRD | 17155 | 47 | Callard <i>et al.</i> , 2018 |
| T7 | JC106-149VC | SUERC-59509 | T7-149VC-421 | 56.39728 | -7.44881 | 136 | Shell fragment | 421 | | 20730 | 100 | Callard <i>et al.</i> , 2018 |
| T7 | JC106-151VC | UCIAMS-179841 | T7-151VC-389 | 56.14046 | -7.53772 | 122 | Foraminifera, mixed assemblage | 389-394 | | 19690 | 90 | Callard <i>et al.</i> , 2018 |
| T7 | JC106-153VC | UCIAMS-164432 | T7-153VC-277 | 56.25168 | -7.58738 | 113.5 | Foraminifera | 277-279 | Glaciomarine/ice proximal in a stiffer mud unit with some IRD | 19210 | 110 | Callard <i>et al.</i> , 2018 |
| T7 | JC106-154VC | UCIAMS-164433 | T7-154VC-211 | 56.32525 | -7.61805 | 138 | Foraminifera | 211-214 | Glaciomarine/ice distal/proximal | 18670 | 90 | Callard <i>et al.</i> , 2018 |

Table 4 All published BRITICE-CHRONO TCN ages.

| Transect | Code | Location | Region | Latitude | Longitude | Elev. (m) | Sample | Lithology | ¹⁰ Be age (ka) ¹ | CRONUScalc v2.0 ¹⁰ Be age (ka) ² | CRONUScalc v2.0 ³⁶ Cl age (ka) ² | Reference |
|----------|---------|-----------------------|----------------------|-----------|-----------|-----------|---------|-------------------------|--|--|--|----------------------|
| T6 | T6BS01 | English Valley | Blue Stack Mountains | 54.7228 | -8.1132 | 149 | boulder | Conglomerate | 13.1 ± 0.9 (0.7) | 13.1 ± 1.3 (0.7) | | Wilson et al. (2019) |
| T6 | T6BS02 | English Valley | Blue Stack Mountains | 54.7225 | -8.114 | 148 | boulder | Sandstone | 15.4 ± 1.0 (0.7) | 15.4 ± 1.4 (0.7) | | Wilson et al. (2019) |
| T6 | T6BS03 | English Valley | Blue Stack Mountains | 54.7231 | -8.1165 | 150 | boulder | Conglomerate | 14.9 ± 0.9 (0.7) | 14.9 ± 1.4 (0.7) | | Wilson et al. (2019) |
| T6 | T6BS04 | English Valley | Blue Stack Mountains | 54.7225 | -8.115 | 163 | boulder | Conglomerate | 14.4 ± 0.8 (0.4) | 14.4 ± 1.2 (0.4) | | Wilson et al. (2019) |
| T6 | T6GCS02 | Glencolumbkille | SW coast Donegal | 54.7079 | -8.761 | 41 | boulder | Schist (Qtz vein) | 16.2 ± 1.0 (0.7) | 16.2 ± 1.5 (0.7) | | Wilson et al. (2019) |
| T6 | T6GCS03 | Glencolumbkille | SW coast Donegal | 54.7076 | -8.7589 | 36 | boulder | Schist (Qtz vein) | 17.3 ± 1.1 (0.7) | 17.3 ± 1.6 (0.7) | | Wilson et al. (2019) |
| T6 | T6GCS04 | Glencolumbkille | SW coast Donegal | 54.7076 | -8.7589 | 34 | boulder | Schist (Qtz vein) | 16.5 ± 1.0 (0.7) | 16.5 ± 1.5 (0.7) | | Wilson et al. (2019) |
| T6 | T6PG01 | Poisoned Glen | Donegal | 55.01505 | -8.10675 | 73 | Boulder | Granite | 17.2 ± 1.1 (0.8) | 17.2 ± 1.6 (0.8) | | Wilson et al. (2019) |
| T6 | T6PG04 | Poisoned Glen | Donegal | 55.01495 | -8.10653 | 73 | Boulder | Granite | 16.2 ± 1.0 (0.8) | 16.2 ± 1.5 (0.8) | | Wilson et al. (2019) |
| T6 | T6PG05 | Poisoned Glen | Donegal | 55.01498 | -8.10572 | 75 | Boulder | Granite | 13.0 ± 0.9 (0.6) | 13.0 ± 1.2 (0.6) | | Wilson et al. (2019) |
| T6 | T6ROS01 | Rosguill | Donegal | 55.2269 | -7.84304 | 65 | Boulder | Granite | 18.7 ± 1.0 (0.6) | 18.7 ± 1.6 (0.6) | | Wilson et al. (2019) |
| T6 | T6ROS02 | Rosguill | Donegal | 55.2252 | -7.84062 | 105 | Boulder | Granite | 21.4 ± 1.4 (1.0) | 21.0 ± 2.0 (1.0) | | Wilson et al. (2019) |
| T6 | T6ROS04 | Rosguill | Donegal | 55.22412 | -7.84055 | 105 | Boulder | Granite | 18.9 ± 1.0 (0.6) | 18.9 ± 1.6 (0.6) | | Wilson et al. (2019) |
| T6 | T6BEN01 | Ben Bulbin | Sligo | 54.36215 | -8.4939 | 204 | Boulder | Sandstone | 13.0 ± 0.7 (0.5) | 13.0 ± 1.1 (0.5) | | Schiele (2017) |
| T6 | T6BEN02 | Ben Bulbin | Sligo | 54.361967 | -8.494217 | 198 | Boulder | Sandstone | 14.3 ± 0.8 (0.5) | 14.3 ± 1.2 (0.5) | | Schiele (2017) |
| T6 | T6BEN03 | Ben Bulbin | Sligo | 54.363433 | -8.494533 | 203 | Boulder | Sandstone | 14.3 ± 0.8 (0.5) | 14.3 ± 1.2 (0.5) | | Schiele (2017) |
| T6 | T6BEN04 | Ben Bulbin | Sligo | 54.363617 | -8.494717 | 200 | Boulder | Sandstone | 15.7 ± 0.9 (0.5) | 15.7 ± 1.4 (0.5) | | Schiele (2017) |
| T6 | T6KC01 | Kilcar | Donegal | 54.6187 | -8.6096 | 50 | Boulder | Dolerite | | 18.2 ± 1.7 (0.7) | | Wilson et al. (2019) |
| T6 | T6KC02 | Kilcar | Donegal | 54.6187 | -8.6096 | 50 | Boulder | Dolerite | | 37.5 ± 6.3 (2.1) | | Wilson et al. (2019) |
| T6 | T6KC03 | Kilcar | Donegal | 54.6187 | -8.6096 | 50 | Boulder | Dolerite | | 42.8 ± 6.1 (2.0) | | Wilson et al. (2019) |
| T6 | T6KC04 | Kilcar | Donegal | 54.6189 | -8.609 | 45 | Boulder | Dolerite | | 37.4 ± 5.4 (1.7) | | Wilson et al. (2019) |
| T6/T7 | T7MH02 | Malin Head | N Coast Donegal | 55.38112 | -7.37255 | 65 | Bedrock | Quartzite | 23.2 ± 1.4 (0.9) | 23.2 ± 2.1 (0.9) | | Wilson et al. (2019) |
| T6/T7 | T7MH03 | Malin Head | N Coast Donegal | 55.38156 | -7.37716 | 30 | Bedrock | Quartz vein (Quartzite) | 20.7 ± 1.1 (0.7) | 20.7 ± 1.8 (0.7) | | Wilson et al. (2019) |
| T6/T7 | T7MH04 | Malin Head | N Coast Donegal | 55.38033 | -7.37458 | 55 | Bedrock | Quartzite | 25.5 ± 2.1 (1.8) | 25.8 ± 2.8 (1.8) | | Wilson et al. (2019) |
| T7 | T7CAR02 | Carman Mor | Tiree | 56.45521 | -6.92344 | 136 | Boulder | Lewisian Gneiss | 21.1 ± 1.2 (0.7) | 21.1 ± 1.8 (0.7) | | Small et al. (2017) |
| T7 | T7CAR05 | Carman Mor | Tiree | 56.45464 | -6.92271 | 133 | Boulder | Lewisian Gneiss | 20.2 ± 1.1 (0.6) | 20.2 ± 1.7 (0.6) | | Small et al. (2017) |
| T7 | T7CAR07 | Carman Mor | Tiree | 56.45236 | -6.91878 | 111 | Boulder | Lewisian Gneiss | 20.8 ± 1.1 (0.7) | 20.9 ± 1.8 (0.7) | | Small et al. (2017) |
| T7 | T7MIN02 | Mingulay | Mingulay | 56.82096 | -7.63059 | 223 | Boulder | Lewisian Gneiss | 18.7 ± 1.0 (0.5) | 18.7 ± 1.6 (0.5) | | Small et al. (2017) |
| T7 | T7MIN03 | Mingulay | Mingulay | 56.82096 | -7.63059 | 223 | Bedrock | Lewisian Gneiss | 21.6 ± 1.1 (0.6) | 21.6 ± 1.8 (0.6) | | Small et al. (2017) |
| T7 | T7MIN04 | Mingulay | Mingulay | 56.81998 | -7.63172 | 196 | Boulder | Lewisian Gneiss | 17.4 ± 0.9 (0.5) | 17.4 ± 1.5 (0.5) | | Small et al. (2017) |
| T7 | T7MIN06 | Mingulay | Mingulay | 56.81521 | -7.63793 | 52 | Boulder | Lewisian Gneiss | 19.2 ± 1.0 (0.5) | 19.2 ± 1.6 (0.5) | | Small et al. (2017) |
| T7 | T7MIN07 | Mingulay | Mingulay | 56.81521 | -7.63793 | 52 | Bedrock | Lewisian Gneiss | 20.9 ± 1.1 (0.6) | 20.9 ± 1.8 (0.6) | | Small et al. (2017) |
| T7 | T7SGU02 | North Barra | North Barra | 57.05256 | -7.44933 | 65 | Boulder | Lewisian Gneiss | 17.4 ± 1.0 (0.6) | 17.4 ± 1.5 (0.6) | | Small et al. (2017) |
| T7 | T7SGU03 | North Barra | North Barra | 57.05273 | -7.44955 | 69 | Boulder | Lewisian Gneiss | 19.8 ± 1.1 (0.6) | 19.8 ± 1.7 (0.6) | | Small et al. (2017) |
| T7 | T7SGU04 | North Barra | North Barra | 57.05349 | -7.45106 | 78 | Boulder | Lewisian Gneiss | 17.0 ± 0.9 (0.6) | 17.0 ± 1.5 (0.6) | | Small et al. (2017) |
| T7 | T7TMC01 | Torr Mor a'Chonairist | Ross of Mull | 56.28791 | -6.34428 | 42 | Boulder | Schist | 17.3 ± 0.9 (0.5) | 17.3 ± 1.5 (0.5) | | Small et al. (2017) |
| T7 | T7TMC05 | Torr Mor a'Chonairist | Ross of Mull | 56.28716 | -6.34287 | 57 | Boulder | Granite | 17.8 ± 0.9 (0.5) | 17.8 ± 1.5 (0.5) | | Small et al. (2017) |
| T7 | T7TMC06 | Torr Mor a'Chonairist | Ross of Mull | 56.28617 | -6.3411 | 46 | Boulder | Granite | 17.9 ± 1.0 (0.6) | 18.0 ± 1.5 (0.6) | | Small et al. (2017) |
| T7 | S1 | Scriob na Caillich | Jura | 55.9176 | -6.0509 | 106 | Boulder | Quartzite | 17.6 ± 1.2 (0.8) | 17.5 ± 1.6 (0.8) | | Small et al. (2017) |
| T7 | S2 | Scriob na Caillich | Jura | 55.9172 | -6.0512 | 106 | Boulder | Quartzite | 16.5 ± 1.1 (0.8) | 16.4 ± 1.5 (0.8) | | Small et al. (2017) |
| T7 | S3 | Scriob na Caillich | Jura | 55.9176 | -6.0522 | 92 | Boulder | Quartzite | 15.0 ± 1.1 (0.8) | 14.9 ± 1.4 (0.8) | | Small et al. (2017) |

¹Calculated with calculator formerly known as the CRONUS-Earth calculator. (Developmental version; Wrapper script 2.3. Main calculator 2.1, constants 2.2.1, muons 1.1; Balco, et al., 2008) with LM scaling method. Loch Lomond reference production rate (LLPR) (see text), 1mm ka⁻¹ erosion rate, and one sigma external uncertainty (internal in brackets).

²Calculated with CRONUScalc v2.0 (Marrero et al. 2016) with LM scaling method, default global reference production rate, 1mm ka⁻¹ erosion rate, and one sigma external uncertainty (internal in brackets).

Table 5 All legacy and other TCN ages published after the beginning of the BRITICE-CHRONO project and included in the Bayesian age modelling.

| Site | Sample | ^{10}Be (ka) ¹ | CRONUScalc v2.0 ^{10}Be (ka) ² | CRONUScalc v2.0 ^{36}Cl (ka) ² | Material and context | Reference |
|---------------------------------------|-------------|------------------------------------|--|--|---|-----------------------------|
| DONEGAL | | | | | | |
| Malin Head | | | | 25.1 ± 1.1 | Glacially smoothed quartzite bedrock | Bowen et al. (2002) |
| Bloody Foreland | | | | 31.0 ± 17.0 | Not specified, but granite bedrock or boulder | Bowen et al. (2002) |
| Bloody Foreland | BF-01 | 21.2 ± 1.1 (1.0) | 21.0 ± 2.0 (1.1) | | Glacially transported granite boulder | Ballantyne et al. (2007) |
| | BF-02 | 18.5 ± 0.9 (0.8) | 18.6 ± 1.7 (0.9) | | Glacially transported granite boulder | |
| Bloody Foreland | BF-04-01 | 17.9 ± 1.7 (1.6) | 18.0 ± 2.3 (1.8) | | Glacially transported granite boulder | Clark et al. (2009b) |
| | BF-04-03 | 33.5 ± 2.7 (2.6) | 34.0 ± 4.0 (2.9) | | Glacially transported granite boulder | |
| | BF-04-04 | 21.8 ± 1.6 (1.5) | 22.0 ± 2.4 (1.7) | | Glacially transported granite boulder | |
| | BF-04-05 | 21.2 ± 1.7 (1.6) | 21.4 ± 2.5 (1.8) | | Glacially transported granite boulder | |
| | BF-04-06 | 21.2 ± 1.9 (1.9) | 21.4 ± 2.7 (2.1) | | Glacially transported granite boulder | |
| | BF-04-08 | 23.6 ± 2.0 (1.9) | 23.8 ± 2.8 (2.1) | | Glacially transported granite boulder | |
| | BF-04-09 | 21.7 ± 2.1 (2.0) | 21.9 ± 2.8 (2.2) | | Glacially transported granite boulder | |
| | BF-04-10 | 22.1 ± 2.0 (2.0) | 22.3 ± 2.8 (2.2) | | Glacially transported granite boulder | |
| Average | | 21.6 ± 0.7 | 21.7 ± 1.8 | | | |
| Aran Island | ARAN01 | 21.8 ± 0.9 (0.7) | 21.6 ± 1.9 (0.7) | | Glacially transported granite boulder | Cullen (2012) |
| | ARAN02 | 21.5 ± 0.9 (0.7) | 21.3 ± 1.8 (0.7) | | Granite bedrock | |
| Average | | 21.7 ± 0.8 | 21.5 ± 1.8 | | | |
| Glencolumbkille | MAL-03 | 17.8 ± 0.6 (0.5) | 17.9 ± 1.5 (0.5) | | Vein quartz in glacially transported schist boulder | Ballantyne et al. (2007) |
| | MAL-05 | 19.6 ± 0.7 (0.5) | 19.8 ± 1.7 (0.6) | | Vein quartz in schist roche moutonnée | |
| Errigal col | ERGL-COL-01 | 17.6 ± 0.8 (0.6) | 17.4 ± 1.5 (0.6) | | Glacially plucked quartzite bedrock | Ballantyne et al. (2013b) |
| | ERGL-COL-02 | 18.2 ± 0.7 (0.6) | 18.0 ± 1.5 (0.6) | | Glacially plucked quartzite bedrock | |
| | ERGL-COL-04 | 18.1 ± 0.8 (0.6) | 17.9 ± 1.6 (0.6) | | Glacially plucked quartzite bedrock | |
| Average | | 18.0 ± 0.6 | 17.8 ± 1.4 | | | |
| Slieve League | SL-02 | 17.1 ± 0.8 (0.7) | 16.9 ± 1.5 (0.7) | | Quartzite boulder from rockslope-failure debris | Ballantyne et al. (2013b) |
| | SL-03 | 17.8 ± 1.0 (0.9) | 17.6 ± 1.7 (0.9) | | Quartzite boulder from rockslope-failure debris | |
| | SL-04 | 17.1 ± 1.0 (0.9) | 16.9 ± 1.6 (0.9) | | Quartzite boulder from rockslope-failure debris | |
| Average | | 17.3 ± 0.6 | 17.1 ± 1.5 | | | |
| NORTH MAYO | | | | | | |
| Ox Mountains | OX-03-01 | 16.9 ± 1.4 (1.4) | 17.0 ± 2.0 (1.5) | | Vein quartz in glacially transported gneissic boulder | Clark et al. (2009c) |
| | OX-03-02 | 15.7 ± 1.5 (1.4) | 16.0 ± 2.0 (1.6) | | Vein quartz in glacially transported gneissic boulder | |
| | OX-03-03 | 16.4 ± 1.3 (1.3) | 16.4 ± 1.9 (1.4) | | Vein quartz in glacially transported gneissic boulder | |
| | OX-03-05 | 16.9 ± 1.3 (1.2) | 16.9 ± 1.9 (1.4) | | Vein quartz in glacially transported gneissic boulder | |
| | OX-03-06 | 17.0 ± 1.7 (1.7) | 17.0 ± 2.3 (1.8) | | Vein quartz in glacially transported gneissic boulder | |
| Average | | 16.6 ± 0.6 | 16.7 ± 1.5 | | | |
| | OX-03-07 | 19.1 ± 1.6 (1.5) | 19.1 ± 2.3 (1.7) | | Vein quartz in glacially transported gneissic boulder | Clark et al. (2009c) |
| | OX-03-09 | 20.9 ± 1.5 (1.4) | 21.1 ± 2.3 (1.6) | | Vein quartz in glacially transported gneissic boulder | |
| | OX-03-10 | 20.5 ± 1.9 (1.8) | 20.7 ± 2.6 (2.0) | | Vein quartz in glacially transported gneissic boulder | |
| Average | | 20.2 ± 1.1 | 20.3 ± 1.9 | | | |
| HEBRIDES AND SCOTTISH MAINLAND | | | | | | |
| Arran : Glen Dougarie | D1 | 16.1 ± 1 | | | Glacially transported granite boulder | Finlayson et al. (2014) |
| | D2 | 16.9 ± 1 | | | Glacially transported granite boulder | |
| South Uist : Beinn Mhor col | BM-2 | 16.3 ± 0.9 | | | Strongly ice-moulded gneiss bedrock | Stone and Ballantyne (2006) |
| Jura: Scriob na Caillich RSF | SNC02 | 14 ± 1.7 | | | Quartzite boulder | Ballantyne et al., (2014) |
| | SNC03 | 12.3 ± 1.4 | | | Quartzite boulder | |
| | SNC06 | 16.8 ± 1.1 | | | Quartzite boulder | |
| | SNC07 | 16.8 ± 1 | | | Quartzite boulder | |

¹Calculated with calculator formerly known as the CRONUS-Earth calculator (Developmental version; Wrapper script 2.3, Main calculator 2.1, constants 2.2.1, muons 1.1; Balco, et al., 2008) with LM scaling method, Loch Lomond reference production rate (LLPR) (see text), 1mm ka⁻¹ erosion rate, and one sigma external uncertainty (internal in brackets).

²Calculated with CRONUScalc v2.0 (Marrero et al. 2016) with LM scaling method, default global reference production rate, 1mm ka⁻¹ erosion rate, and one sigma external uncertainty (internal in brackets).

Table 6 Previously published legacy ¹⁴C ages.

| Site | Code | Sample type | Stratigraphical context | Conventional Radiocarbon Age (years BP) | +/- 1σ (radiocarbon yrs BP) | Quality | Reference |
|------------------------------|------------|------------------------------------|---|---|-----------------------------|-----------------------|-------------------------|
| TRANSECT 6 | | | | | | | |
| Derryvree | BIRM-166 | TOC | Moss-rich mud overlaid by proglacial sands and till | 30500 | 1100 | Red (because pre-LGM) | Colhoun et al. (1972) |
| | SSR-2713 | Mollusc | | 16940 | 120 | Green | McCabe et al. (1986) |
| | AA53589 | Mollusc | Laminated muds and sands and diamictons interpreted as glaciomarine sediments over glacially striated rock surface | 16980 | 120 | | |
| | AA56703 | Foraminifera | | 16627 | 83 | | |
| Belderg Pier, Co. Mayo | AA56704 | Foraminifera | | 16830 | 130 | Green | McCabe et al. (2005) |
| | AA56706 | Mollusc | | 16389 | 74 | | |
| | AA56707 | Mollusc | | 16328 | 67 | | |
| Fiddauntawanoneen Co. Mayo | SSR-2714 | Mollusc | | 17370 | 100 | Yellow | McCabe et al. (1986) |
| | OxA-3693 | Bone (Red Deer) | | 13622.5 | 136.5 | | |
| | OxA-3706 | Bone (Brown Bear) | Faunal remains in a very thin series of earth and clay strata above "sterile" deposit | 13776.5 | 105.5 | | |
| Kesh Corran Caves, Co. Sligo | OxA-3708 | Bone (Wolf) | | 13030 | 118 | Yellow | Woodman et al. (1997) |
| | OxA-5736 | Bone (Hare) | | 14029.5 | 210.5 | | |
| TRANSECT 7 | | | | | | | |
| Sourlie | SRR3023 | Antler of <i>Rangifer tarandus</i> | Fluvialite sediments between two glacial diamictons | 29900 | 430 | Red (because pre-LGM) | Jardine et al. (1998) |
| | SRR3146 | Plant debris | | 29290 | 350 | | |
| | AA45968 | | | 16120 | 160 | | |
| | AA45967 | | | 15490 | 150 | | |
| Corvish | AA45966 | Foraminifera | Glaciotectonised sediments | 16460 | 430 | Green | McCabe and Clark (2003) |
| | AA33831 | | | 15425 | 95 | | |
| West of Islay | SUERC13122 | Shell | Glaciomarine sediments | 13103 | 40 | Green | Peacock (2008) |
| | SUERC13123 | | | 13054 | 39 | | |
| Loch Indaal | SUERC13124 | Shell | Glaciomarine sediments | 13120 | 39 | Green | Peacock (2008) |
| | | | Mud with occasional dropstones and pecten in life position interpreted as glacial diamict capped by sediments indicating glaciomarine and fully marine conditions | | | | |
| Loch Sunart | UL2853 | Mollusc (<i>Pecten Maximus</i>) | | 14020 | 210 | Green | Baltzer et al. (2010) |
| | | | | | | | |
| Lochgiphead | OxA-1697 | Shell | Glaciomarine sediments | 14481 | 303 | | |
| | OxA-1698 | | | 14848 | 302 | Yellow | Hedges et al. (1989) |

Table 7 The modelled boundary limit ages for the MSIS and DBIS. All boundary ages are expressed as ± 1 sigma. Ages marked * are identified as outliers that did not influence the modelled outputs. Model structures show the named Phases in the Bayesian age models and groups of dating information for the models.

| Malin Sea Ice Stream (T7) | | | | | Donegal Bay Ice Stream (T6) | | | | | |
|----------------------------------|------------------------------|-----------------|----------------|----------------|---------------------------------|---------------------------------------|-----------------|-----------------|--------------------------------|--|
| Model structure | Age information | Modelled age | Boundary age | | Model structure | Age information | Modelled age | Boundary age | | |
| Boundary Base: ice-free Scotland | | | | 34.4 \pm 1.8 | Boundary Base: ice-free Ireland | | | | 35.1 \pm 3.2 | |
| Phase free ages | Sourlie-SRR3023 | 29.9 \pm 0.4 | 33.5 \pm 0.5 | | Phase Zone 1 | Derryvree: BIRM-166 | 30.5 \pm 1.1 | 33.5 \pm 1.2 | | |
| | Sourlie-SRR3146 | 29.2 \pm 0.4 | 32.9 \pm 0.5 | | Boundary BLO-Build-up of ice | | | | 26.6 \pm 1.3 | |
| Boundary BLO-base | | | | 27.9 \pm 2.2 | | JC106-112VC-51 | 22.6 \pm 0.07 | 26.4 \pm 0.1 | | |
| Phase Zone 1 | T7JC106-125VC117 | 22.9 \pm 0.06 | 26.8 \pm 0.2 | | Phase Zone UC106-112VC-59.5 | | | | 22.6 \pm 0.07 26.4 \pm 0.1 | |
| | T7JC106-125VC115 | 22.8 \pm 0.06 | 26.7 \pm 0.3 | | Boundary BL1 | | | | 26.3 \pm 0.1 | |
| Boundary BL1 | | | | 26.3 \pm 0.3 | | T6CE-08-018_CC | 20.2 \pm 0.09 | 23.8 \pm 0.2 | | |
| Phase Zone 2 | UCIAMS-164440 T7-146VC-389 | 20.7 \pm 0.1 | 24.4 \pm 0.3 | | Phase Zone 2 | SUERC-63558 T6-103VC-145 | 22.5 \pm 0.07 | 26.2 \pm 0.2 | | |
| | UCIAMS-176383 T7-146VC-369 | 22.0 \pm 0.1 | 25.9 \pm 0.1 | | | UCIAMS-164437 T6-102VC-247 | 21.0 \pm 0.1 | 24.8 \pm 0.2 | | |
| | UCIAMS-176382 T7-146VC-223 | 20.2 \pm 0.08 | 23.9 \pm 0.2 | | | UCIAMS-164431 T6-101VC-548-551 | 20.1 \pm 0.1 | 23.8 \pm 0.2 | | |
| Boundary BL2 | | | | 23.5 \pm 0.3 | Boundary BL2 | | | | 22.9 \pm 0.7 | |
| Phase Zone 3 | UCIAMS-179841 T7_151VC_389 | 19.7 \pm 0.1 | 23.1 \pm 0.3 | | | ARAN01 | 21.8 \pm 0.9 | 21.6 \pm 0.6 | | |
| | UCIAMS-164432 T7-153VC-277 | 19.2 \pm 0.1 | 22.7 \pm 0.3 | | | ARAN02 | 21.5 \pm 0.9 | 21.5 \pm 0.6 | | |
| | UCIAMS-164433 T7-154VC-211 | 18.7 \pm 0.1 | 22.2 \pm 0.3 | | | BF-01 Bloody Foreland | 21.2 \pm 1.1 | 21.4 \pm 0.6 | | |
| Boundary BL3 | | | | 22 \pm 0.3 | | BF-02 Bloody Foreland | 18.5 \pm 0.9 | * | | |
| | BF-01 Bloody Foreland | 21.2 \pm 1.1 | 21.6 \pm 0.4 | | Phase Zone 3 | BF-04-01 Bloody Foreland | 17.9 \pm 1.7 | * | | |
| | BF-02 Bloody Foreland | 18.5 \pm 0.9 | * | | | BF-04-04 Bloody Foreland | 21.8 \pm 1.6 | 21.6 \pm 0.7 | | |
| | BF-04-01 Bloody Foreland | 17.9 \pm 1.7 | * | | | BF-04-05 Bloody Foreland | 21.2 \pm 1.7 | 21.5 \pm 0.7 | | |
| | BF-04-04 Bloody Foreland | 21.8 \pm 1.6 | 21.6 \pm 0.4 | | | BF-04-06 Bloody Foreland | 21.2 \pm 1.9 | 21.5 \pm 0.7 | | |
| | BF-04-05 Bloody Foreland | 21.2 \pm 1.7 | 21.6 \pm 0.4 | | | BF-04-08 Bloody Foreland | 23.6 \pm 2.0 | 21.8 \pm 0.7 | | |
| | BF-04-06 Bloody Foreland | 21.2 \pm 1.9 | 21.6 \pm 0.4 | | | BF-04-09 Bloody Foreland | 21.7 \pm 2.0 | 21.6 \pm 0.7 | | |
| Phase Zone 4 | BF-04-08 Bloody Foreland | 23.6 \pm 2.0 | 21.7 \pm 0.4 | | | BF-04-10 Bloody Foreland | 22.1 \pm 2.0 | 21.6 \pm 0.7 | | |
| | BF-04-09 Bloody Foreland | 21.7 \pm 2.0 | 21.6 \pm 0.4 | | Boundary BL3 | | | | 20.5 \pm 0.3 | |
| | BF-04-10 Bloody Foreland | 22.1 \pm 2.0 | 21.6 \pm 0.4 | | | UCIAMS-164429 T6-099VC-474 | | 20.2 \pm 0.2 | | |
| | T7ALT802 Altwinny Bay | 30.4 \pm 4.9 | * | | | SSR-2713 Belderg Pier, Co. Mayo | 16.9 \pm 0.1 | 19.9 \pm 0.2 | | |
| | T7FAWN02 Fawnmore | 25.8 \pm 4.2 | 21.7 \pm 0.4 | | | SSR-2714 Fiddauntawnanoneen, Co. Mayo | 17.4 \pm 0.1 | 20.3 \pm 0.3 | | |
| | T7FAWN03 Fawnmore | 27.1 \pm 3.7 | 21.7 \pm 0.4 | | | AA56707 Belderg Pier, Co. Mayo | 16.3 \pm 0.07 | 19.3 \pm 0.2 | | |
| | T7MH04, Malin Head | 25.5 \pm 2.1 | 21.7 \pm 0.4 | | | AA56706 Belderg Pier, Co. Mayo | 16.4 \pm 0.07 | 19.3 \pm 0.2 | | |
| | T7MH02 Malin Head | 23.2 \pm 1.4 | 21.7 \pm 0.4 | | Phase Zone 4 | AA56704 Belderg Pier, Co. Mayo | 16.8 \pm 0.1 | 19.8 \pm 0.2 | | |
| | T7MH03 Malin Head | 20.7 \pm 1.1 | 21.6 \pm 0.4 | | | AA53589 Belderg Pier, Co. Mayo | 16.6 \pm 0.08 | 20 \pm 0.2 | | |
| Boundary BL4 | | | | 21.2 \pm 0.5 | | AA56703 Belderg Pier, Co. Mayo | 16.6 \pm 0.08 | 19.6 \pm 0.1 | | |
| | T7CAR02 Tiree | 21.1 \pm 1.2 | 20.6 \pm 0.5 | | | Beta432794 JC106-97VC-468cm | 16.8 \pm 0.06 | 19.8 \pm 0.1 | | |
| | T7CAR05 Tiree | 20.2 \pm 1.1 | 20.5 \pm 0.4 | | | Beta432793 JC106-92VC-259cm | 16.5 \pm 0.06 | 19.5 \pm 0.1 | | |
| | T7CAR07 Tiree | 20.8 \pm 1.1 | 20.5 \pm 0.5 | | | T6GULR01 | 24.1 \pm 1.9 | * | | |
| Phase Zone 5 | T7CARV01 Carey Valley | 22.6 \pm 2.4 | 20.6 \pm 0.5 | | | T6GULR02 | 25.2 \pm 1.9 | * | | |
| | T7CARV02 Carey Valley | 22.1 \pm 2.4 | 20.6 \pm 0.5 | | Boundary BL4 | | | | 19 \pm 0.4 | |
| | T7GLEN01 Glenshesk Valley | 30.4 \pm 4.2 | * | | | T6ROS01 Rosguill | 18.7 \pm 1.0 | 18.2 \pm 0.6 | | |
| | T7GLEN02 Glenshesk Valley | 23.6 \pm 3.4 | 20.6 \pm 0.5 | | | T6ROS02 Rosguill | 21.4 \pm 1.4 | * | | |
| | SUERC-59509 T7-149VC-421 | 17.1 \pm 0.05 | 20.3 \pm 0.2 | | | T6ROS03 Rosguill | 18.9 \pm 1.0 | 18.2 \pm 0.6 | | |
| Boundary BL5 | | | | 20 \pm 0.3 | | T6GCS-02 | 16.2 \pm 1.0 | 17.3 \pm 0.6 | | |
| Phase Zone 6 | T6ROS01 Rosguill | 18.7 \pm 1.0 | 19.7 \pm 0.3 | | | T6GCS-03 | 17.3 \pm 1.1 | 17.7 \pm 0.6 | | |
| | T6ROS02 Rosguill | 21.4 \pm 1.4 | 19.8 \pm 0.3 | | | T6GCS-04 | 16.5 \pm 1.0 | 17.4 \pm 0.6 | | |
| | T6ROS03 Rosguill | 18.9 \pm 1.0 | 19.7 \pm 0.3 | | | MAL03 | 17.8 \pm 0.6 | 17.8 \pm 0.5 | | |
| Boundary BL6 | | | | 19.5 \pm 0.3 | | MAL05 | 19.6 \pm 0.7 | * | | |
| | T7MIN02 Mingulay | 18.7 \pm 1.0 | 19.3 \pm 0.3 | | Phase Zone 5 | T6KC-01 | 37.4 \pm 5.4 | 17.9 \pm 0.7 | | |
| Phase Zone 7 | T7MIN03 Mingulay | 21.6 \pm 1.1 | 19.3 \pm 0.3 | | | T6KC-02 | 37.5 \pm 6.3 | * | | |
| | T7MIN04 Mingulay | 17.4 \pm 0.9 | 19.2 \pm 0.3 | | | T6KC-03 | 42.8 \pm 6.1 | * | | |
| | T7MIN06 Mingulay | 19.2 \pm 1.0 | 19.3 \pm 0.3 | | | T6KC-04 | 37.4 \pm 5.4 | * | | |
| | T7MIN07 Mingulay | 20.9 \pm 1.1 | 19.3 \pm 0.3 | | | ERGL-Col-01 | 17.6 \pm 0.8 | 17.7 \pm 0.6 | | |
| Boundary BL7 | | | | 19 \pm 0.3 | | ERGL-Col-02 | 18.2 \pm 0.7 | 18.1 \pm 0.5 | | |
| | AA45968 Corvish | 16.1 \pm 0.2 | 18.8 \pm 0.3 | | | ERGL-Col-04 | 18.1 \pm 0.8 | 18 \pm 0.6 | | |
| Phase Zone 8 | AA45967 Corvish | 14.5 \pm 0.2 | 18.4 \pm 0.2 | | | SL-02 | 17.1 \pm 0.8 | 17.5 \pm 0.6 | | |
| | AA45966 Corvish | 16.5 \pm 0.4 | 18.8 \pm 0.3 | | | SL-03 | 17.8 \pm 1.0 | 17.8 \pm 0.6 | | |
| | AA33831 Corvish | 15.4 \pm 0.1 | 18.3 \pm 0.2 | | | SL-04 | 17.1 \pm 1.0 | 17.6 \pm 0.6 | | |
| Boundary BL8 | | | | 18.1 \pm 0.7 | | T6PG-01 | 17.2 \pm 1.1 | 17.7 \pm 0.6 | | |
| | S1 Jura | 17.6 \pm 1.2 | 17.1 \pm 0.9 | | | T6PG-04 | 16.2 \pm 1.0 | 17.3 \pm 0.6 | | |
| | S2 Jura | 16.5 \pm 1.1 | 16.5 \pm 1.1 | | | T6PG-05 | 13.0 \pm 0.9 | * | | |
| | S3 Jura | 15.0 \pm 1.1 | 15 \pm 1.1 | | Boundary BL5 | | | | 16.8 \pm 0.5 | |
| | SNC-06 Jura | 16.8 \pm 1.1 | 16.7 \pm 1.1 | | | OX-03-01 | 16.9 \pm 1.4 | 16.2 \pm 0.6 | | |
| | SNC-07 Jura | 16.8 \pm 1.0 | 16.7 \pm 0.9 | | Phase Zone 6 | OX-03-02 | 15.7 \pm 1.5 | 16.1 \pm 0.6 | | |
| | SNC-02 Jura | 14.0 \pm 1.7 | * | | | OX-03-03 | 16.4 \pm 1.3 | 16.1 \pm 0.6 | | |
| | SNC-03 Jura | 12.3 \pm 1.4 | * | | | OX-03-05 | 16.9 \pm 1.3 | 16.2 \pm 0.6 | | |
| Phase Zone 9 | T7SGU02 North Barra | 17.4 \pm 1.0 | 17.1 \pm 0.9 | | | OX-03-06 | 17.0 \pm 1.7 | 16.2 \pm 0.6 | | |
| | T7SGU03 North Barra | 19.8 \pm 1.1 | * | | Boundary BL6 | | | | 15.3 \pm 0.6 | |
| | T7SGU04 North Barra | 17.0 \pm 0.9 | 16.9 \pm 0.9 | | | T6BS-04 | 14.4 \pm 0.8 | 14.5 \pm 0.5 | | |
| | T7TMC01 Torr Mor a'Chonairst | 17.3 \pm 0.9 | 17.1 \pm 0.9 | | | T6BS-01 | 13.1 \pm 0.9 | * | | |
| | T7TMC05 Torr Mor a'Chonairst | 17.8 \pm 0.9 | 17.3 \pm 0.9 | | | T6BS-02 | 15.4 \pm 1.0 | * | | |
| | T7TMC06 Torr Mor a'Chonairst | 17.9 \pm 1.0 | 17.3 \pm 0.9 | | Phase Zone 7 | T6BS-03 | 14.9 \pm 0.9 | 14.6 \pm 0.5 | | |
| | Arran D1 | 16.1 \pm 1.0 | 16.2 \pm 0.9 | | | T6BEN01 | 13.0 \pm 0.7 | * | | |
| | Arran D2 | 16.9 \pm 1.0 | 16.8 \pm 0.9 | | | T6BEN02 | 14.3 \pm 0.8 | 14.5 \pm 0.5 | | |
| | SUERC13122 W Islay | 13.1 \pm 0.04 | 15.2 \pm 1.6 | | | T6BEN03 | 14.3 \pm 0.8 | 14.5 \pm 0.5 | | |
| | SUERC13123 Loch Indaal | 13.1 \pm 0.04 | 15.1 \pm 1.2 | | | T6BEN04 | 15.7 \pm 0.9 | 15.7 \pm 0.9 | | |
| | SUERC13124 Loch Indaal | 13.1 \pm 0.04 | 15.2 \pm 1.4 | | Boundary Ice free Midlands | | | | 13.9 \pm 0.4 | |
| | UL2853 Baltzer | 14.0 \pm 0.2 | 17 \pm 0.9 | | | OxA-3706 | 13.8 \pm 0.1 | 13.4 \pm 0.3 | | |
| Boundary BL9 | | | | 14.9 \pm 1.5 | | Phase Zone 7 | OxA-3693 | 13.6 \pm 0.14 | * | |
| | OxA-1698 | 14.9 \pm 0.3 | 14.7 \pm 1.6 | | | OxA-3708 | 13.0 \pm 0.1 | * | | |
| Zone 10 | OxA-1697 | 14.5 \pm 0.3 | 14.6 \pm 1.5 | | | OxA-5736 | 14.0 \pm 0.2 | 13.6 \pm 0.3 | | |
| Boundary BL10-end | | | | 14.3 \pm 1.8 | Boundary End of sequence | | | | 13.1 \pm 0.9 | |

Figure captions

Figure 1: Main map presents an overview of the study area showing the west coast of Scotland and northwest of Ireland with the locations of legacy and BRITICE-CHRONO samples used in this paper, as well as other locations mentioned in the text. Background bathymetry and topography were downloaded from the EMODnet data services (<https://portal.emodnet-bathymetry.eu/services/>) and are presented here as shaded-relief with 20x vertical exaggeration to visualise specifically the geomorphological features on the shelf (colour scale is only indicative due to processing). Inset presents the proposed maximum ice extent, the outline of the Donegal-Barra Fan (DBF) and mapped moraines and grounding-zone wedges (GZW) in the region (from [BRITICE Glacial Map v2.0](#); Clark et al., 2017 and references therein); the location of ice streams, main ice flow directions and ice flow divides (see Greenwood and Clark, 2009a, Greenwood and Clark, 2009b); and the location of BRITICE-CHRONO transects 6 (Donegal Bay) and 7 (Malin Sea) discussed in this paper.

Figure 2: A) Serial section of the main exposure at Altwinny Bay. OSL sample locations are indicated by the labelled red dots, whilst the boxes labelled B-F show the coverage of the facies photographs in panels B-F. Note that clast depictions are not to scale but are instead representative of relative grain size variation between units. B-F) photographs of the main facies exposed. The OSL sample locations T7ALTB01 and 02 are indicated by the red circles. The white arrows highlight some of the abundant erratic clasts within the section that are likely carried to the site by Malin Sea ice.

Figure 3: Optically-stimulated luminescence data. Abanico plots (Dietze, et al., 2016) of the D_e values determined for OSL dating applied at (A) Altwinny Bay, (B) Carey Valley, (C) Castleroe, (D) Fawnmore, and (E) Glenshesk Valley. The plots present the D_e distributions in two plots that share a common z-axis of D_e values: (i) a bivariate plot where each D_e value is presented in relation to its precision (shown on the x-axis, where those more precisely known are plotted to the right); and (ii) a univariate plot showing the age frequency distribution of D_e values, which does not give any presentation of the precision of individual D_e values. The grey shading across both plots shows the D_e used in age calculation for each distribution (2σ shown on they-axis). The combination of these two plots aids interpretation of the scatter in the D_e distributions, where samples with a greater range of D_e values on the z-axis have larger amounts of scatter in the D_e distribution.

Figure 4: Photographs of exposures at Fawnmore Quarry A) section 1 and B) section 2. The labelled boxes show the locations covered by the photographs in C-E. Close-up photographs of the units from which C) T7FAWN01, D) T7FAWN02, and E) T7FAWN03 were sampled. The circles highlight sample positions.

Figure 5 A) Generalized vertical log and environmental interpretation of the sediments exposed at Castleroe with X-axis scaling denoting C (clay), Si (silt), S (sand), G (Gravel) and Dm (diamicton). Standard lithofacies codes follow Evans and Benn (Fig. 2.15: 2004), with prefixes F (fines), S (sand), G (gravel), D (diamict), and suffixes planar (p) or trough (t) cross-stratification, delta foresets (fo), massive or structureless (S/Fm), horizontal stratification (h), rippled (r), laminations (l) with or without drop-stones (d), gravels matrix-supported massive (Gms), gravels clast-supported massive (Gm), diamict matrix-supported, massive (Dmm) and diamict matrix-supported stratified (Dms). OSL sample positions are indicated by the labelled crossed circles. The labelled bars along the depth

1
2 axis indicate the coverage of photographs in B-C. B, C) Photographs of the units sampled
3 for OSL dating. The OSL sample locations are indicated by the labelled circles.
4

5 Figure 6 A) Photomontage of the main section at Glenshesk Valley. Lithofacies codes are
6 the same as Fig. 5 (see Evans and Benn, 2004). The labelled boxes show the locations
7 covered by the photographs in B-C. Close-up photographs of the units from which B)
8 T7GLEN01 and C) T7GLEN02 were sampled. The circles highlight sample positions.
9

10 Figure 7: A) Generalized vertical succession of sediments exposed within Carey Valley
11 (after McCabe and Eyles, 1988). Lithofacies codes are the same as Fig. 5 (see Evans and
12 Benn, 2004). OSL sample positions are indicated by the labelled crossed circles. The
13 labelled bars along the depth axis indicate the coverage of photographs in B-C. B, C)
14 Photographs of the units sampled for OSL dating. The OSL sample locations are indicated
15 by the circles.
16
17

18 Figure 8: A) Annotated photo-montage of the main section at Lough Nacung quarry.
19 Lithofacies codes are the same as Fig. 5 (see Evans and Benn, 2004). The labelled boxes
20 indicate the locations of photographs shown in B-C. Close-up photographs of the units
21 sampled for B) T6LNAC01 and C) T6LNAC02. The circles highlight the position of the OSL
22 samples.
23
24

25 Figure 9: Optically-stimulated luminescence data. Abanico plots (Dietze, et al., 2016) of
26 the D_e values determined for OSL dating applied at (A) Brockhill Quarry, (B) Glenulra, and
27 (C) Lough Nacung. The plots present the D_e distributions in two plots that share a
28 common z-axis of D_e values: (i) a bivariate plot where each D_e value is presented in
29 relation to its precision (shown on the x-axis, where those more precisely known are
30 plotted to the right); and (ii) a univariate plot showing the age frequency distribution of D_e
31 values, which does not give any presentation of the precision of individual D_e values. The
32 grey shading across both plots shows the D_e used in age calculation for each distribution
33 (2σ shown on they-axis). The combination of these two plots aids interpretation of the
34 scatter in the D_e distributions, where samples with a greater range of D_e values on the
35 z-axis have larger amounts of scatter in the D_e distribution.
36
37
38

39 Figure 10: A) Generalized vertical succession of the sediments in Glenulra valley (after
40 McCabe, et al., 2007a). Lithofacies codes are the same as Fig. 5 (see Evans and Benn,
41 2004). The location of photographs in panels B and C are indicated by the labelled bars
42 along the depth axis. Photographs of the units sampled for B) T6GULR02 and C)
43 T6GULR01 with sample locations are indicated by the circles.
44
45

46 Figure 11: A) Generalized vertical succession of the sediments at Brockhill Quarry (after
47 McCabe, et al., 1986). Lithofacies codes are the same as Fig. 5 (see Evans and Benn,
48 2004). The location of photographs in panels B and C are indicated by the labelled bars
49 along the depth axis. Photographs of the units sampled for B) T6BROC01 and C)
50 T6BROC02 with sample locations are indicated by the circles.
51
52

53 Figure 12: Bayesian chronosequence age-model output of dating constraints using Oxcal
54 4.3. (A) the MSIS (T7) and (B) DBIS (T6). The model structure shown uses OxCal
55 brackets (left) and keywords that define the relative order of events (Bronk Ramsey,
56 2009a). Each original distribution (hollow) represents the relative probability of each age
57 estimate with posterior density estimate (solid) generated by the modelling. Shown are
58 ^{14}C ages (black), OSL ages (orange), cosmogenic nuclide ages (blue) and modelled
59 boundary ages (Red). Outliers are denoted by '?' and their probably (P) of being an outlier
60 indicated by low values <5 (95% confidence). Model agreement indices for individual ages

1
2 show their fit to the model with >60% the widely used threshold for 'good' fit (Bronk
3 Ramsey, 2009b).
4

5 Figure 13: Maximum and retreat grounding-line positions for the Malin Shelf Ice Stream
6 (T7 transect) and across the present-day coastal hinterland. Location of the
7 geochronological sites constraining the Bayesian modelling, modelled ages for retreat
8 positions, major moraines and grounding-zone wedges on the shelf and on land (from
9 [BRITICE Glacial Map v2.0](#); Clark et al., 2017 and references therein) and isochrones are
10 shown. 'BL' = Boundary Layers pre-LGM ice free to 10. Background bathymetry and
11 topography from EMODnet data services (<https://portal.emodnet-bathymetry.eu/services/>).
12
13

14 Figure 14: Maximum and retreat grounding-line positions for the Donegal Bay Ice Stream
15 (T6 transect) and across the present-day coastal hinterland. Location of the
16 geochronological sites constraining the Bayesian modelling, modelled ages for retreat
17 positions, moraines on the shelf and on land (from [BRITICE Glacial Map v2.0](#); Clark et al.,
18 2017 and references therein) and isochrones are shown. 'BL' = Boundary Layers pre-LGM
19 ice free to 8. Background bathymetry and topography from EMODnet data services
20 (<https://portal.emodnet-bathymetry.eu/services/>).
21
22

23 Figure 15: For A) the Donegal Bay Ice Stream and B) the Malin Sea Ice Stream, all plotted
24 against age (ka) showing, (bottom) the boundary ages (circle and ± 1 sigma whisker plots)
25 and retreat zones of the respective Bayesian models and the rates of net axial ice margin
26 retreat. (Middle) Modelled palaeo water depths (relative to present day bathymetry) for the
27 inner and outer shelf derived from a glacial isostatic adjustment (GIA) model (Bradley, et
28 al., 2011) updated to include the latest BRITICE-CHRONO ice sheet reconstruction and
29 accounting for global ice sheet variations. (Top) Mean and 95% ice bed elevations from
30 the NextMap elevation and EMODnet bathymetry (www.emodnet-hydrography.eu/). C) Ice
31 rafted debris (IRD) flux records from marine cores within the Donegal-Barra Fan MD04-
32 2822 (Hibbert, et al., 2009) and MD05-2006 (Knutz, et al., 2001, Knutz, et al., 2002)
33 plotted against an updated (Waelbroeck, et al., 2019). Heinrich Events H2 and H1 are
34 highlighted grey (Bond, et al., 1992). D) Ocean-climate parameters showing (bottom) sea
35 surface temperature records determined for the North Atlantic using SST ($^{\circ}\text{C}$) calculated
36 using planktonic foraminifera for core SO82-02 at 59°N , 31°W (red line) (Rasmussen, et
37 al., 2016, Van Kreveld, et al., 2000) plotted using an updated age model (Waelbroeck, et
38 al., 2019) and the MD01-2461 site from the Porcupine Seabight at 51.7°N , 12.9°W (blue
39 line) (Peck, et al., 2006, Peck, et al., 2007). (Middle) $\delta^{18}\text{O}$ concentrations, Greenland
40 Stadials (GS) and Interstadials (GI) from the GISP2 and GRIP Greenland ice cores
41 (Rasmussen, et al., 2014), plotted with and modelled surface-air temperatures (black line)
42 relative to present for land masses north of $\sim 45^{\circ}\text{N}$ (Bintanja, et al., 2005). (Top) Ice
43 volume equivalent sea level (Lambeck, et al., 2014) and summer insolation (pecked) for
44 60°N (Berger and Loutre, 1991).
45
46
47
48
49

50 Figure 16: Overview of modelled isochrones and retreat rates across the two transects of
51 the Malin Sea and Donegal Bay Ice Streams with relevant geomorphological context (from
52 [BRITICE Glacial Map v2.0](#); Clark et al., 2017 and references therein). Dashed lines
53 indicate more tentative isochrone positions due to lack of geomorphological evidence at
54 the required spatial resolution. Background bathymetry and topography from EMODnet
55 data services (<https://portal.emodnet-bathymetry.eu/services/>).
56
57
58
59
60

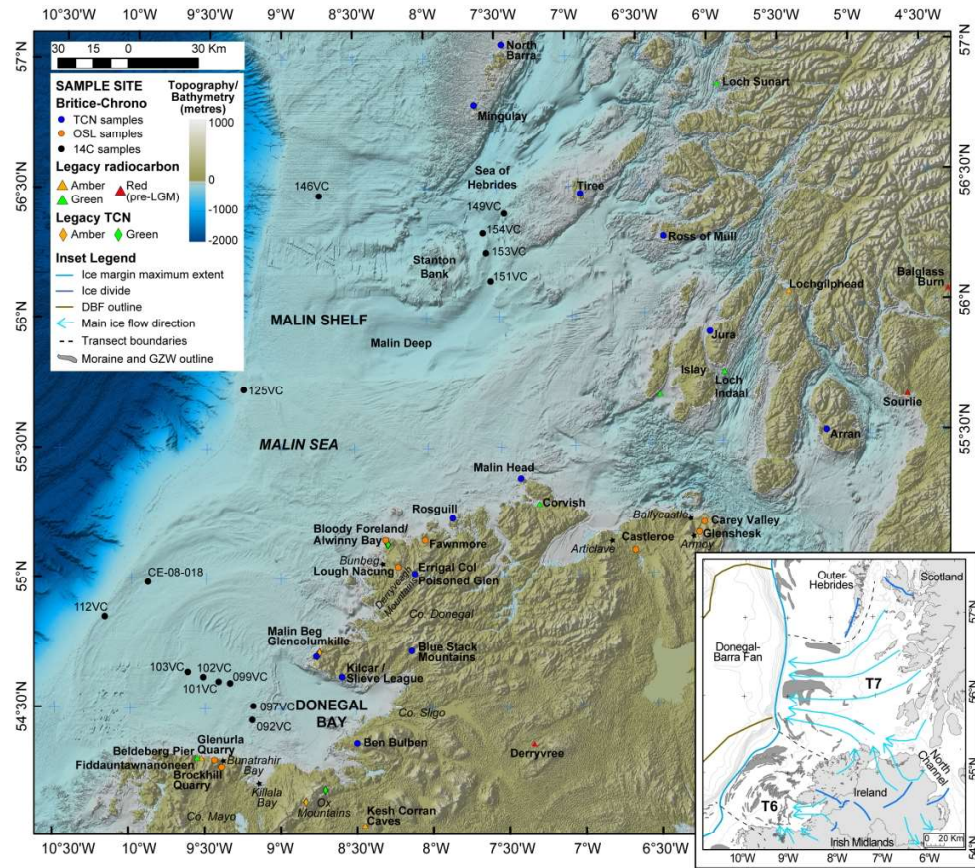


Figure 1: Main map presents an overview of the study area showing the west coast of Scotland and northwest of Ireland with the locations of legacy and BRITICE-CHRONO samples used in this paper, as well as other locations mentioned in the text. Background bathymetry and topography were downloaded from the EMODnet data services (<https://portal.emodnet-bathymetry.eu/services/>) and are presented here as shaded-relief with 20x vertical exaggeration to visualise specifically the geomorphological features on the shelf (colour scale is only indicative due to processing). Inset presents the proposed maximum ice extent, the outline of the Donegal-Barra Fan (DBF) and mapped moraines and grounding-zone wedges (GZW) in the region (from BRITICE Glacial Map v2.0; Clark et al., 2017 and references therein); the location of ice streams, main ice flow directions and ice flow divides (see Greenwood and Clark, 2009a, Greenwood and Clark, 2009b); and the location of BRITICE-CHRONO transects 6 (Donegal Bay) and 7 (Malin Sea) discussed in this paper.

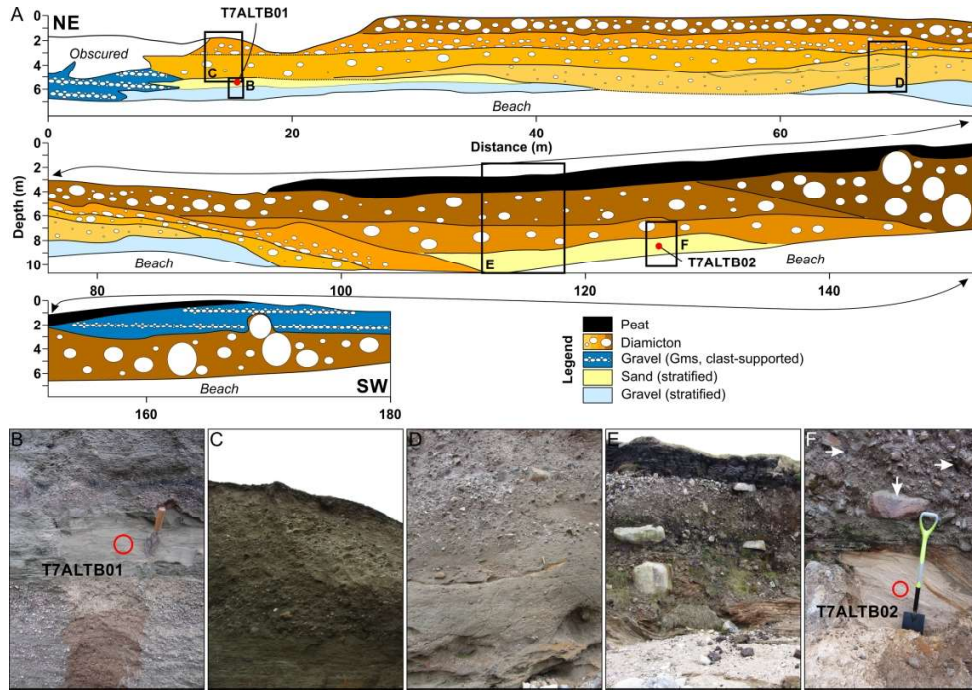


Figure 2: A) Serial section of the main exposure at Altwinny Bay. OSL sample locations are indicated by the labelled red dots, whilst the boxes labelled B-F show the coverage of the facies photographs in panels B-F. Note that clast depictions are not to scale but are instead representative of relative grain size variation between units. B-F) photographs of the main facies exposed. The OSL sample locations T7ALTB01 and 02 are indicated by the red circles. The white arrows highlight some of the abundant erratic clasts within the section that are likely carried to the site by Malin Sea ice.

252x176mm (300 x 300 DPI)

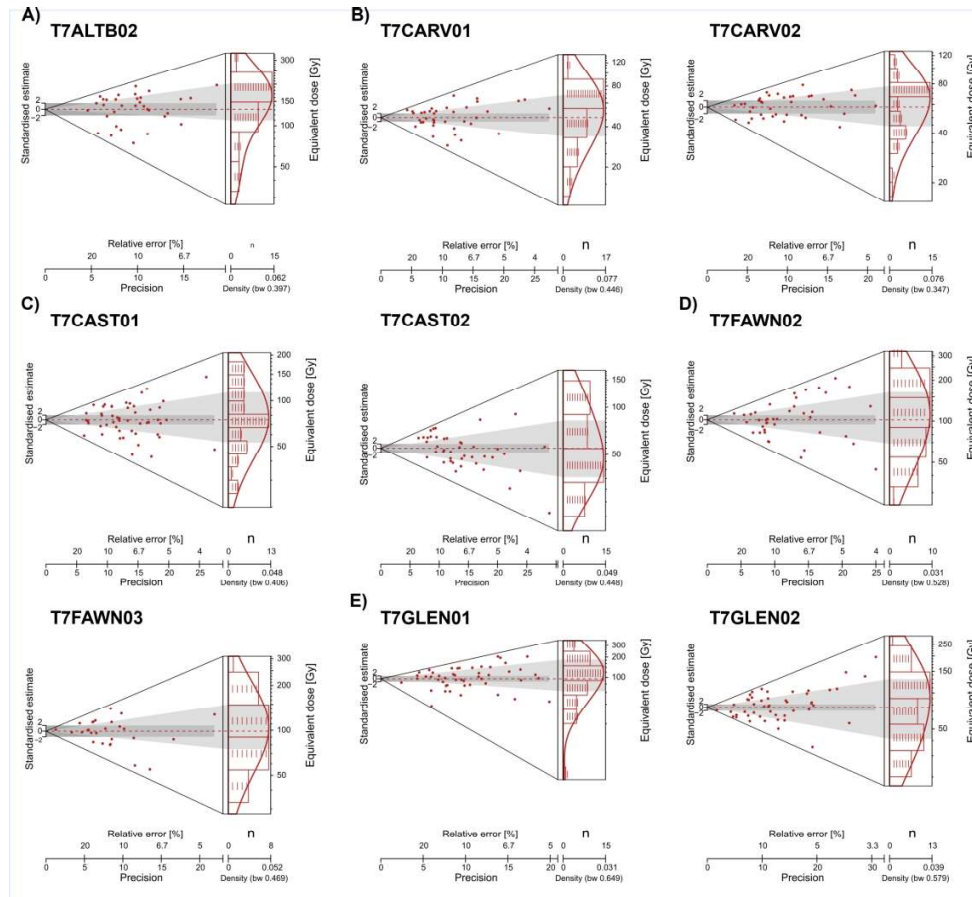


Figure 3: Optically-stimulated luminescence data. Abanico plots (Dietze et al., 2016) of the D_e values determined for OSL dating applied at (A) Altwinny Bay, (B) Carey Valley, (C) Castleroe, (D) Fawnmore, and (E) Glenshesk Valley. The plots present the D_e distributions in two plots that share a common z-axis of D_e values: (i) a bivariate plot where each D_e value is presented in relation to its precision (shown on the x-axis, where those more precisely known are plotted to the right); and (ii) a univariate plot showing the age frequency distribution of D_e values, which does not give any presentation of the precision of individual D_e values. The grey shading across both plots shows the D_e used in age calculation for each distribution (2σ shown on they-axis). The combination of these two plots aids interpretation of the scatter in the D_e distributions, where samples with a greater range of D_e values on the z-axis have larger amounts of scatter in the D_e distribution.

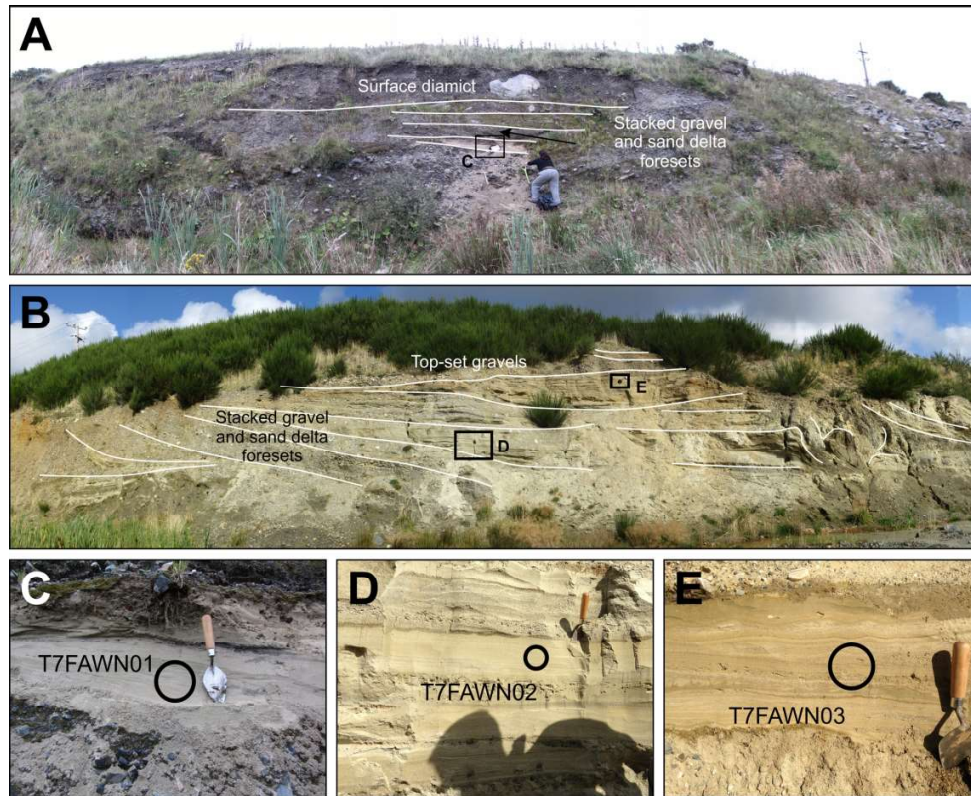


Figure 4: Photographs of exposures at Fawnmore Quarry A) section 1 and B) section 2. The labelled boxes show the locations covered by the photographs in C-E. Close-up photographs of the units from which C) T7FAWN01, D) T7FAWN02, and E) T7FAWN03 were sampled. The circles highlight sample positions.

180x146mm (300 x 300 DPI)

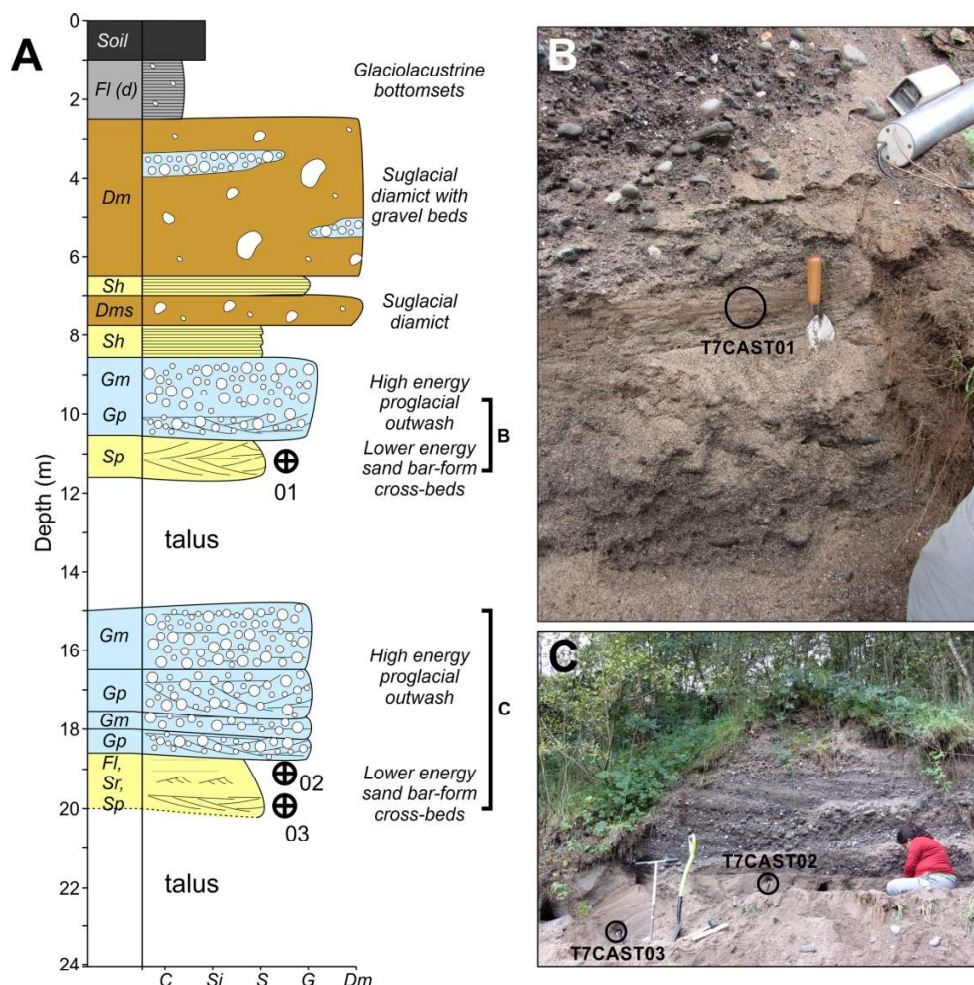


Figure 5 A) Generalized vertical log and environmental interpretation of the sediments exposed at Castleroe with X-axis scaling denoting C (clay), Si (silt), S (sand), G (Gravel) and Dm (diamicton). Standard lithofacies codes follow Evans and Benn (Fig. 2.15: 2004), with prefixes F (fines), S (sand), G (gravel), D (diamict), and suffixes planar (p) or trough (t) cross-stratification, delta foresets (fo), massive or structureless (S/Fm), horizontal stratification (h), rippled (r), laminations (l) with or without drop-stones (d), gravels matrix-supported massive (Gms), gravels clast-supported massive (Gm), diamict matrix-supported, massive (Dmm) and diamict matrix-supported stratified (Dms). OSL sample positions are indicated by the labelled crossed circles. The labelled bars along the depth axis indicate the coverage of photographs in B-C. B, C) Photographs of the units sampled for OSL dating. The OSL sample locations are indicated by the labelled circles.

185x185mm (300 x 300 DPI)

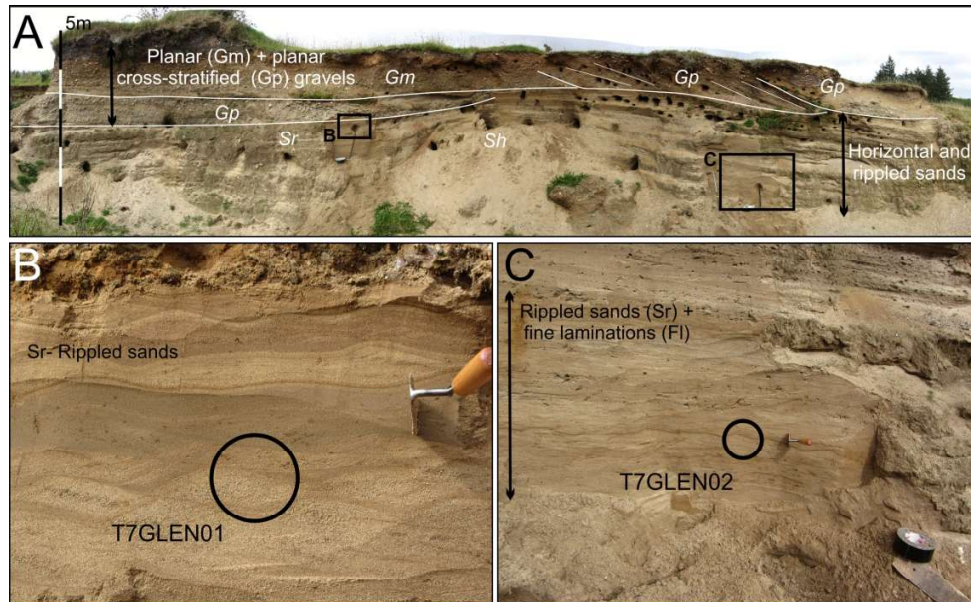


Figure 6 A) Photomontage of the main section at Glenshesk Valley. Lithofacies codes are the same as Fig. 5 (Fig. 2.15: Evans and Benn, 2004). The labelled boxes show the locations covered by the photographs in B-C. Close-up photographs of the units from which B) T7GLEN01 and C) T7GLEN02 were sampled. The circles highlight sample positions.

180x111mm (300 x 300 DPI)

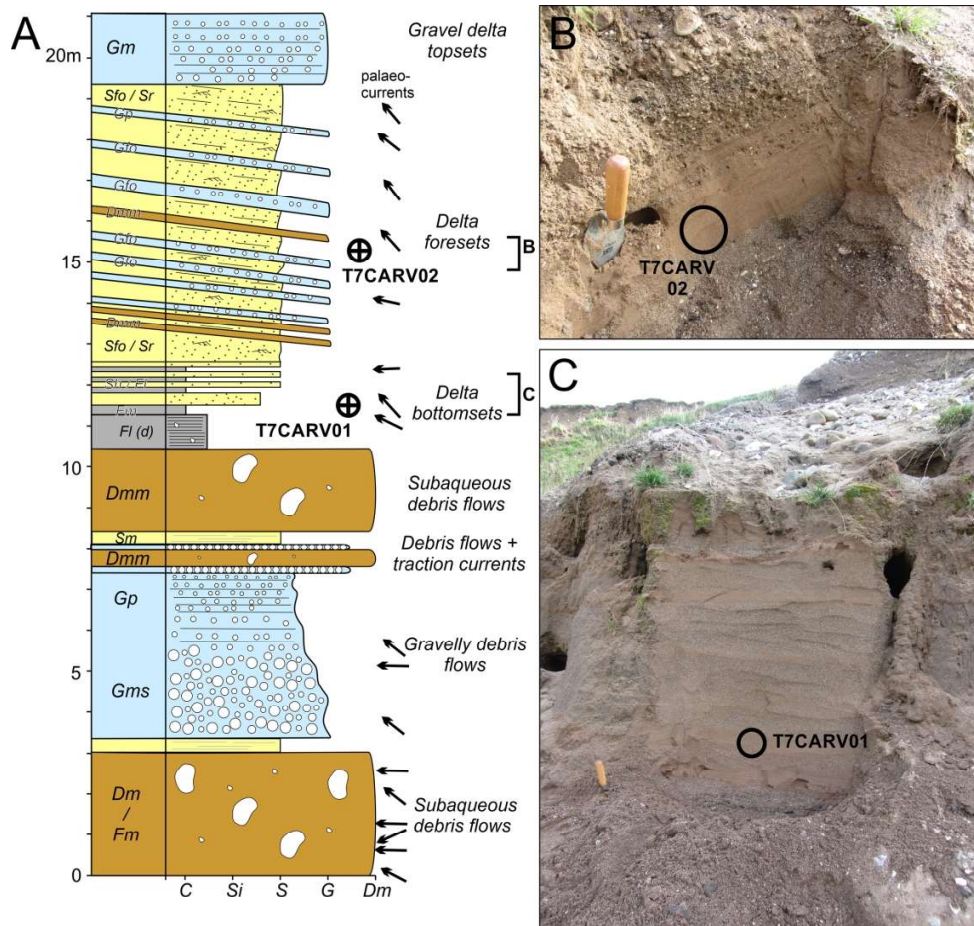


Figure 7: A) Generalized vertical succession of sediments exposed within Carey Valley (after McCabe and Eyles, 1988). Lithofacies codes are the same as Fig. 5 (Fig. 2.15: Evans and Benn, 2004). OSL sample positions are indicated by the labelled crossed circles. The labelled bars along the depth axis indicate the coverage of photographs in B-C. B, C) Photographs of the units sampled for OSL dating. The OSL sample locations are indicated by the circles.

186x176mm (300 x 300 DPI)



Figure 8: A) Annotated photo-montage of the main section at Lough Nacung quarry. Lithofacies codes are the same as Fig. 5 (Fig. 2.15: Evans and Benn, 2004). The labelled boxes indicate the locations of photographs shown in B-C. Close-up photographs of the units sampled for B) T6LNAC01 and C) T6LNAC02. The circles highlight the position of the OSL samples.

240x138mm (300 x 300 DPI)

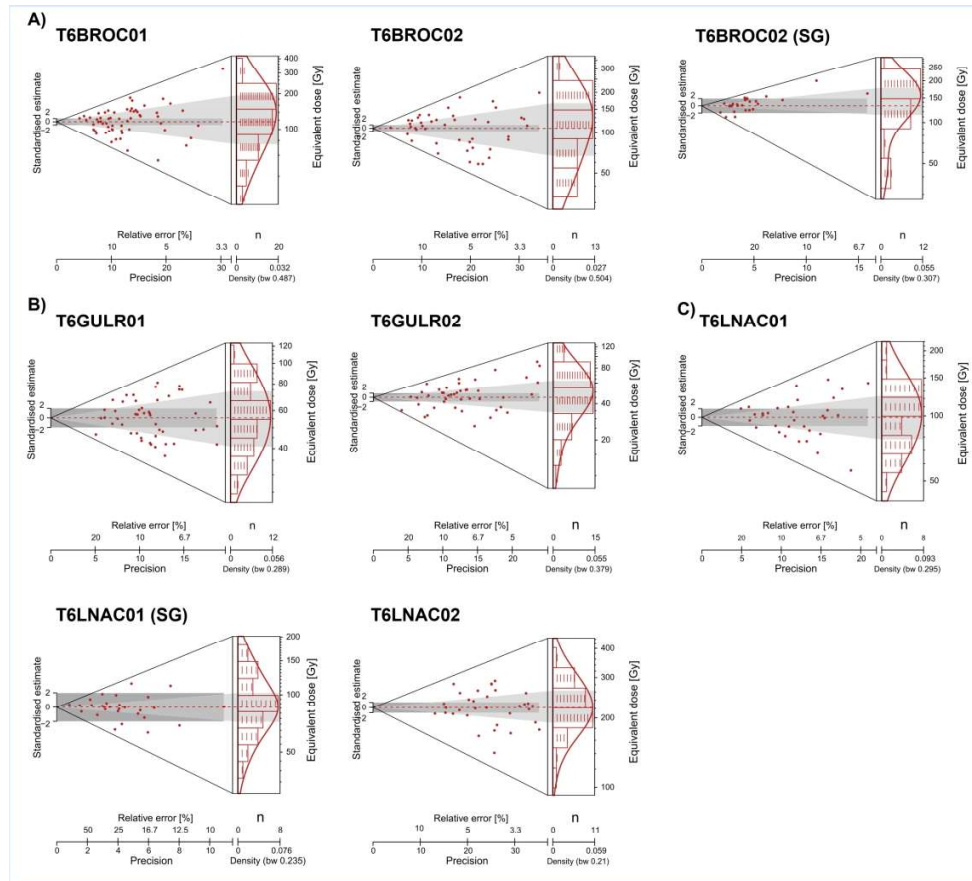


Figure 9: Optically-stimulated luminescence data. Abanico plots (Dietze et al., 2016) of the De values determined for OSL dating applied at (A) Brockhill Quarry, (B) Glenulra, and (C) Lough Nacung. The plots present the De distributions in two plots that share a common z-axis of De values: (i) a bivariate plot where each De value is presented in relation to its precision (shown on the x-axis, where those more precisely known are plotted to the right); and (ii) a univariate plot showing the age frequency distribution of De values, which does not give any presentation of the precision of individual De values. The grey shading across both plots shows the De used in age calculation for each distribution (2σ shown on they-axis). The combination of these two plots aids interpretation of the scatter in the De distributions, where samples with a greater range of De values on the z-axis have larger amounts of scatter in the De distribution.

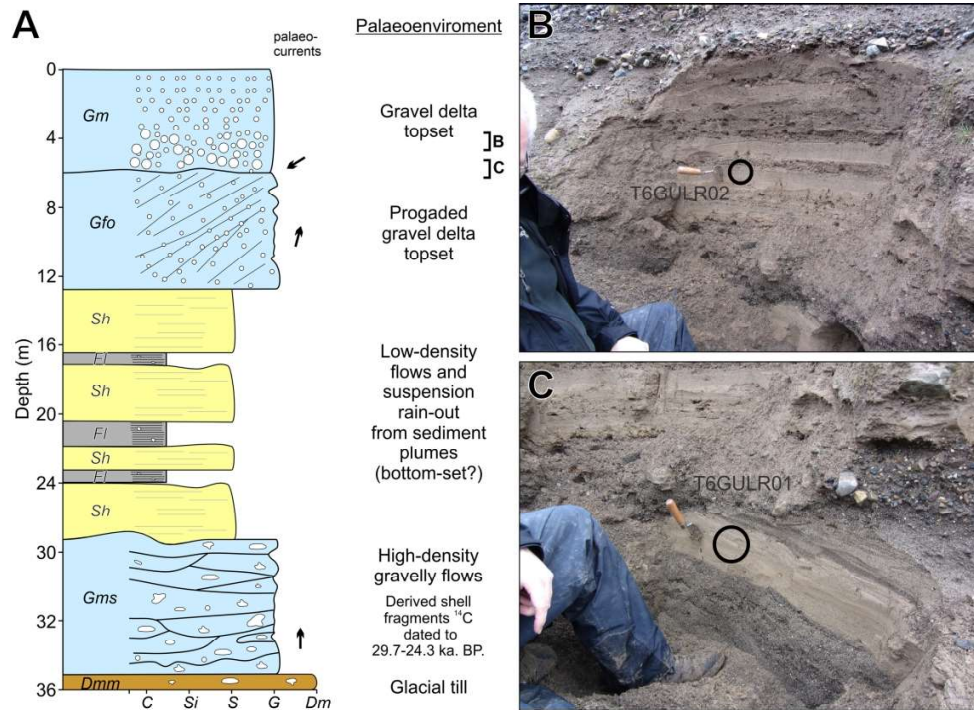


Figure 10: A) Generalized vertical succession of the sediments in Glenultra valley (after McCabe et al., 2007a). Lithofacies codes are the same as Fig. 5 (Fig. 2.15: Evans and Benn, 2004). The location of photographs in panels B and C are indicated by the labelled bars along the depth axis. Photographs of the units sampled for B) T6GULR02 and C) T6GULR01 with sample locations are indicated by the circles.

208x151mm (300 x 300 DPI)

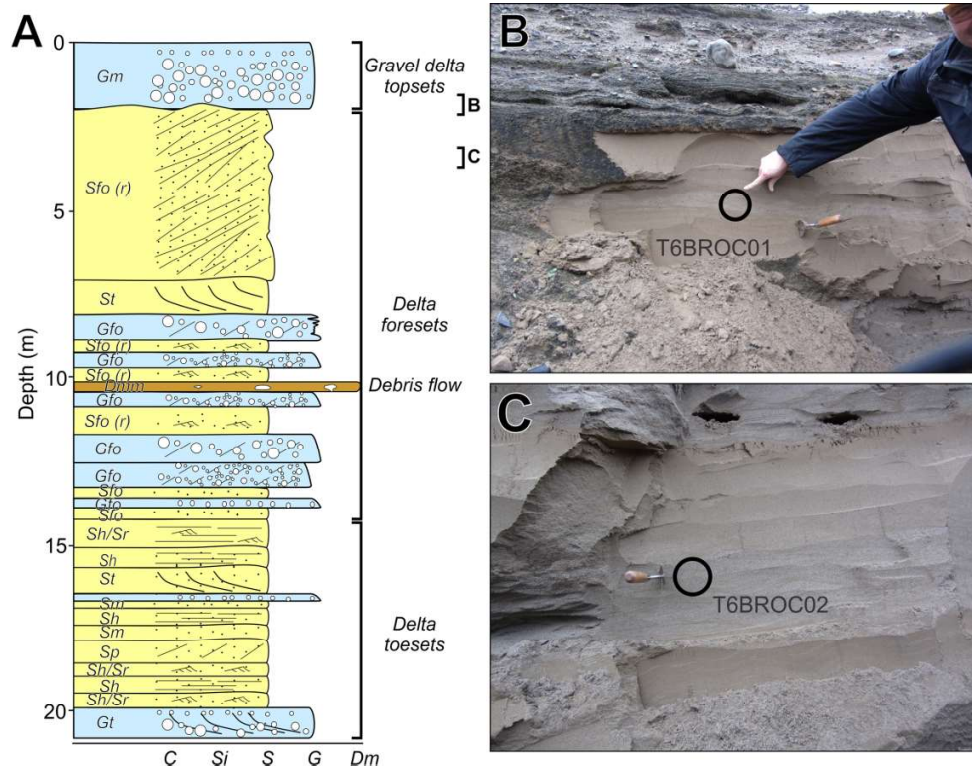


Figure 11: A) Generalized vertical succession of the sediments at Brockhill Quarry (after McCabe et al., 1986). Lithofacies codes are the same as Fig. 5 (Fig. 2.15: Evans and Benn, 2004). The location of photographs in panels B and C are indicated by the labelled bars along the depth axis. Photographs of the units sampled for B) T6BROC01 and C) T6BROC02 with sample locations are indicated by the circles.

182x142mm (300 x 300 DPI)

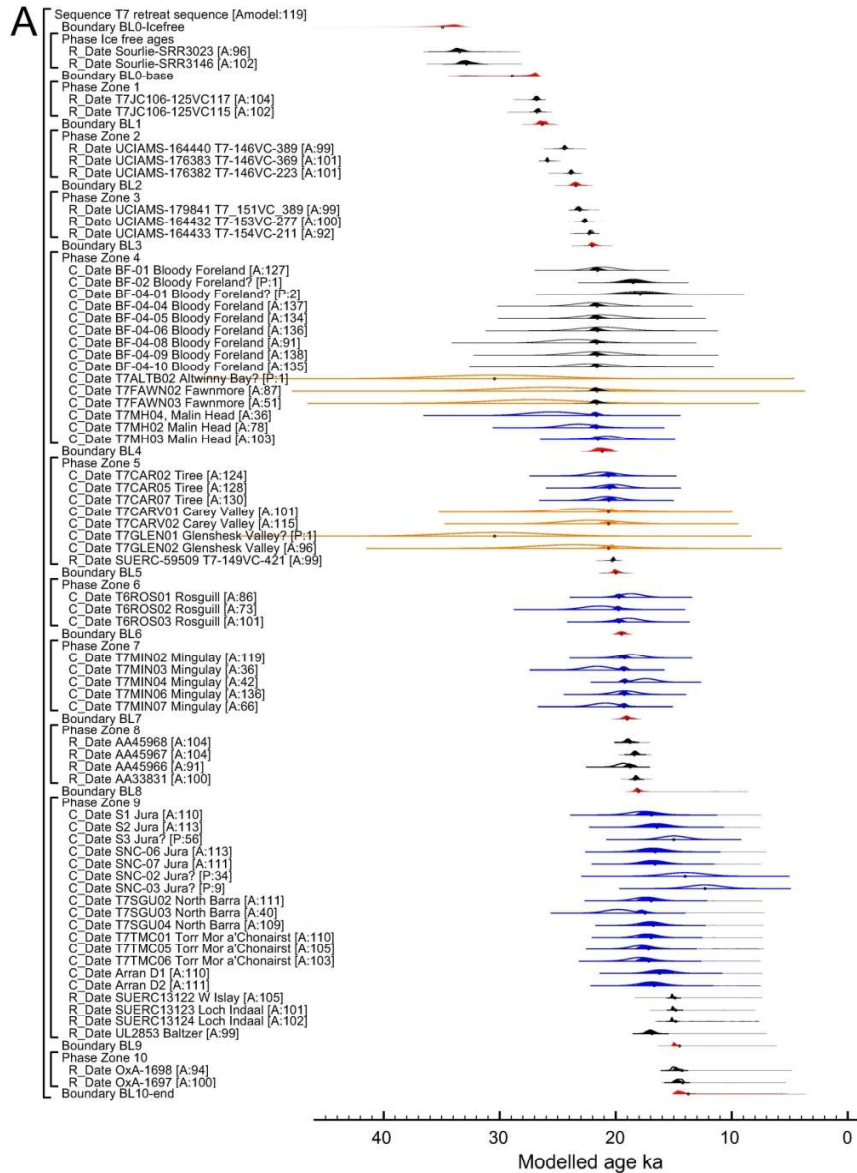


Figure 12: Bayesian chronosequence age-model output of dating constraints using Oxcal 4.3. (A) the MSIS (T7) and (B) DBIS (T6). The model structure shown uses OxCal brackets (left) and keywords that define the relative order of events (Bronk Ramsey, 2009a). Each original distribution (hollow) represents the relative probability of each age estimate with posterior density estimate (solid) generated by the modelling. Shown are 14C ages (black), OSL ages (orange), cosmogenic nuclide ages (blue) and modelled boundary ages (Red). Outliers are denoted by '?' and their probably (P) of being an outlier indicated by low values <5 (95% confidence). Model agreement indices for individual ages show their fit to the model with >60% the widely used threshold for 'good' fit (Bronk Ramsey, 2009b).

136x186mm (300 x 300 DPI)

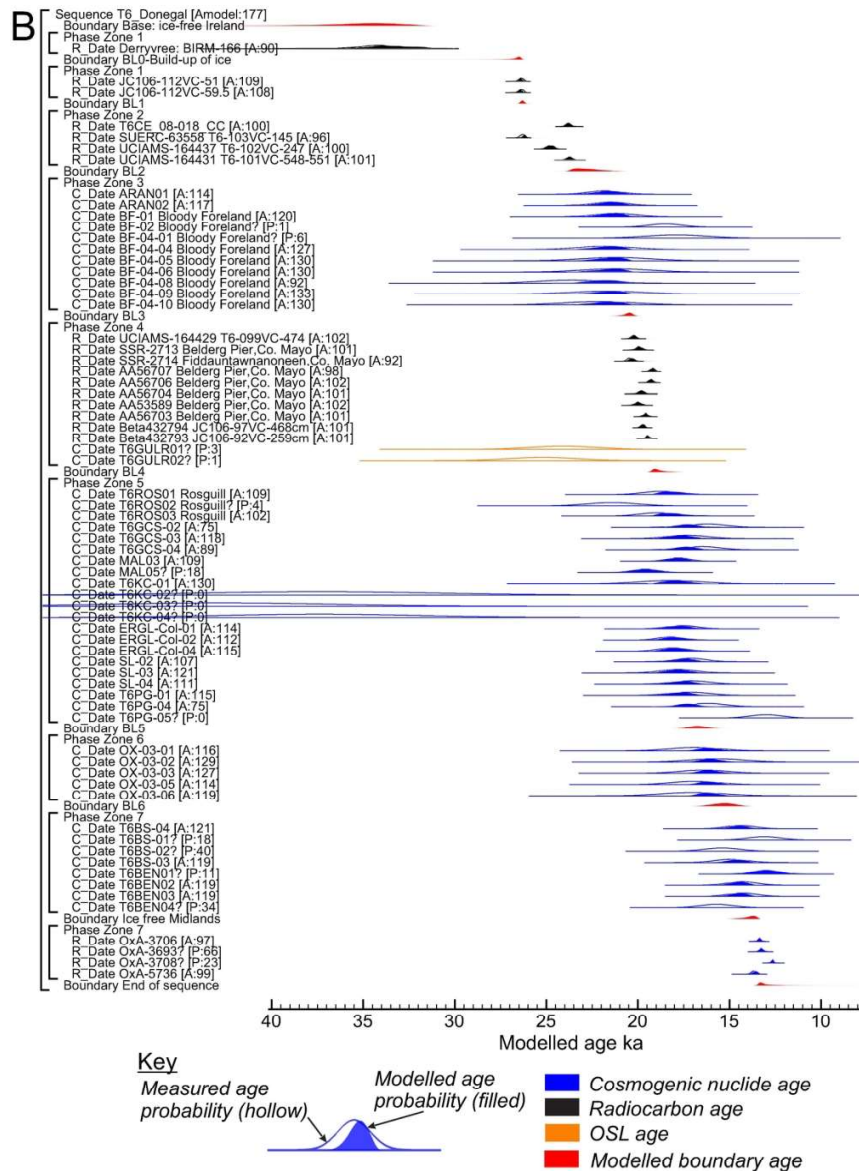


Figure 12: Bayesian chronosequence age-model output of dating constraints using Oxcal 4.3. (A) the MSIS (T7) and (B) DBIS (T6). The model structure shown uses OxCal brackets (left) and keywords that define the relative order of events (Bronk Ramsey, 2009a). Each original distribution (hollow) represents the relative probability of each age estimate with posterior density estimate (solid) generated by the modelling. Shown are ¹⁴C ages (black), OSL ages (orange), cosmogenic nuclide ages (blue) and modelled boundary ages (Red). Outliers are denoted by '?' and their probably (P) of being an outlier indicated by low values <5 (95% confidence). Model agreement indices for individual ages show their fit to the model with >60% the widely used threshold for 'good' fit (Bronk Ramsey, 2009b).

137x186mm (300 x 300 DPI)

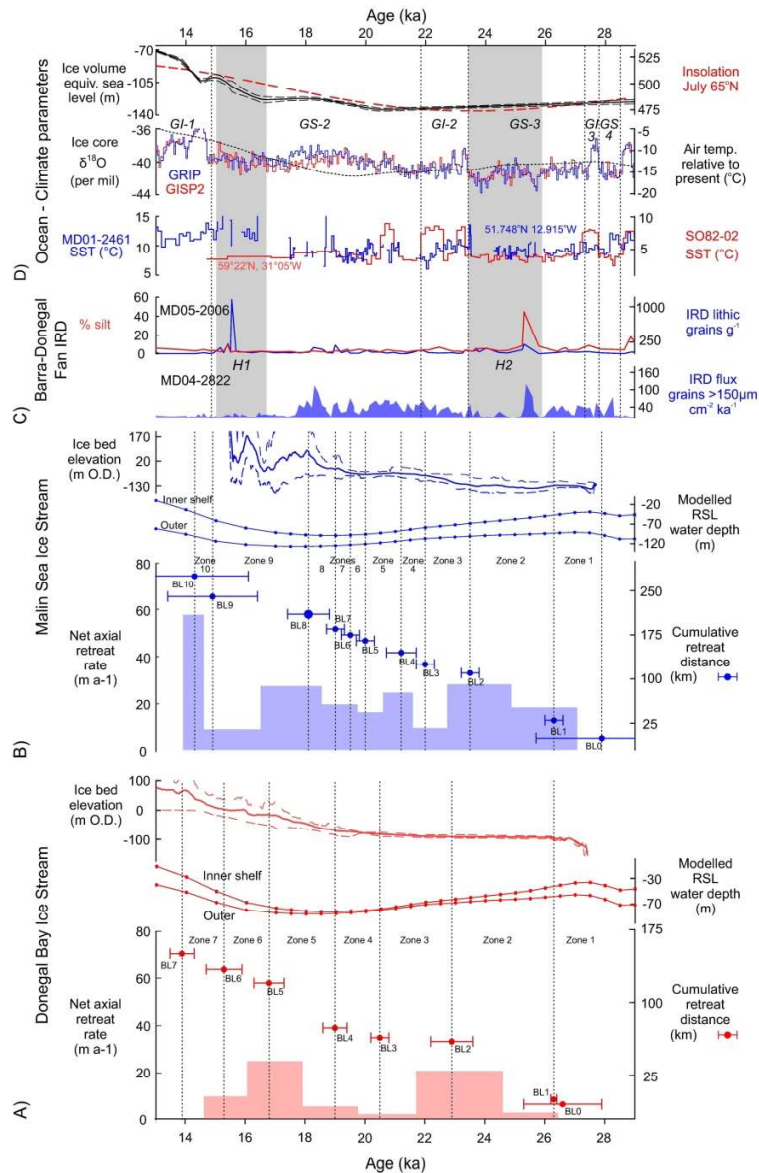


Figure 15: For A) the Donegal Bay Ice Stream and B) the Malin Sea Ice Stream, all plotted against age (ka) showing, (bottom) the boundary ages (circle and ± 1 sigma whisker plots) and retreat zones of the respective Bayesian models and the rates of net axial ice margin retreat. (Middle) Modelled palaeo water depths (relative to present day bathymetry) for the inner and outer shelf derived from a glacial isostatic adjustment (GIA) model (Bradley et al., 2011) updated to include the latest BRITICE-CHRONO ice sheet reconstruction and accounting for global ice sheet variations. (Top) Mean and 95% ice bed elevations from the NextMap elevation and EMODnet bathymetry (www.emodnet-hydrography.eu/). C) Ice rafted debris (IRD) flux records from marine cores within the Donegal-Barra Fan MD04-2822 (Hibbert et al., 2009) and MD05-2006 (Knutz et al., 2001; Knutz et al., 2002) plotted against an updated (Waelbroeck et al., 2019). Heinrich Events H2 and H1 are highlighted grey (Bond et al., 1992). D) Ocean-climate parameters showing (bottom) sea surface temperature records determined for the North Atlantic using SST (°C) calculated using planktonic foraminifera for core SO82-02 at 59°N, 31°W (red line) (Rasmussen et al., 2016; Van Kreveld et al., 2000) plotted using an updated age model (Waelbroeck et al., 2019) and the MD01-2461 site from the Porcupine Seabight at 51.7°N, 12.9°W (blue line) (Peck et al., 2006; Peck et al., 2007). (Middle) $\delta^{18}\text{O}$

1
2
3 concentrations, Greenland Stadials (GS) and Interstadials (GI) from the GISP2 and GRIP Greenland ice cores
4 (Rasmussen et al., 2014), plotted with and modelled surface-air temperatures (black line) relative to
5 present for land masses north of ~45°N (Bintanja et al., 2005). (Top) Ice volume equivalent sea level
6 (Lambeck et al., 2014) and summer insolation (pecked) for 60°N (Berger and Loutre, 1991).

7
8 177x276mm (300 x 300 DPI)
9

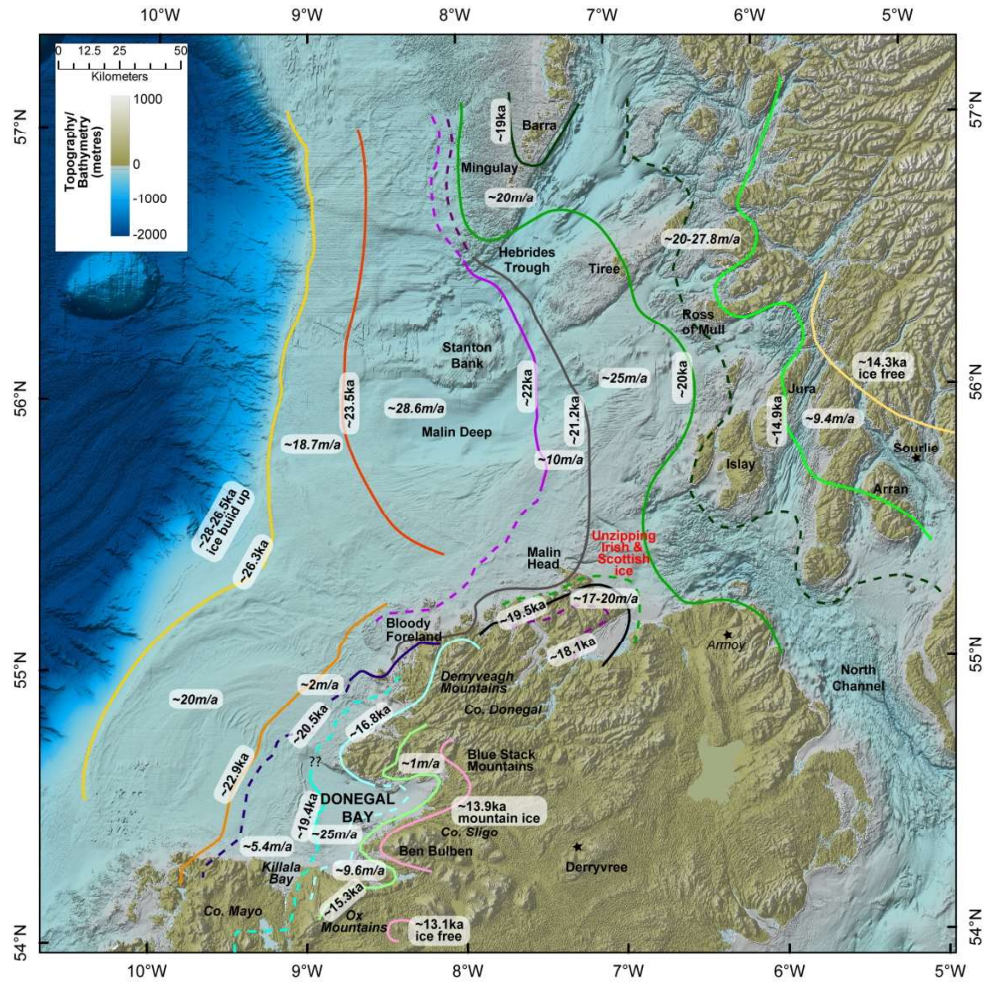


Figure 16: Overview of modelled isochrones and retreat rates across the two transects of the Malin Sea and Donegal Bay Ice Streams with relevant geomorphological context (from BRITICE Glacial Map v2.0; Clark et al., 2017 and references therein). Dashed lines indicate more tentative isochrone positions due to lack of geomorphological evidence at the required spatial resolution. Background bathymetry and topography from EMODnet data services (<https://portal.emodnet-bathymetry.eu/services/>).